DISSERTATION

LOW-COST DEVICES FOR OCCUPATIONAL AND ENVIRONMENTAL EXPOSURE ASSESSMENT

Submitted by

Casey Quinn

Department of Environmental and Radiological Health Sciences

In partial fulfillment of the requirements

For the Degree of Doctor of Philosophy

Colorado State University

Fort Collins, Colorado

Fall 2018

Doctoral Committee:

Advisor: John Volckens
Co-Advisor: Charles Henry

Sheryl Magzamen
Georgiana Brooke Anderson
Stephen Reynolds

ABSTRACT

LOW-COST DEVICES FOR OCCUPATIONAL AND

ENVIRONMENTAL EXPOSURE ASSESSMENT

The measurement of chemical and physical stressors in occupational and environmental settings traditionally requires sophisticated equipment, trained professionals, and laboratory-based analyses. These requirements are cost and time prohibitive and, thus, limit the quantity and frequency of exposure monitoring. This dissertation focuses on the development of low-cost monitoring tools for evaluation of air and water quality.

Water Quality Assessment

Metal contamination of natural and drinking water systems poses hazards to public and environmental health. Quantifying metal concentrations in water typically requires sample collection in the field followed by expensive laboratory analysis that can take days to weeks to obtain results. The first portion of this work was to develop a low-cost, field-deployable method to quantify trace levels of copper in drinking water by coupling solid-phase extraction/preconcentration with a microfluidic paper-based analytical device. This method has the advantages of being hand-powered (instrument-free) and using a simple 'read by eye' quantification motif (based on color distance). Tap water samples collected across Fort Collins, CO were tested with this method and validated against ICP-MS. We demonstrate the ability to quantify the copper content of tap-water within 30% of a reference technique at levels ranging from 20 to 500,000 ppb. The application of this technology, which should be sufficient as a rapid screening tool, can lead to faster, more cost-effective detection of soluble metals in water systems.

Air Quality Assessment

Personal monitors for air quality are expensive and cumbersome, which hinders epidemiologic and occupational exposure assessments. The Automated Microenvironmental Aerosol Sampler (AMAS) is a low-cost, wearable device containing four filter-pump assemblies designed to measure personal exposure

particulate matter air pollution. This novel device collects size-selective samples of particulate matter from within distinct personal microenvironments (i.e. at home, at work, and in transit). The AMAS uses on-board sensors (GPS, light intensity, temperature, pressure, and acceleration) coupled with an algorithm (developed and described in to this work) to determine when an individual enters a given microenvironment and then initiates sampling through one of three filter assemblies.

Low-cost devices capable of in-field quantification of pollutant hazards can allow researchers to afford more monitoring and analysis equipment and increase the size of epidemiology and industrial hygiene cohorts.

ACKNOWLEDGEMENTS

I have tried hard all of my life to avoid additional education; however, I now find myself at the terminus of yet another degree (26 years of schooling… but who's counting other than my nephew). I am very grateful to have been afforded the many opportunities to continue my academic growth, and I hope that the knowledge and skills I've gained can be used to have a positive impact on society.

I owe my accomplishments to date, in large part, to the support that my spouse Jill Schulte, my parents C.A. Quinn, Joyce Quinn, Dana Quinn, and Larry Nelson, my sister Christa Quinn-Prideaux and many other family members and close friends have provided over the years. In particular I am grateful for the support and patience from Jill. She has been pivotal in ensuring that I complete this work, and she has endured the near-constant whirring of multiple air samplers that I've tested over the years scattered throughout the house. I would also like to express my gratitude for my family and friends whom have supported me over the years and for enduring countless hours of listening to me ramble (much of the time incoherently) about what I'm working on. In particular I am deeply grateful to those who were so kind to help accommodate my visits to Colorado and provided a place to stay.

I would also like to thank my current advisors John Volckens and Chuck Henry and for their patience, guidance, and support during the duration of this work. In particular, I wish to thank them for entrusting me with the management of the many opportunities they provided, allowing me to learn new skills, and the freedom to complete my dissertation from afar allowing me to balance my personal and professional needs. Additionally, I wish to thank John for his persistence to persuade me to embark on yet another academic challenge that has provided invaluable knowledge and skills. In addition to my official advisors I am truly grateful to Dave Leith (the all-knowing intern) for his pro bono advising and Sheryl Magzamen for her support, advice, and match-making skills. I also owe much of my success to my colleagues Daniel David Miller-Lionberg, David Cate, and Todd Hochwitz. The technologies developed and described herein would not have been possible without their support and efforts. I am also extremely grateful for all the friendships, support, and efforts that all of my fellow members of the Volckens and Henry Research Groups have

provided over the years including Jacklyn Adkins, Kelsey Bilsback, James Cao, Nicholas Good, Nathan Henry, Brie Hawley, Scott Kelleher, Kevin Klunder, Kirsten Koehler, Jake Lord, John Mehaffy, Jaruwan Mettakoonpitak, Mike Nguyen, Christian L'Orange, Thomas Reilly III, Josh Smith, and Eric Wendt. I am also grateful to everyone from the Department of Environmental and Radiological Sciences, Mechanical Engineering, Engines and Energy Conversion Laboratory, and the Energy Institute whom I have worked with and whom have assisted me over the past many years including Marc Baumgardner, Megan Benka-Coker, Wande Benka-Coker, Thomas Bradley, Ben Geller, Mac McGoldrick, Jason Prapas, "brother" Jason Quinn, Nick Wagner, and Dan Zimmerle.

The development of the Automated Microenvironmental Aerosol Sampler (AMAS) couldn't have been developed without our collaborations with Rivendell School in Fort Collins, the Center for Advanced Research and Technology (CART) in Fresno, CA. More importantly this work couldn't have been completed without the participation by the students at those institutions and my colleagues at Colorado State University who agreed to carry aerosol samplers and collect the data described herein. Finally, I would like to thank our collaborators from the University of California, Berkeley and California State University, Fresno, in particular the assistance from S. Katherine Hammond, Betsey Noth, and Jaymin Kwon for their assistance and management of the data collection efforts in Fresno, CA.

Additional thanks to my amazing research committee that includes John Volckens, Chuck Henry, Sheryl Magzamen, Brooke Anderson, and Stephen Reynolds for providing great advice and assistance throughout this entire process and taking the time to help review this document.

The water quality work was supported by grant 1415655 from the National Science Foundation and a State of Colorado Advanced Industries Grant. The AMAS work was supported by grant ES24719 from the National Institute of Environmental Health Sciences, and by grant OH010662 from the National Institute for Occupational Safety and Health. This AMAS work was also supported by the Children's Health & Air Pollution Study (CHAPS), an NIH/EPA-funded Children's Environmental Health and Disease Prevention Research Center (EPA: RD83543501, NIH: ES022849.

DEDICATION

This work is dedicated to my good friend Brian Trainor, who gave me wonderful advice and insisted that I take the GRE and apply for a research position at the Engines and Energy Conversion Laboratory. That insistence has led to the completion of the work described herein, but more importantly, has impacted my personal and professional life in ways I would not have imagined.

Thank you.

You are missed.

TABLE OF CONTENTS

LIST OF NOMENCLATURE

AMAS	Automated Microenvironmental Aerosol Sampler
CAD	Computer Animated Design
CDC	Centers for Disease Control and Prevention
d_{50}	50% collection efficiency of particles with an aerodynamic diameter of 2.5µm
EPA	Environmental Protection Agency
ICP-MS	Inductively Coupled Plasma Mass Spectrometry
I2C	Inter-Integrated Circuit
LED	Light Emitting Diode
µPAD	Microfluidic Paper Analytical Devices
NIOSH	National Institute of Occupational Safety and Health
OSHA	Occupational Safety and Health Administration
$PM_{2.5}$	Particulate Matter Less than 2.5 Microns in Aerodynamic Diameter
PCB	Printed Circuit Board
SOC	State of Charge
UART	Universal Asynchronous Receiver-Transmitter
UPAS	Ultrasonic Personal Aerosol Sampler

CHAPTER 1: INTRODUCTION

Environmental Pollution & Public Health

We live in an era when people throughout the world can easily gain access to cellular phones and the internet[1] but still lack basic resources such as clean air and water.[2-9] Poor environmental conditions have enormous implications for public health and disease outcomes. Recent research has estimated that exposure to environmental pollution was the cause of 12.6 million (23%)[10] global premature deaths in 2012; approximately eight million of those deaths were attributable to noncommunicable diseases.[11] A further breakdown of these premature deaths suggests that contaminated drinking water causes 502,000 diarrheal deaths each year,[12] and exposure to air pollution causes 4.2 million deaths each year.[2, 13] In addition to premature deaths, exposure to air and water pollution has casual associations with chronic conditions like schistosomiasis[12], asthma, and cardiovascular disease.[2, 13] Thus, improving and sustaining the quality of our environment is fundamental to enhancing quality of life worldwide.

Exposure Inequities

Exposure to environmental pollution presents a health burden to all individuals; however, mortality and morbidity rates indicate that the burden does not impact all communities and populations equally. Minorities, lower-income groups, and residents of developing countries are more vulnerable and susceptible to environmental pollution exposure.[14-18] In 2011, the Centers for Disease Control and Prevention (CDC) estimated that over 39.5 million Americans have been diagnosed with asthma[19], with a higher prevalence in black and multi-race individuals who live in a household with an annual income of less than $15,000 per year.[20-22] Asthma disproportionately affects children and is known to result in a large number of school absences. Water quality issues also disproportionately affect low-income communities and people of color. The lead contamination incident in drinking water in Flint, Michigan impacted a community with a high poverty rate (>41%) and a predominate population of people of color (>62%).[23, 24] Similar incidents have been documented around the world where underserved populations face a disproportionately large burden from exposure to environmental pollutants.[25]

The Burden of Proof

Historically, human exposure to environmental pollution has been exacerbated by a culture of corporate profit incentives and insufficient penalties for violations of environmental laws; however, there have been recent examples that have shown some change on these fronts.[26, 27, 28] In part, this leniency, at least here in the U.S., has been tied with the use of a technique called "manufactured uncertainty" and is described at length by the former Assistant Secretary of the Occupational Safety and Health Administration (OSHA) David Michaels.[29] In brief, manufactured uncertainty is an approach that large corporations and influential groups have used to deflect scientific proof that a contaminant has a causal link to a health outcome, which can delay responsibility for decades. The most notable examples have involved the tobacco,[30] lead,[31] and asbestos[32] industries, all of which used manufactured uncertainty for financial gain at the expense of environmental and public health. In a climate of uncertainty around the consequences of environmental pollution, such industries are able to undermine efforts to regulate contaminants and evade responsibility for the health consequences from exposure to industrial pollution.

A Gap in Exposure Science: Insufficient Data

Public health researchers can provide estimates of the health implications resulting from exposure to environmental pollutants; however, associating health outcomes with environmental pollutants is complex and challenging.[33] The lack of data to support citizen complaints or observations made by public health officials is a limitation in exposure science and is one reason manufactured uncertainty can be used to delay the implementation of protective measures against exposures to contaminants.[3] To reduce the impacts of manufactured uncertainty, large and sufficiently-powered studies are needed. Studies that include spatially- and temporally-resolved monitoring are better able to pinpoint the environmental causes of health outcomes.[34] However, the expense and complexity of pollutant detection and monitoring means that quantitative assessments are frequently cost-prohibitive and limited in scope. Therefore, qualitative assessments are frequently conducted and usually only for initial screening. For example, occupational health qualitative assessments are commonly used to estimate exposures. However, research has shown that initial qualitative judgments of workplace conditions are only about 30% accurate and can falsely deem

quantitative assessment unnecessary, potentially leaving workers unprotected.[35] Additionally, exposure to many contaminants is not uniform over time or spatially homogenous and thus requires repeated sampling.[36, 37] Expanding the reach of quantitative evaluations by reducing the cost and complexity of contaminant detection and monitoring is needed to strengthen the power of environmental health assessments.

Pollutant Sample Collection & Analysis

Sample collection and analysis are two key steps for evaluating exposures to air and water pollutants. Traditional sample collection usually requires a specialized lab to analyze the samples. Traditional methods for the collection of water samples are relatively simple, but the samples can be heavy and cumbersome if large volumes of water are needed. In contrast, personal sampling for airborne pollutants is more complex. Some traditional personal aerosol samplers collect one time-integrated sample per measurement by collecting particulate matter onto a filter for a specified amount of time. Filter-based samplers have a number of logistical challenges: they require the use of multiple devices to capture spatial differences in exposure, the filters must be carefully handled, and samples require laboratory analysis after they have been collected. However, filter-based samplers do provide the opportunity to analyze the composition of the air pollution. Other personal exposure samplers continuously monitor aerosol concentration or composition (i.e. black carbon). Continuous, or real-time, monitoring methods can provide spatial-temporal evaluation of air quality and generally do not require laboratory analyses; however, these methods typically only monitor for a single aerosol characteristic (i.e. black carbon, aerosol mass or number concentration, etc.). In addition, their accuracy relative to reference instruments is typically lower than that of filter-based methods.[38]

The need for laboratory analysis of collected samples imposes additional challenges for sample collection in remote or resource-limited areas and limits the ability to capture exceptional exposure events that may occur infrequently. In 2015, the U.S. Environmental Protection Agency (EPA) inadvertently released three million gallons of mine water containing high concentrations of metals from the Gold King Mine in Colorado into the Animas River. The U.S. EPA collected water samples downstream immediately

after the incident occurred; however, the laboratory results were not available for 48 hours.[39] While the water samples were being analyzed the local residents were told to cease use of all wells and water supplies until the plume had passed and the laboratory results were released to the public. This example demonstrates the need for quantitative sample analysis methods that can provide expedited results.

Improving Environmental Pollution Assessment

Personal monitoring of environmental pollutants has traditionally been cost prohibitive for individuals or community groups to undertake themselves. In addition, low-income communities and people of color have historically been underrepresented in large-scale studies conducted by research institutions.[40] Fortunately, the technology wave that has brought cellular communications to the masses has helped reduce the cost of electronics (especially sensors), which in turn, has the potential to reduce the cost of equipment and methods used for contaminant sample collection and analysis.[38, 41-43] Low-cost sampling and analysis techniques can lower the economic barriers to evaluating environmental exposures and can empower communities by allowing individuals and community groups to directly monitor contaminants of concern. The use of low-cost sensors can also expand the reach of research studies to a greater number of participants, making them more likely to capture the heterogeneity of exposures across a community.

One novel air quality sampler, the low-cost Ultrasonic Personal Aerosol Sampler (UPAS)[44], is an example of a device that has been developed to help reduce the cost of personal air quality sample collection and thus increase the number of samples that can be collected. The UPAS costs less than $1500 for each personal sampler, about one third the cost of the equipment used in traditional outdoor air monitoring and occupational exposure monitoring.

All air and water samples that are collected for pollution monitoring must either be evaluated in real-time by onboard sensors, returned to a laboratory for analysis, or be evaluated by an in-field evaluation method. Microfluidic paper-based analytical devices (μPADs) are low-cost devices that are being developed for in-field detection and analysis of numerous environmental contaminants. Low-cost sample collection and analysis with devices such as the UPAS and μPADs are invaluable resources for researchers,

citizen scientists, and activists as these new tools help us further understand how environmental pollution impacts public health.

Objectives

This work makes three novel contributions to the field of exposure science. The first portion of this work (Chapter 2) details the development of a method capable of measuring copper levels in drinking water. This novel method combines sample preconcentration with a distance-based μPAD. Combining these two methods provides the ability to detect copper at ppb levels comparable to traditional methods such as inductively coupled plasma spectrometry (ICP-MS) but in the field without complex instrumentation. Chapters 3 & 4 describe the development of the Automated Microenvironmental Aerosol Sampler (AMAS) to provide the ability to collect filter samples in multiple locations throughout a sample period. The AMAS is a novel personal aerosol sampler that is capable of collecting fine particulate matter ($PM_{2.5}$) by microenvironment (i.e. home, school, work, transit). Chapter 3 describes a pilot test that demonstrated the viability of the AMAS. Chapter 4 describes the development of an enhanced microenvironment classification algorithm that was developed primarily for the AMAS but can also be applied to archived data. Chapter 5 summarizes the main findings (and limitations) of this work and discusses potential opportunities for ongoing research and development.

REFERENCES

1. World Bank, *World Development Report 2016: Digital Dividends*; **2016**.
2. Brauer, M.; Freedman, G.; Frostad, J.; Van Donkelaar, A.; Martin, R. V.; Dentener, F.; Dingenen, R. v.; Estep, K.; Amini, H.; Apte, J. S., Ambient air pollution exposure estimation for the global burden of disease 2013. *Environmental science & technology* **2015,** *50*, (1), 79-88.
3. Guarnieri, M.; Balmes, J. R., Outdoor air pollution and asthma. *The Lancet* **2014,** *383*, (9928), 1581-1592.
4. Järup, L., Hazards of heavy metal contamination. *British medical bulletin* **2003,** *68*, (1), 167-182.
5. Nel, A., Air pollution-related illness: effects of particles. *Science* **2005,** *308*, (5723), 804-806.
6. Pal, A.; He, Y.; Jekel, M.; Reinhard, M.; Gin, K. Y.-H., Emerging contaminants of public health significance as water quality indicator compounds in the urban water cycle. *Environment international* **2014,** *71*, 46-62.
7. Pope III, C. A.; Dockery, D. W., Health effects of fine particulate air pollution: lines that connect. *Journal of the air & waste management association* **2006,** *56*, (6), 709-742.
8. Rhind, S., Anthropogenic pollutants: a threat to ecosystem sustainability? *Philosophical Transactions of the Royal Society B: Biological Sciences* **2009,** *364*, (1534), 3391-3401.
9. Eisner, M.; Yelin, E.; Katz, P.; Earnest, G.; Blanc, P., Exposure to indoor combustion and adult asthma outcomes: environmental tobacco smoke, gas stoves, and woodsmoke. *Thorax* **2002,** *57*, (11), 973-978.
10. Prüss-Ustün, A.; Wolf, J.; Corvalán, C.; Neville, T.; Bos, R.; Neira, M., Diseases due to unhealthy environments: an updated estimate of the global burden of disease attributable to environmental determinants of health. *Journal of public health* **2016,** *39*, (3), 464-475.
11. Suk, W. A.; Ahanchian, H.; Asante, K. A.; Carpenter, D. O.; Diaz-Barriga, F.; Ha, E.-H.; Huo, X.; King, M.; Ruchirawat, M.; da Silva, E. R., Environmental pollution: an under-recognized threat to children's health, especially in low-and middle-income countries. *Environmental Health Perspectives* **2016,** *124*, (3), A41.
12. World Health Organization, Drinking-water: Key Facts. http://www.who.int/news-room/fact-sheets/detail/drinking-water (June 2018).
13. Cohen, A. J.; Brauer, M.; Burnett, R.; Anderson, H. R.; Frostad, J.; Estep, K.; Balakrishnan, K.; Brunekreef, B.; Dandona, L.; Dandona, R., Estimates and 25-year trends of the global burden of disease attributable to ambient air pollution: an analysis of data from the Global Burden of Diseases Study 2015. *The Lancet* **2017,** *389*, (10082), 1907-1918.
14. Bell, M. L.; Ebisu, K., Environmental inequality in exposures to airborne particulate matter components in the United States. *Environmental health perspectives* **2012,** *120*, (12), 1699.
15. Brown, P., Race, class, and environmental health: a review and systematization of the literature. *Environmental Research* **1995,** *69*, (1), 15-30.
16. Mohai, P.; Pellow, D.; Roberts, J. T., Environmental justice. *Annual Review of Environment and Resources* **2009,** *34*, 405-430.
17. Morello-Frosch, R.; Jesdale, B. M., Separate and unequal: residential segregation and estimated cancer risks associated with ambient air toxics in US metropolitan areas. *Environmental health perspectives* **2006,** *114*, (3), 386.
18. O'Neill, M. S.; Jerrett, M.; Kawachi, I.; Levy, J. I.; Cohen, A. J.; Gouveia, N.; Wilkinson, P.; Fletcher, T.; Cifuentes, L.; Schwartz, J., Health, wealth, and air pollution: advancing theory and methods. *Environmental health perspectives* **2003,** *111*, (16), 1861.
19. Centers for Disease Control and Prevention, Asthma facts—CDC's national asthma control program grantees. *Atlanta, GA: US Department of Health and Human Services, Centers for Disease Control and Prevention* **2013**.
20. Forno, E.; Celedón, J. C., Asthma and ethnic minorities: socioeconomic status and beyond. *Current opinion in allergy and clinical immunology* **2009,** *9*, (2), 154.

21. Akinbami, L. J.; Bailey, C. M.; Johnson, C. A.; King, M. E.; Liu, X.; Moorman, J. E.; Zahran, H. S., Trends in asthma prevalence, health care use, and mortality in the United States, 2001-2010. **2012**.
22. Barnett, S. B. L.; Nurmagambetov, T. A., Costs of asthma in the United States: 2002-2007. *Journal of allergy and clinical immunology* **2011,** *127*, (1), 145-152.
23. Bellinger, D. C., Lead Contamination in Flint — An Abject Failure to Protect Public Health. *New England Journal of Medicine* **2016,** *374*, (12), 1101-1103.
24. Butler, L. J.; Scammell, M. K.; Benson, E. B., The Flint, Michigan, Water Crisis: A Case Study in Regulatory Failure and Environmental Injustice. *Environmental Justice* **2016,** *9*, (4), 93-97.
25. Brulle, R. J.; Pellow, D. N., Environmental justice: human health and environmental inequalities. *Annu. Rev. Public Health* **2006,** *27*, 103-124.
26. Adeola, F. O., Cross-national environmental injustice and human rights issues: A review of evidence in the developing world. *American Behavioral Scientist* **2000,** *43*, (4), 686-706.
27. Dutta, M.; Sreedhar, R.; Basu, A., The blighted hills of Roro, Jharkhand, India: a tale of corporate greed and abandonment. *International journal of occupational and environmental health* **2003,** *9*, (3), 254-259.
28. Katz, R. S., Environmental pollution: corporate crime and cancer mortality. *Contemporary justice review* **2012,** *15*, (1), 97-125.
29. Michaels, D.; Monforton, C., Manufacturing uncertainty: contested science and the protection of the public's health and environment. *American journal of public health* **2005,** *95*, (S1), S39-S48.
30. Kessler, D., *A question of intent: A great American battle with a deadly industry*. Great American Battle with wit: **2002**.
31. Warren, C., *Brush with death: a social history of lead poisoning*. JHU Press: **2001**.
32. Ozonoff, D., Failed warnings: asbestos-related disease and industrial medicine. *The health and safety of workers* **1988**, 139-218.
33. Briggs, D., Environmental pollution and the global burden of disease. *British medical bulletin* **2003,** *68*, (1), 1-24.
34. Rappaport, S., Assessment of long-term exposures to toxic substances in air. *The Annals of occupational hygiene* **1991,** *35*, (1), 61-122.
35. Arnold, S. F.; Stenzel, M.; Drolet, D.; Ramachandran, G., Using checklists and algorithms to improve qualitative exposure judgment accuracy. *Journal of occupational and environmental hygiene* **2016,** *13*, (3), 159-168.
36. Lyles, R. H.; Kupper, L. L.; Rappaport, S. M., A lognormal distribution-based exposure assessment method for unbalanced data. *The Annals of occupational hygiene* **1997,** *41*, (1), 63-76.
37. Rappaport, S.; Lyles, R.; Kupper, L., An exposure—assessment strategy accounting for within-and-between-worker sources of variability. *The Annals of occupational hygiene* **1995,** *39*, (4), 469-495.
38. Kumar, P.; Morawska, L.; Martani, C.; Biskos, G.; Neophytou, M.; Di Sabatino, S.; Bell, M.; Norford, L.; Britter, R., The rise of low-cost sensing for managing air pollution in cities. *Environment international* **2015,** *75*, 199-205.
39. *Gold King Mine Release: Inspector General Response to Congressional Requests*; Environmental Protection Agency: Washington, D.C., **2017**.
40. Burchard, E. G.; Oh, S. S.; Foreman, M. G.; Celedón, J. C., Moving toward true inclusion of racial/ethnic minorities in federally funded studies. A key step for achieving respiratory health equality in the United States. *American journal of respiratory and critical care medicine* **2015,** *191*, (5), 514-521.
41. Hasenfratz, D.; Saukh, O.; Sturzenegger, S.; Thiele, L. In *Participatory air pollution monitoring using smartphones*, in Proceedings of the 1st International Workshop onMobile Sensing: From Smartphones and Wearables to Big Data, 2012; 2012.
42. Meredith, N. A.; Quinn, C.; Cate, D. M.; Reilly, T. H., 3rd; Volckens, J.; Henry, C. S., Paper-based analytical devices for environmental analysis. *Analyst* **2016,** *141*, (6), 1874-87.
43. Koehler, K. A.; Peters, T. M., New methods for personal exposure monitoring for airborne particles. *Current environmental health reports* **2015,** *2*, (4), 399-411.
44. Volckens, J.; Quinn, C.; Leith, D.; Mehaffy, J.; Henry, C. S.; Miller-Lionberg, D., Development and evaluation of an ultrasonic personal aerosol sampler. *Indoor air* **2017,** *27*, (2), 409-416.

CHAPTER 2: SOLID-PHASE EXTRACTION COUPLED TO A PAPER-BASED TECHNIQUE FOR TRACE COPPER IN DRINKING WATER

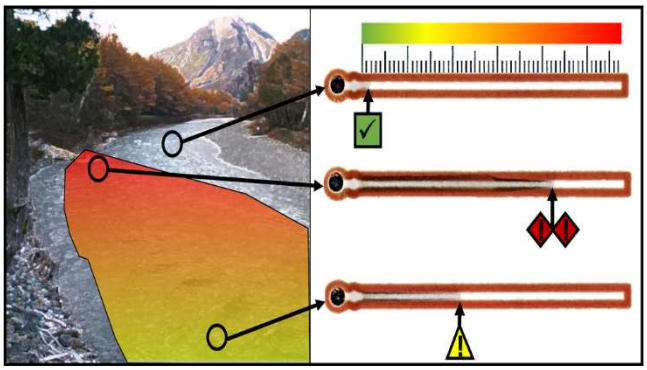

Figure 2-1: Example demonstration of how trace levels of copper in water samples could be quickly quantified in the field by coupling solid-phase extraction/preconcentration with a microfluidic paper-based analytical device.

Chapter Overview

The content of this chapter was published in *Environmental Science & Technology* and is reproduced here.[1] Metal contamination of natural and drinking water systems poses hazards to public and environmental health. Quantifying metal concentrations in water typically requires sample collection in the field followed by expensive laboratory analysis that can take days to weeks to obtain results. The objective of this work was to develop a low-cost, field-deployable method to quantify trace levels of copper in drinking water by coupling solid-phase extraction/preconcentration with a microfluidic paper-based analytical device. This method has the advantages of being hand-powered (instrument-free) and using a

simple 'read by eye' quantification motif (based on color distance). Tap water samples collected across Fort Collins, CO were tested with this method and validated against ICP-MS. We demonstrate the ability to quantify the copper content of tap-water within 30% of a reference technique at levels ranging from 20 to 500,000 ppb. The application of this technology, which should be sufficient as a rapid screening tool, can lead to faster, more cost-effective detection of soluble metals in water systems.

Introduction

Recent municipal[2] and environmental[3] water contamination events have highlighted public health concerns regarding water quality. Events like those in Flint, MI and the Gold King Mine in Colorado have produced considerable outrage[4, 5] and have increased public demand for improved monitoring.[6] Affected stakeholders have placed particular emphasis on increasing the spatial and temporal resolution of monitoring, in an effort to promote more effective risk communication (and control efforts) during a contamination event.[7, 8] Standard reference methods for trace metals analysis, however, rely on expensive equipment and time-intensive procedures. Therefore, a need exists for water quality monitoring methods that are rapid, low-cost, and scalable to the needs not only of regulatory agencies but also the general public.

Microfluidic paper analytical devices (μPADs) represent an emerging technology platform that shows promise for scalable, low-cost monitoring of water quality. Most μPAD applications have focused on medical diagnostics,[9-11] but this technology is also well poised to make advances in environmental monitoring.[12] The present work focuses on μPAD detection of Cu in drinking water. Although low-levels of Cu intake are essential for human and aquatic health, high levels of intake can be toxic.[13, 14] The U.S. Environmental Protection Agency (EPA) requires monitoring of Cu in drinking water under the 1991 Copper and Lead rule[15] and also under the National Recommended Aquatic Life Criteria.[16] The current EPA Action Level (concentration that when exceeded warrants remedial action) for Cu in drinking water is 1.3 ppm.[17] Although colorimetric intensity[18-27] and distance-based[28, 29] μPADs have been developed for Cu, these existing designs have limitations. Intensity-based μPADs require the evaluation of the color hue and/or intensity, which can be difficult to access accurately without the aid of imaging equipment and

software. Distance-based μPADs are easier to evaluate in the field as they can be read by eye; however, such methods, to date, cannot detect Cu concentrations at or below the EPA limit of 1.3 ppm.

Solid-phase extraction of metal ions has been previously demonstrated as a sample preparation technique for Flame Atomic Absorption Spectrometry,[30-32] X-Ray Fluorescence,[33, 34] Diffuse Reflectance Spectroscopy,[35-37] and for intensity-based μPADs.[38] In this work, Empore™ chelation disks were used to extract the metal ions from the sample to reduce the potential for interferences from sample matrix effects and to preconcentrate Cu from tap water samples for subsequent quantification using a distance-based μPAD. While we focused on Cu, the method has broad utility to other types of analytes.[39] Once captured, the Cu was extracted from the disk with 100 μL of acid and eluted onto a distance-based μPAD for direct quantification. Using this approach, a detection limit of 20 ppb was achieved, approximately two orders of magnitude lower than methods without preconcentration. Finally, Cu levels were measured in drinking water from multiple sites and gave good agreement for paired samples analyzed by ICP-MS.

Experimental Methods

Chemicals

Ultrapure water (18.2 MΩcm) from a Mill-Q system was used for the preparation of solutions and cleaning of supplies and equipment (Merck Millipore, Darmstadt, Germany). Analytical-grade chemical reagents were used. Copper(II) sulfate pentahydrate, dithiooxamide (98.5%), and hydroxylamine hydrochloride were purchased from Sigma-Aldrich (St. Louis, MO, USA). Sodium acetate, nitric acid, sodium hydroxide, glacial acetic acid, and isopropanol were obtained from Fisher Scientific (Pittsburgh, PA, USA).

μPAD Fabrication

The distance-based μPAD design[40] and dithiooxamide Cu detection ink reported by Cate et. al.[28] were leveraged in this work. The μPAD was created on Whatman (grade 4) filter paper (GE Healthcare Bio-Sciences, Pittsburgh, PA, USA) using a red wax barrier to enhance visibility of the colorimetric product. The distance-based μPAD design is shown in the supporting materials (Figure A1). In brief, red wax

barriers (46 devices per 8”x11” sheet) were printed on filter paper using a wax printer (Xerox ColorQube 8860). Next, a piezoelectric ink-jet printer (Epson R280) deposited the dithiooxamide reagent along the flow channel according to a pre-determined gradient (five printing cycles in all) with more reagent deposited near the sample addition zone and decreasing amounts of reagent along the detection zone. The reagent gradient improves the linear response by offsetting the Lucas-Washburn[41] capillary flow as found by Cate et. al.[28] For this work, dithiooxamide was printed as two gradients (Figure A1) in series. At the midpoint of the detection zone a second identical gradient was started; this second gradient provided a visible warning indication for the presence of high Cu concentrations (Figure A1). After printing, a 350 nL aliquot of 10%(w/w) hydroxylamine was pipetted onto the pretreatment zone. Next, the Whatman paper was placed inside a lamination sheet and passed through a laminator (Apache AL13P) six times at 340°F to melt the wax through the paper and to seal the device. The wax barrier and the plastic laminate sheets provide hydrophobic barriers to confine the sample flow within the channel and to prevent evaporation during analysis. A 3 mm hole was then punched into each device to form a sample addition zone; clear packing tape was applied to the underside of each hole creating a small reservoir for sample addition.

Preconcentration and µPAD Analysis

The sample workflow for analysis of Cu is depicted in Figure 2-2. Standard solutions prepared from analytic reagents were used to calibrate the method.

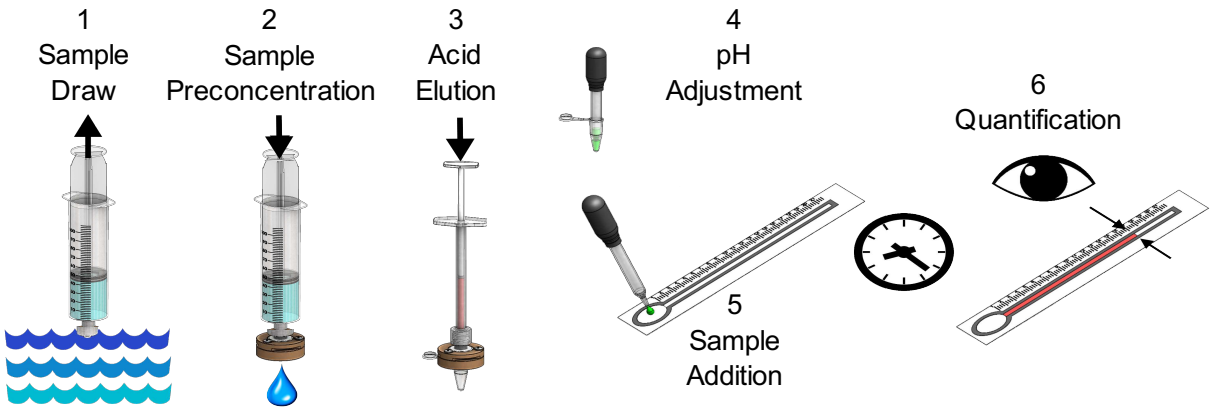

Figure 2-2: Schematic for sample collection, preconcentration, and µPAD analysis in six steps: 1) Sample water is drawn into a syringe, 2) Sample water is passed through an Empore™ chelation disk for

metal capture, 3) A drop of acid is passed through the Empore™ chelation disk, releasing the metal ions back into solution and depositing them into a micro-centrifuge tube containing pre-mixed amounts of base and buffer, 4) A pH adjusted aliquot is pulled from the centrifuge tube 5) The aliquot is added to the distance-based μPAD, 6) After 30 min (once the sample has fully been wicked along the length of the μPAD), the color formation distance is read to determine the sample concentration.

Sample Preconcentration

Initial development of the preconcentration technique leveraged work by Gazda et. al.,[36] which used a polystyrene-divinylbenzene Empore™ solid-phase extraction Chelation disk (3M) housed in a 13 mm Millipore Swinnex filter holder; however, modifications were made to optimize this technique. We used computer-aided design software (SolidWorks® ANSYS, Inc., Canonsburg, PA, USA) and rapid-prototype machining to develop a holder that is chemically resistant (made from Sabic Ultem 1000 thermoplastic) and thus, reusable with 10 mm chelation disks. Head space for the chelation disk was integrated into the upper portion of the filter holder to accommodate the swelling that occurs when the disk is wetted; this feature reduces the amount of backpressure during preconcentration (Figure 2-2 step 2). Drain manifold tracks were added to the lower portion of the filter holder and a polyether ether ketone (PEEK) mesh was used to eliminate blockage of the outlet of the filter cartridge. As a result, the holder allows for a high acid extraction efficiency (Figure 2-2, step 3) with a minimal acid wash volume. The final preconcentration design consisted of a 10 mm punch of solid-phase extraction chelation disk (3M) paired with a 10 mm punch of fine woven PEEK mesh which were placed inside the custom holder (Figure 2-3).

Copper was adsorbed to the disk by passing a 30-mL aqueous sample through the Empore™ chelation disk by hand with a disposable syringe. Each 30-mL sample required approximately five minutes to complete the preconcentration (Figure 2-2, steps 1-3). Most of that time was attributed to the sample preconcentration (Figure 2-2, step 2) due to the limited flow rate of the chelation disk; estimated flow rates were comparable to the 3M documentation (<10 $minL^{-1}$).[42] Next, 100 μL of 3M nitric acid was pushed through the disk and eluent was collected in a 0.2 mL centrifuge tube that is snapped onto the outlet of the custom filter holder. A pH of 4.0 is ideal for the Cu-dithiooxamide color formation to avoid interference

from Ni and Co.[28, 43, 44] The eluent was adjusted to a pH of 4.0 with 40 µL of 4M sodium hydroxide pipetted into the centrifuge tube prior to the acid wash. After the acid wash, a 20 µL aliquot of 6.3M sodium acetate buffer was added and the centrifuged tube was then shaken to mix the contents.

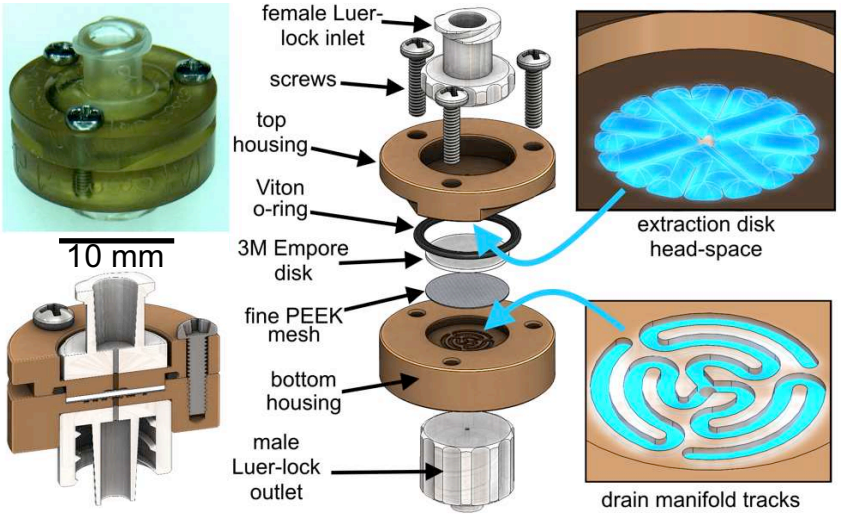

Figure 2-3: Design schematic for solid-phase extraction/preconcentration using a 3M Empore™ chelation disk.

µPAD Analysis

Following preconcentration, an aliquot of buffered eluent was transferred from the centrifuge tube and placed in the sample well of the distance-based µPAD via pipette. Aliquots of 5, 10, and 20 µL were taken for select, high-concentration samples to evaluate the effects of sample dilution. If a 5 or 10 µL aliquot was transferred from the preconcentrated solution, a 15 or 10 µL aliquot of deionized water was added via pipette to the sample well to create a final volume of 20 µL to be analyzed by the µPAD. The 20 µL aliquot required approximately 30 min to wick the full length (56 mm) of the µPAD detection zone. Once dried, the distance of the most downstream tip of color formation along the µPAD was measured using a ruler to the nearest millimeter. The limit of detection was determined as the color band that precipitated a minimum of 1 mm from the beginning of the detection channel, per the definition used by Cate et. al.[28] Additionally, each µPAD was scanned (Xerox DocuMate 3220 Scanner, color photo setting, 600 dpi resolution) and the length of the dark grey/black color formation was measured using ImageJ software (NIH). The ImageJ

measurements are the values reported in this work; however, the use of the ruler-based measurements would not have substantially impacted the accuracy or the results presented per findings by Cate et. al.[28]

Preconcentration and µPAD Calibrations.

The concentration of the aliquot tested via the µPAD can be adjusted by either varying the amount of sample volume passed through the Empore™ disk or the aliquot volume pulled from the preconcentration centrifuge tube. The metric to relate the aliquot concentration to the original sample is called the preconcentration factor and is defined in Equation A1. The preconcentration factor may be impacted by variability in the Empore™ disk capture and elution efficiencies; this work assumed these to be unity based on preliminary tests (Figure A2, Table A1, Table A2).

To improve Cu detection sensitivity, the linear range was sacrificed by reducing the number of print passes and modifying the gradient as reported by Cate et. al.[28] A log-linear calibration curve was generated with Cu standard solutions (25-500 ppm) and is shown Figure A3 with the supporting data displayed Table A3. The calibration was generated with data points taken from independent batches of µPAD printings to test the reproducibility of the method (Table A3). Preconcentrated samples were analyzed using the aforementioned calibration curve with the sample water concentrations determined by scaling the results (x-axis) according to the preconcentration factor. Three preconcentration factors were tested in this work: 47, 94, and 188×. These preconcentration factors were achieved using a 30 mL sample volume and either 5, 10, or 20 µL aliquot draws for µPAD analysis (15 or 10 µL aliquots of DI water were added to the 5 and 10 µL draws).

Drinking Water Analysis.

Per EPA's requirement for tap water testing for Cu (40 CFR 141.86(a)), first-draw tap water samples were collected in 500 mL, wide-mouth bottles (Thermo Scientific Nalgene HDPE); 20 samples were drawn on the same day from different buildings around the Colorado State University campus and 14 samples were drawn that same week in August 2015 by volunteers from their residences in Fort Collins, Colorado. Each sample was preconcentrated, and three aliquots from each preconcentrated sample were analyzed for Cu concentrations using the method described above. All 34 water samples were validated by inductively

coupled plasma mass spectrometry (ICP-MS) according to the method provided in the Chapter 2 Appendix. Data analyses were conducted using R 3.4.1 (R Core Team, Vienna, Austria) and ggmap[45] was used to display the spatial distribution of the water samples collected and analyzed.

Results and Discussion

Standard Copper Solution Calibrations

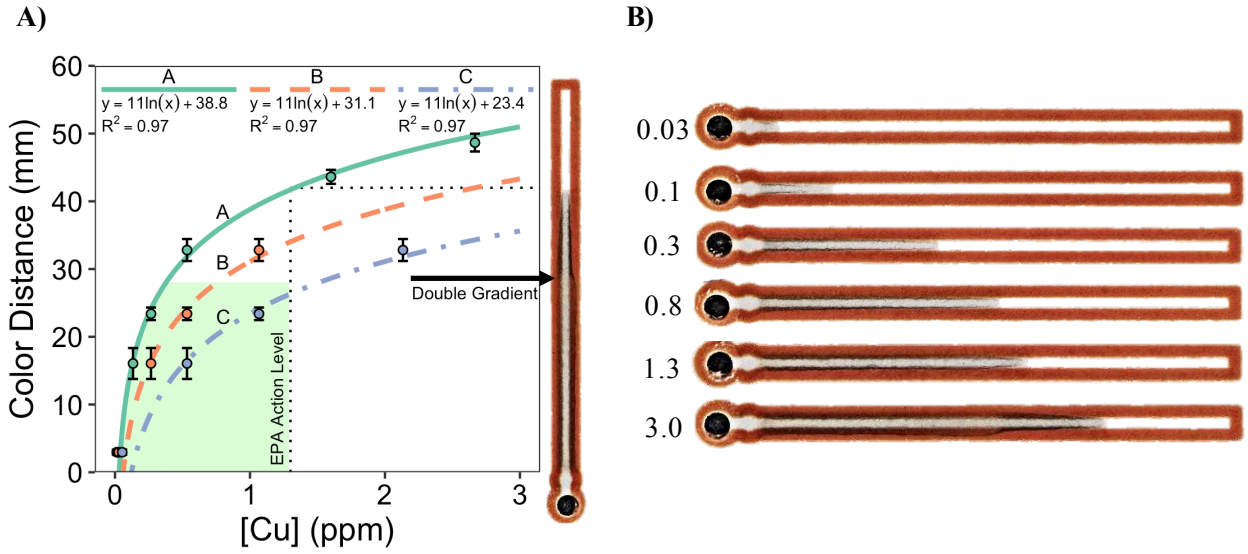

Figure 2-4: A) µPAD calibration curves for standard Cu solutions preconcentrated by 188, 94, and 47×. (A) 20 µL aliquot, 188×; (B) 10 µL aliquot+5 µL DI H_2O, 94×; (C) 5 µL aliquot+15 µL DI H_2O, 47×. A solution with a concentration at the EPA Action Level (1.3 ppm Cu) was evaluated with the 20 µL aliquot,188× preconcentration/µPAD method and is shown to the right of the calibration curves. The location of the double gradient (Figure A1) on the µPAD (28 mm) is marked by the arrow. The region where the µPAD can reliably quantify Cu in water is highlighted in green**. B)** Examples of Cu concentrations ranging from 0.03 to 3.0 ppm using a 188× preconcentration factor.

Calibration curves for preconcentration factors of 188, 94, and 47× are shown in Figure 2-4A (A to C), respectively. The primary calibration curve with the highest preconcentration factor (188×; Figure 2-4A) used a 20 µL aliquot transferred from the centrifuge tube to the µPAD. Shown next to the plot is an image of a µPAD result for a sample containing 1.3 ppm Cu (the EPA action limit) that was analyzed with a 20

µL aliquot at a preconcentration factor of188×. Examples for Cu concentrations ranging from 0.03 to 3.0 ppm using a 188× preconcentration factor are shown in Figure 2-4B.

Water Samples.

Measured copper concentrations (mean ± one standard deviation) using the µPAD technique with a 20 µL preconcentration aliquot (n=34 samples) are compared to the ICP method (Table A5-Table A8) in Figure 2-5.

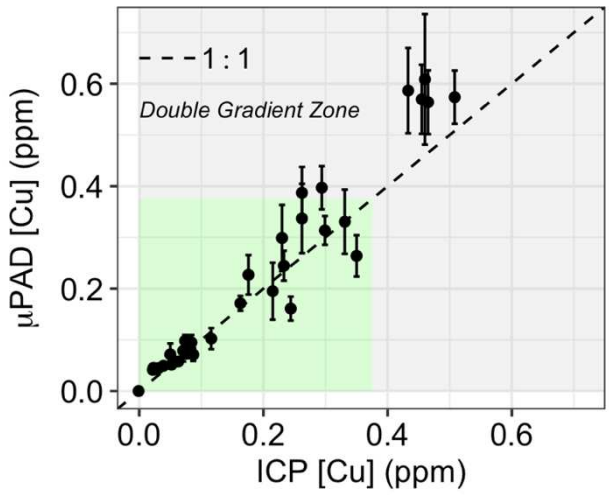

Figure 2-5: Comparison of 20 µL aliquot,188× preconcentration µPAD and ICP methods for trace Cu detection in drinking water (one-to-one line denoted by the dashed line). Double gradient starts at 0.375 ppm as denoted by the grey shaded region.

The results demonstrate the ability to quantify Cu in tap water within 30% of the reference technique. In general, samples with a concentration less than 0.375 ppm (point where the double gradient starts) had good agreement (R^2=0.84, slope = 0.88, intercept = 0.007), lower variability, and lower bias between the preconcentration-µPAD method and the ICP analysis (RMSE = 45 ppb). Above 0.375 ppm, the µPAD results demonstrate an increased positive bias (RMSE = 120 ppb) and increased variability, as shown in Figure 2-5 and Figure A1. The µPAD variability appears heteroscedastic, as shown by the increase of the standard deviation with respect to increasing Cu concentration. The heteroscedastic nature of distance-based error in µPADs was first reported by Cate et. al.[28] and was subsequently explained by Noblitt et. al.[46]

Only one sample (P15) contained Cu levels that were below the detection limits for both preconcentration-μPAD (20 ppb) and ICP (0.19 ppb) methods.

The five samples with concentration greater than 0.375 ppm were re-analyzed using 10 μL (94×) and 5 μL (47×) aliquot volumes to demonstrate the ability to improve the preconcentration-μPAD estimates by diluting the preconcentration eluent and thus reducing the color formation distance. This approach reduced the error and bias associated with these five samples, as shown in Figure 2-6, by limiting the color formation distance to less than the double gradient distance. For reporting, if increased accuracy would be needed the use of the 5 μL (47×) aliquot preconcentration results would be recommended due to the reduced error and bias. The increased bias induced by the double gradient may be caused by the change in flow due to a sharp increase in color formation product.

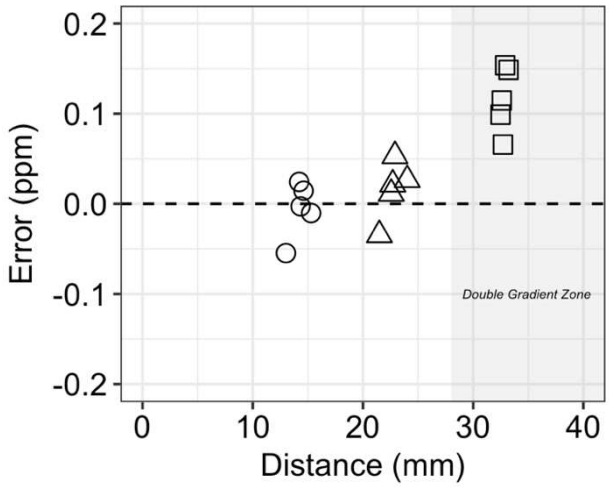

Figure 2-6: Difference in Cu concentrations (ppm) between μPAD and ICP methods for the five samples (C04, C09, C10, C16, C17) that had greater than 0.375 ppm Cu. Circles represent 5 μL aliquots (47× preconcentration factor); triangles represent 10 μL (94×); squares represent 20 μL (188×).

The distribution of the samples across Fort Collins and the Colorado State University campus are shown on the maps in Figure 2-7. The 34 samples spanned Cu concentrations from below the detection limit (20 ppb) to 508 ppb, thus demonstrating that this method can cover a wide dynamic range. The samples collected from the Colorado State University campus had higher 90th percentile Cu concentrations (460 ppb, n = 20) than surrounding residential areas (110 ppb, n = 14). The measured concentrations in this work

are similar to the 90th percentile values reported for the Colorado State University Main Campus (514 ppb, n = N/A)[47] and the City of Fort Collins (80 ppb, n = 52).[48] The highest Cu concentrations (>400 ppb, n=5) were found in some of the oldest buildings on campus are shown in Figure 2-7 (orange/red dots), and are likely the result of old infrastructure and/or pipe corrosion.

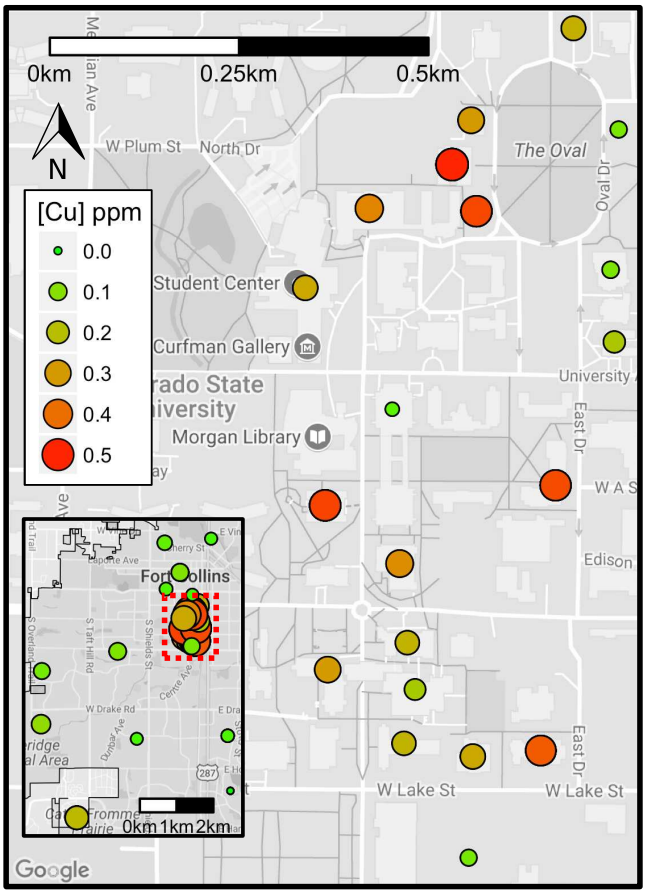

Figure 2-7: Cu concentrations by sample location. Inset shows all samples collected across Fort Collins (n=33) in August of 2015. The Colorado State University main campus is enclosed with the red dotted lines on the inset, and the samples (n=19) collected there are displayed on the main map. Maps were generated with the ggmap[45] library using R 3.4.1 (R Core Team, Vienna, Austria).

Implications for Metal Detection in Water Sources

A preconcentration technique coupled with a distance-based μPAD with minimal equipment requirements has been developed. This new method can be used for quantitative detection of Cu at parts-per-billion levels in water and has been validated against ICP-MS. Although both qualitative and

quantitative colorimetric kits for Cu detection are commercially available (in addition to aforementioned laboratory methods), the distance-based measurement described here offers several key advantages. For example, distance-based detection is more precise than existing low-cost methods that rely on color chart comparisons.[49] Although a single measurement is limited to a smaller range of concentrations (e.g. 20-375 ppb when using a 188× preconcentration factor), one can adapt the method to measure a wide range of Cu concentrations (from approximately 20 to 500,000 ppb) by adjusting the volume of sample that is preconcentrated and/or adjusting the aliquot volume that is added to the μPAD.

The implementation of a second gradient along the μPAD detection region provides a warning indicator that the optimal detection range has been exceeded (Figure 2-4); this line also may be used to alert a user that Cu concentrations have reached or exceeded action limits. Finally, the output from the μPAD can be easily captured using a smartphone for long-term data storage, the advantages of which have been described in a number of reports.[50-58] A phone application similar to these could be developed to measure the length of the color formation and automatically report that data back to a central data server. Adding this functionality would allow the image/results to be quickly relayed back to a central location.

There are several limitations worth noting. 1) The color formation produced by the Cu-dithiooxamide complex is relatively faint especially when Cu concentrations are low (Figure 2-4). The use of another complexing reagent with higher molar absorptivity would improve readability. Bathocuproine has been successfully used in μPADs for the detection of Cu;[24] however, the development of a bathocuproine ink compatible with an ink-jet printer has yet to be developed. Silver nanoparticles (AgNP) have been used with traditional μPADs to detect ppb levels of Cu.[25] The use of AgNP could be a potential candidate for future work and improve the sensitivity of the method; however, deposition of the AgNP on the μPAD and immobilization of the Cu-AgNP complex would need to be considered. Recent work has successfully demonstrated the use of Meso-tetrakis(1,2-dimethylpyrazolium-4-yl)porphyrin sulfonate (TDMPzP), a water-soluble porphyrin derivative for Cu detection using a distance-based μPAD.[29] The TDMPzP ligand provides a very visible response to Cu and future work will likely try to couple this μPAD motif with the preconcentration technique to quantify ppb Cu in water. 2) The distance-based μPAD demonstrated in this

work required 30 minutes to complete sample wicking and color formation. The Cu-TDMPzP color formation will help reduce the quantification time by providing a distinct color formation. Work is also underway to reduce the time to transport the sample aliquot along the length of the μPAD measurement zone. 3) Currently Cu is the only analyte that has been evaluated with this method; however, there is potential to extend this method to other metals. For example, colorimetric reagents have been described for arsenic,[59] chromium,[18] nitrate/nitrite,[60] and lead,[38] all of which are regulated in drinking water by the U.S. Environmental Protection Agency.

The preconcentration-μPAD system has the potential to provide water quality experts, technicians, and other stakeholders with a tool that can provide quick and inexpensive analysis of a large number of water samples. This method will not eliminate the need for standard laboratory sample analysis; however, this method can be used for the identification of a pollutant source in a river section, provide spatial-temporal feedback during accidental events (similar to the Gold King Mine incident), or provide municipalities with a cost-effective means to implement a monitoring network without a substantial investment of resources.

REFERENCES

1. Quinn, C. W.; Cate, D. M.; Miller-Lionberg, D. D.; Reilly III, T.; Volckens, J.; Henry, C. S., Solid-Phase Extraction Coupled to a Paper-Based Technique for Trace Copper Detection in Drinking Water. *Environmental science & technology* **2018,** *52*, (6), 3567-3573.
2. Butler, L. J.; Scammell, M. K.; Benson, E. B., The Flint, Michigan, Water Crisis: A Case Study in Regulatory Failure and Environmental Injustice. *Environmental Justice* **2016,** *9*, (4), 93-97.
3. Emergency Response to August 2015 Release from Gold King Mine. http://www.epa.gov/goldkingmine (Jan. 2018).
4. Bellinger, D. C., Lead Contamination in Flint — An Abject Failure to Protect Public Health. *New England Journal of Medicine* **2016,** *374*, (12), 1101-1103.
5. Rodriguez-Freire, L.; Avasarala, S.; Ali, A.-M. S.; Agnew, D.; Hoover, J. H.; Artyushkova, K.; Latta, D. E.; Peterson, E. J.; Lewis, J.; Crossey, L. J.; Brearley, A. J.; Cerrato, J. M., Post Gold King Mine Spill Investigation of Metal Stability in Water and Sediments of the Animas River Watershed. *Environmental Science & Technology* **2016,** *50*, (21), 11539-11548.
6. Rutt, R. L.; Bluwstein, J., Quests for Justice and Mechanisms of Suppression in Flint, Michigan. *Environmental Justice* **2017,** *10*, (2), 27-35.
7. *Drinking Water Action Plan*; United States Environmental Protection Agency: Washington D.C., **2016**.
8. Scully, J. R., The Corrosion Crisis in Flint, Michigan: A Call for Improvements in Technology. *The Bridge of the National Academy of Engineering* **2016,** *46*, (2), 9-29.
9. Cate, D. M.; Adkins, J. A.; Mettakoonpitak, J.; Henry, C. S., Recent developments in paper-based microfluidic devices. *Anal Chem* **2015,** *87*, (1), 19-41.
10. Yang, Y.; Noviana, E.; Nguyen, M. P.; Geiss, B. J.; Dandy, D. S.; Henry, C. S., Paper-Based Microfluidic Devices: Emerging Themes and Applications. *Analytical Chemistry* **2017,** *89*, (1), 71-91.
11. Yetisen, A. K.; Akram, M. S.; Lowe, C. R., Paper-based microfluidic point-of-care diagnostic devices. *Lab on a chip* **2013,** *13*, (12), 2210-51.
12. Meredith, N. A.; Quinn, C.; Cate, D. M.; Reilly, T. H., 3rd; Volckens, J.; Henry, C. S., Paper-based analytical devices for environmental analysis. *Analyst* **2016,** *141*, (6), 1874-87.
13. Council, N. R., *Copper in Drinking Water*. The National Academies Press: Washington, DC, **2000**; p 162.
14. Dorsey, A.; Ingerman, L., *Toxicological Profile for Copper*; United States Department of Health and Human Services: Atlanta, GA, **2004**.
15. Lead and Copper Rule. https://www.epa.gov/dwreginfo/lead-and-copper-rule (Jan. 2018).
16. Aquatic Life Criteria. https://www.epa.gov/wqc/national-recommended-water-quality-criteria-aquatic-life-criteria-table (Jan. 2018).
17. Drinking Water Contaminants. http://water.epa.gov/drink/contaminants/ (Jan. 2018).
18. Cate, D. M.; Nanthasurasak, P.; Riwkulkajorn, P.; L'Orange, C.; Henry, C. S.; Volckens, J., Rapid Detection of Transition Metals in Welding Fumes Using Paper-Based Analytical Devices. *Annals of occupational hygiene* **2014,** *58*, (4), 413-423.
19. Chaiyo, S.; Siangproh, W.; Apilux, A.; Chailapakul, O., Highly selective and sensitive paper-based colorimetric sensor using thiosulfate catalytic etching of silver nanoplates for trace determination of copper ions. *Analytica chimica acta* **2015,** *866*, 75-83.
20. Hossain, S. Z.; Brennan, J. D., β-Galactosidase-based colorimetric paper sensor for determination of heavy metals. *Analytical chemistry* **2011,** *83*, (22), 8772-8778.
21. Jayawardane, B. M.; Cattrall, R. W.; Kolev, S. D., The use of a polymer inclusion membrane in a paper-based sensor for the selective determination of Cu (II). *Analytica chimica acta* **2013,** *803*, 106-112.
22. Li, M.; Cao, R.; Nilghaz, A.; Guan, L.; Zhang, X.; Shen, W., "Periodic-Table-Style" Paper Device for Monitoring Heavy Metals in Water. *Analytical chemistry* **2015,** *87*, (5), 2555-2559.

23. Liu, L.; Lin, H., Paper-Based Colorimetric Array Test Strip for Selective and Semiquantitative Multi-Ion Analysis: Simultaneous Detection of Hg2+, Ag+, and Cu2+. *Analytical Chemistry* **2014,** *86*, (17), 8829-8834.
24. Mentele, M. M.; Cunningham, J.; Koehler, K.; Volckens, J.; Henry, C. S., Microfluidic paper-based analytical device for particulate metals. *Anal Chem* **2012,** *84*, (10), 4474-80.
25. Ratnarathorn, N.; Chailapakul, O.; Henry, C. S.; Dungchai, W., Simple silver nanoparticle colorimetric sensing for copper by paper-based devices. *Talanta* **2012,** *99*, 552-557.
26. Rattanarat, P.; Dungchai, W.; Cate, D.; Volckens, J.; Chailapakul, O.; Henry, C. S., Multilayer paper-based device for colorimetric and electrochemical quantification of metals. *Analytical chemistry* **2014,** *86*, (7), 3555-3562.
27. Sadollahkhani, A.; Hatamie, A.; Nur, O.; Willander, M.; Zargar, B.; Kazeminezhad, I., Colorimetric disposable paper coated with ZnO@ ZnS core–shell nanoparticles for detection of copper ions in aqueous solutions. *ACS applied materials & interfaces* **2014,** *6*, (20), 17694-17701.
28. Cate, D. M.; Noblitt, S. D.; Volckens, J.; Henry, C. S., Multiplexed paper analytical device for quantification of metals using distance-based detection. *Lab on a Chip* **2015,** *15*, (13), 2808-2818.
29. Pratiwi, R.; Nguyen, M. P.; Ibrahim, S.; Yoshioka, N.; Henry, C. S.; Tjahjono, D. H., A selective distance-based paper analytical device for copper(II) determination using a porphyrin derivative. *Talanta* **2017,** *174*, 493-499.
30. Baytak, S.; Kasumov, V. T., Preconcentration and Determination of Copper (II) by Novel Solid-Phase Extraction and High-Resolution Continuum Source Flame Atomic Absorption Spectrometry. *Analytical Letters* **2017,** *50*, (1), 105-116.
31. Díaz-de Alba, M.; Galindo-Riaño, M. D.; García-Vargas, M., Solid phase extraction of copper traces using poly(styrene-divinylbenzene) membrane disks modified with pyridoxal salicyloylhydrazone in water samples. *Talanta* **2012,** *100*, 432-438.
32. Saxena, R.; Meena, P. L.; Tiwari, S., Determination of copper in industrial water by innovative flow injection flame atomic absorption spectrometry. *Instrumentation Science & Technology* **2016,** *44*, (2), 210-222.
33. Abe, W.; Isaka, S.; Koike, Y.; Nakano, K.; Fujita, K.; Nakamura, T., X-ray fluorescence analysis of trace metals in environmental water using preconcentration with an iminodiacetate extraction disk. *X-Ray Spectrometry* **2006,** *35*, (3), 184-189.
34. Hou, X.; Peters, H. L.; Yang, Z.; Wagner, K. A.; Batchelor, J. D.; Daniel, M. M.; Jones, B. T., Determination of trace metals in drinking water using solid-phase extraction disks and X-ray fluorescence spectrometry. *Applied spectroscopy* **2003,** *57*, (3), 338-342.
35. Fritz, J. S.; Arena, M. P.; Steiner, S. A.; Porter, M. D., Rapid determination of ions by combined solid-phase extraction–diffuse reflectance spectroscopy. *Journal of Chromatography A* **2003,** *997*, (1), 41-50.
36. Gazda, D. B.; Fritz, J. S.; Porter, M. D., Determination of nickel (II) as the nickel dimethylglyoxime complex using colorimetric solid phase extraction. *Analytica Chimica Acta* **2004,** *508*, (1), 53-59.
37. Gazda, D. B.; Fritz, J. S.; Porter, M. D., Multiplexed colorimetric solid-phase extraction: determination of silver (I), nickel (II), and sample pH. *Analytical chemistry* **2004,** *76*, (16), 4881-4887.
38. Satarpai, T.; Shiowatana, J.; Siripinyanond, A., Paper-based analytical device for sampling, on-site preconcentration and detection of ppb lead in water. *Talanta* **2016,** *154*, 504-510.
39. Souza-Silva, É. A.; Jiang, R.; Rodríguez-Lafuente, A.; Gionfriddo, E.; Pawliszyn, J., A critical review of the state of the art of solid-phase microextraction of complex matrices I. Environmental analysis. *TrAC Trends in Analytical Chemistry* **2015,** *71*, 224-235.
40. Cate, D. M.; Dungchai, W.; Cunningham, J. C.; Volckens, J.; Henry, C. S., Simple, distance-based measurement for paper analytical devices. *Lab on a Chip* **2013,** *13*, (12), 2397-2404.
41. Washburn, E. W., *Phys. Rev* **1921,** *17*, 273.
42. *Empore™ Solid Phase Extraction Disks - Technical Information*; Chelating - 6208HB 98-0504-1677-9; 3M: Eagan, MN, **2009**.
43. Jacobs, W. D.; H. Yoe, J., Simultaneous spectrophotometric determination of traces of cobalt, nickel and copper with dithio-oxamide. *Analytica Chimica Acta* **1959,** *20*, 332-339.

44. Soylak, M.; Erdogan, N. D., Copper (II)–rubeanic acid coprecipitation system for separation–preconcentration of trace metal ions in environmental samples for their flame atomic absorption spectrometric determinations. *Journal of hazardous materials* **2006,** *137*, (2), 1035-1041.
45. Kahle, D.; Wickham, H., ggmap: Spatial Visualization with ggplot2. *R Journal* **2013,** *5*, (1).
46. Noblitt, S. D.; Berg, K. E.; Cate, D. M.; Henry, C. S., Characterizing nonconstant instrumental variance in emerging miniaturized analytical techniques. *Analytica Chimica Acta* **2016,** *915*, 64-73.
47. *2016 Drinking Water Quality Report For Calendar Year 2015*; Colorado State University: Fort Collins, CO, **2016**.
48. *2016 Drinking Water Quality Report For Calendar Year 2015* City of Fort Collins: Fort Collins, CO, **2016**.
49. HACH, Copper Color Disc, 0-4 mg/L. https://www.hach.com/copper-color-disc-0-4-mg-l/product?id=8276546107 (Jan. 2018).
50. Chang, B.-Y., Smartphone-based Chemistry Instrumentation: Digitization of Colorimetric Measurements. *Bulletin of the Korean Chemical Society* **2012,** *33*, (2), 549-552.
51. Fronczek, C. F.; San Park, T.; Harshman, D. K.; Nicolini, A. M.; Yoon, J.-Y., Paper microfluidic extraction and direct smartphone-based identification of pathogenic nucleic acids from field and clinical samples. *RSC Advances* **2014,** *4*, (22), 11103-11110.
52. Lopez-Ruiz, N.; Curto, V. F.; Erenas, M. M.; Benito-Lopez, F.; Diamond, D.; Palma, A. J.; Capitan-Vallvey, L. F., Smartphone-based simultaneous pH and nitrite colorimetric determination for paper microfluidic devices. *Anal Chem* **2014,** *86*, (19), 9554-62.
53. Martinez, A. W.; Phillips, S. T.; Carrilho, E.; Thomas III, S. W.; Sindi, H.; Whitesides, G. M., Simple telemedicine for developing regions: camera phones and paper-based microfluidic devices for real-time, off-site diagnosis. *Analytical chemistry* **2008,** *80*, (10), 3699-3707.
54. Mudanyali, O.; Dimitrov, S.; Sikora, U.; Padmanabhan, S.; Navruz, I.; Ozcan, A., Integrated rapid-diagnostic-test reader platform on a cellphone. *Lab on a chip* **2012,** *12*, (15), 2678-86.
55. Sicard, C.; Glen, C.; Aubie, B.; Wallace, D.; Jahanshahi-Anbuhi, S.; Pennings, K.; Daigger, G. T.; Pelton, R.; Brennan, J. D.; Filipe, C. D., Tools for water quality monitoring and mapping using paper-based sensors and cell phones. *Water research* **2015,** *70*, 360-369.
56. Thom, N. K.; Lewis, G. G.; Yeung, K.; Phillips, S. T., Quantitative Fluorescence Assays Using a Self-Powered Paper-Based Microfluidic Device and a Camera-Equipped Cellular Phone. *RSC advances* **2014,** *4*, (3), 1334-1340.
57. Wang, Y.; Ge, L.; Wang, P.; Yan, M.; Yu, J.; Ge, S., A three-dimensional origami-based immuno-biofuel cell for self-powered, low-cost, and sensitive point-of-care testing. *Chemical communications* **2014,** *50*, (16), 1947-9.
58. Yetisen, A. K.; Martinez-Hurtado, J.; Garcia-Melendrez, A.; da Cruz Vasconcellos, F.; Lowe, C. R., A smartphone algorithm with inter-phone repeatability for the analysis of colorimetric tests. *Sensors and Actuators B: Chemical* **2014,** *196*, 156-160.
59. Nath, P.; Arun, R. K.; Chanda, N., A paper based microfluidic device for the detection of arsenic using a gold nanosensor. *RSC Advances* **2014,** *4*, (103), 59558-59561.
60. Jayawardane, B. M.; Wei, S.; McKelvie, I. D.; Kolev, S. D., Microfluidic paper-based analytical device for the determination of nitrite and nitrate. *Anal Chem* **2014,** *86*, (15), 7274-9.

CHAPTER 3: PERSONAL EXPOSURE TO $PM_{2.5}$ BLACK CARBON AND AEROSOL OXIDATIVE POTENTIAL USING AN AUTOMATED MICROENVIRONMENTAL AEROSOL SAMPLER (AMAS)

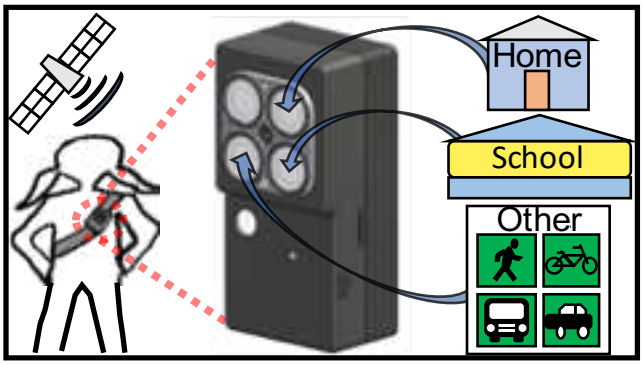

Figure 3-1: An overview of the Automated Microenvironmental Aerosol Sampler (AMAS) functionality.

Chapter Overview

The content of this chapter has been submitted for review to *Environmental Science & Technology* and is reproduced here. Traditional methods for measuring personal exposure to fine particulate matter ($PM_{2.5}$) are cumbersome and lack spatiotemporal resolution; methods that are time-resolved are limited to a single species/component of PM. To address these limitations, we developed an automated microenvironmental aerosol sampler (AMAS), capable of resolving personal exposure by microenvironment. The AMAS is a wearable device that uses a GPS sensor algorithm in conjunction with a custom valve manifold to sample $PM_{2.5}$ onto distinct filter channels to evaluate home, school, and other (e.g., outdoors, in transit, etc.)

exposures. Pilot testing was conducted in Fresno, CA where 25 high-school participants (n=37 sampling events) wore an AMAS for 48-hour periods in November 2016. Data from 20 (54%) of the 48-hour samples collected by participants were deemed valid and the filters were analyzed for $PM_{2.5}$ black carbon (BC) using light transmissometry and aerosol oxidative potential (OP) using the dithiothreitol (DTT) assay. The amount of inhaled $PM_{2.5}$ was calculated for each microenvironment to evaluate the health risks associated with exposure. On average, the estimated amount of inhaled $PM_{2.5}$ BC ($\mu g\ day^{-1}$) and OP ($[(\mu M\ min^{-1})\ day^{-1}$) was greatest at home, owing to the proportion of time spent within that microenvironment. Validation of the AMAS demonstrated good relative precision (8.7% among collocated instruments) and a mean absolute error of 22% for BC and 33% for OP when compared to a traditional personal sampling instrument. This work demonstrates the feasibility of new technology designed to quantify personal exposure to $PM_{2.5}$ species within distinct microenvironments.

Introduction

Particulate matter (PM) air pollution is the leading environmental risk factor for global morbidity and mortality.[1] Evidence connecting PM exposure and adverse health effects has been gathered primarily from studies that rely upon fixed, outdoor PM monitoring sites to estimate air pollution exposure.[2-5] Although central-site monitoring is an effective way to estimate population-level exposures, such monitors are largely ineffective at estimating personal exposure, as PM tends to be spatially and temporally heterogeneous and because individuals are frequently moving from one microenvironment (e.g., home, school, other) to the next.[6-10] Thus, studies that use central-site monitors to estimate air pollution effects at the individual level often suffer from exposure misclassification.[11]

More recently, exposure modeling frameworks, such as temporal land-use regression, have been developed to estimate individual exposure on finer spatial and temporal scales.[12-16] These advanced spatiotemporal models, however, also struggle to capture the known variability in individual-level PM exposure.[17-19] Alternatively, personal exposure monitoring (i.e., using a wearable device to measure PM within an individual's breathing zone), represents a direct measure of an individual's exposure to PM.[20, 21]

The use of active-sampling personal monitors also permits the evaluation of PM composition (i.e. black carbon [BC], organic compounds, metals, and aerosol oxidative potential [OP]).[22-24]

Personal sampling technologies, however, have a number of limitations. Traditional personal samplers, for example, collect one time-integrated sample per measurement (i.e., PM is collected onto a single filter substrate); thus, exposure cannot be resolved spatially or temporally.[25] To address this limitation, studies have either paired multiple filter samplers together to resolve exposures by microenvironment[26] or coupled a direct-reading instrument with a global positioning system (GPS) to resolve these exposures with data processing/analyses.[27-29] Though direct-reading instruments can provide time-resolved exposure data, these instruments tend to be expensive (limiting sample size) and often report only levels of a single species (e.g., $PM_{2.5}$ mass or black carbon [BC]).[30-34] Finally, many personal samplers are bulky, noisy, and intrusive leading to low rates of compliance among participants.[34] These limitations highlight a need for personal PM monitors that are inexpensive, wearable, and capable of resolving speciated PM exposures as a function of distinct microenvironments – the goal of this work.

The Automated Microenvironmental Aerosol Sampler (AMAS) is a wearable, active aerosol sampling device containing four separate filter channels. Each filter channel is used to sample fine particulate matter ($PM_{2.5}$) from pre-determined personal microenvironments based on global positioning system (GPS) location. We evaluated the ability of the AMAS to determine personal exposures by microenvironment (home, school, and other) in a pilot study with high school students in Fresno, California. Collected $PM_{2.5}$ filter samples (n=126 microenvironments) were evaluated for both BC[35-37] and OP[38-40] using established methods.

Materials and Methods

Hardware

The AMAS (Figure 3-2, Figure B1, Table B1) was designed to be small enough (105 mm × 51 mm × 56 mm) and light enough (240 g) to be worn by school-aged children (i.e., ages ~7-18 yrs). The AMAS pump and flow-control systems are derived from previous efforts to develop a single-filter $PM_{2.5}$ sampler called the Ultrasonic Personal Aerosol Sampler (UPAS).[41] The UPAS is a wearable, filter-based aerosol

sampler that contains a piezoelectric micropump, a mass flow sensor, and a suite of environmental sensors (temperature, pressure, relative humidity, acceleration, and light). A key feature of the UPAS pump is that it operates at ultrasonic frequency, producing low noise (< 55dB) in a compact form factor.[41] The AMAS is differentiated from the UPAS by the addition of a global navigation satellite system (GNSS CAM-M8Q, Ublox, Thalwil, Switzerland) and a novel, four-channel flow manifold: each channel is comprised of a separate $PM_{2.5}$ cyclone inlet (1.5 L min^{-1} flow rate, Figure B2) and a 15 mm sampling filter. Airflow through each channel is controlled by a custom-designed valve manifold (Figure 3-2B). This manifold contains four miniature planetary gear motors (206-108, Precision Microdrives™, London, UK), each connected to a custom-machined axial valve that lies between the pump manifold and a given inlet. The four valves are actuated independently by a microcontroller algorithm (described below) to allow airflow through a single filter channel on demand.

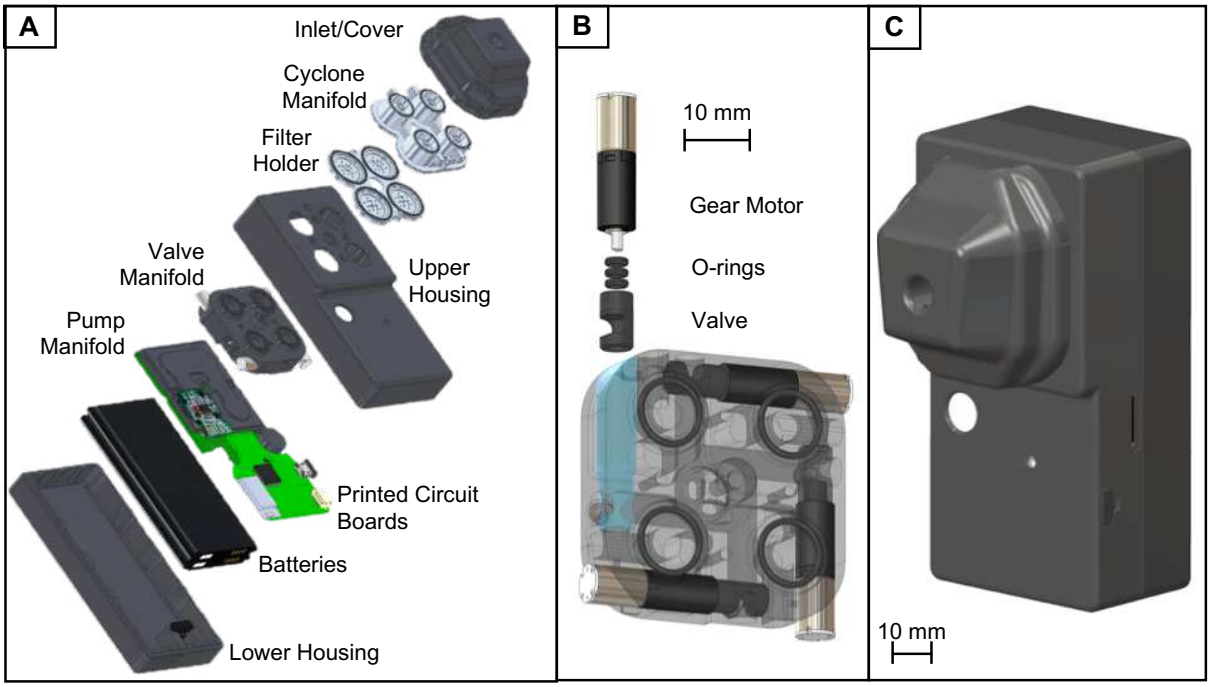

Figure 3-2: AMAS design and hardware. A) Exploded view of all hardware components. B) Partial exploded view of the valve manifold. C) Fully-assembled AMAS prototype.

The inlet manifold consists of a single aluminum filter holder that houses all four filters, integrates the cyclone inlets into a single combined inlet and cover to make the device more aesthetically pleasing, and also contains multidirectional air inlet paths to reduce the possibility of blocked air flow during use. The AMAS is powered by two batteries (SAEBBG900BBU, Samsung, Seoul, South Korea) that can be recharged (even while sampling) via a standard micro-USB connection.

Firmware

The AMAS functionality is controlled with firmware developed for a microcontroller (mbed™; ARM® Ltd., Cambridge, UK) that has been integrated into a printed circuit board (Figure 3-2A). The firmware enables AMAS setup and programing via Bluetooth and in conjunction with a smartphone application (Android[42] and iOS[43] versions; see Figure B3 for screenshots of the app interface). The app allows the user to input microenvironment GPS coordinates, set basic operational settings, and initiate sampling (each of these settings is stored in non-volatile memory). Additionally, the AMAS firmware implements the microenvironmental algorithm, regulates sample volumetric flow rate, and monitors battery life. A multi-color light-emitting diode on the exterior of the upper housing serves as a visual indicator (to the user) about the operational state of the AMAS. A green light indicates normal operation, a blue light is shown while the AMAS is charging, a yellow light is displayed when the battery is under ~20% charge, and the light turns red when the pumps shut down (~10% of battery charge). Shutting the pumps off when the batteries are critically low allows all AMAS sensors (other than the pumping system) to remain operational until the device can be charged. Sensors data are logged to non-volatile memory at 0.2 Hz, with the exception of the total acceleration (square root of the sum of the squares of the three acceleration axes) and light sensor data (ultraviolet, visible, and infrared), which were logged at 1 Hz.

Algorithm

A key element of the AMAS is the ability to detect pre-defined microenvironments in real time and initiate sampling through a designated filter channel. For this study, there were three microenvironments: 1) “home” - a 75 m radius around the central point of the home; 2) “school” - a 100 m radius around the central point of the school; and 3) “other” - anytime the AMAS was not located in either the home or school

microenvironments. Prior to sampling, the GPS coordinates corresponding to the participant's home and school were determined using Google Maps and programmed into the AMAS via the smartphone application. The algorithm could accept two home and two school locations for each participant. In cases where a child spent time in two home locations, these were considered as a single microenvironment (i.e., the samples from both homes were collected on the same filter). The same procedure was applied to the school microenvironment because participating students traveled between two different schools (their primary school and the Center for Advanced Research and Technology [CART], where the participants visited each day and also where they received and returned the AMAS) during the 48-hour sampling period.

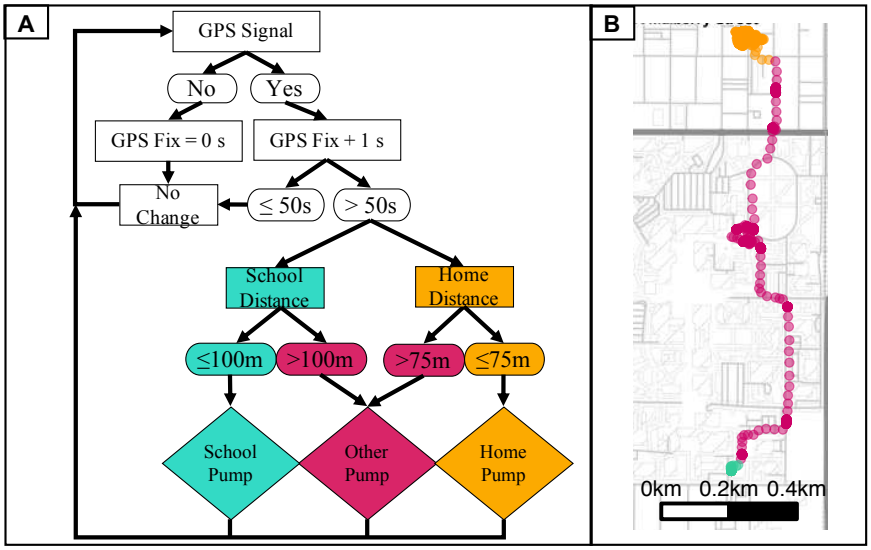

Figure 3-3: AMAS algorithm used to determine the microenvironment location (school, home, or other) and to initiate sample collection into the corresponding filter channel. An example trace is shown to demonstrate home, school, and other microenvironments (orange, green, and red respectively). The map was generated with the ggmap[44] library using R 3.4.1 (R Core Team, Vienna, Austria).

the samples from both homes were collected on the same filter). The same procedure was applied to the school microenvironment because participating students traveled between two different schools (their primary school and the Center for Advanced Research and Technology [CART], where the participants visited each day and also where they received and returned the AMAS) during the 48-hour sampling period.

The microenvironment detection algorithm used logic tied to the on-board GPS to estimate when an individual entered or exited a given microenvironment; the flow chart, shown in Figure 3-3, outlines this algorithm. The first decision point in the algorithm was to determine the presence of a GPS signal. If a signal was detected and had been present for at least 50 s, then the radial distances to the home and school central points were calculated. If the calculated distance was less than 75 m from a home location or less than 100 m from a school location, then the appropriate filter channel (home or school) was activated. If neither a home nor a school microenvironment was detected, the filter channel designated as other was activated. In the cases where no GPS signal was acquired, the last known location was used. If the last known location was >100 m from a school or >75 m from a home microenvironment, the 'other' filter channel was used.

Sample Collection

High school students between the ages of 16 and 18 were recruited from CART in Fresno, CA to evaluate the AMAS. Each student wore the AMAS for a 48-hr monitoring period and students were eligible to participate in the pilot multiple times. All study procedures were approved by the Institutional Review Board at the University of California at Berkeley and participants either provided informed consent or assent with consent from their parent/guardian.

For each 48-hour sample period, five reference samplers were deployed alongside AMAS prototypes (assigned to participants at random) to compare performance. The reference sampler consisted of a backpack containing a traditional personal air sampler with a $PM_{2.5}$ size-selective inlet (PEM 761-203A, SKC, Inc., Eighty Four, PA, USA), a personal sampling pump (BGI OMNI 3000, Mesa Labs, Lakewood, CO, USA), and a 25mm filter cassette (Figure B4). The AMAS filters were cut from Pallflex® Fiberfilm™ (T60A20; Pall Life Sciences, Ann Arbor, MI) sheets using a 15 mm punch. The reference sampler used 25 mm filters cut from Pallflex® Fiberfilm™ sheets (10 of 15) and 25 mm Teflon filters (5 of 15; PT25P-PF03; Measurement Technology Laboratories (MTL), Minneapolis, MN). The backpack filter samples were collected at 4 L min^{-1}, while the AMAS collected filter samples at 1.5 L min^{-1}. Additionally, a research member collocated and transported five AMAS between microenvironments for 48 hours to evaluate

instrument precision. After sampling, filters were sealed in plastic cassettes and stored at -20 °C until they were shipped to Colorado State University and analyzed for BC and OP (within 3 months of sample collection).

AMAS Evaluation

The AMAS battery life, power failure rate, and microenvironment detection algorithm were evaluated as part of the pilot study. Logged readings of AMAS pump and battery status were used to determine the AMAS battery life and power failure rate. The raw GPS data were used to evaluate the microenvironment designations determined with the algorithm for bad transitions (instances where the algorithm detected a home-to-school or school-to-home transition without detecting a transition to the other microenvironment). Additionally, the distances from the home and school microenvironments at the time of a transition from either a home or school to the other microenvironment were analyzed to evaluate the responsiveness of the algorithm.

Black Carbon Analysis

Black carbon loading on each sampling filter was assessed by optical transmissometry at 880 nm (SootScan OT-21, Magee Scientific, Berkeley, CA, USA). Mass absorption cross-sections of 12.2[45] and 9.18[37] $cm^2\ \mu g^{-1}$ were used for the Pallflex® Fiberfilm™ and MTL Teflon filters, respectively, following published data for the differential absorption properties of these filters. The 25 mm filters used a standard filter holder provided by Magee Scientific; however, the 15mm filters required a custom aluminum filter holder. The custom filter holder (Figure B5) was designed with computer-aided design software (SolidWorks® ANSYS, Inc., Canonsburg, PA, USA) and machined specifically for this study. Each filter was scanned twice; once prior to sampling and once after the 48-hour collection period. The Teflon filters were analyzed with a Pallflex® Fiberfilm™ filter underneath (as a light diffuser) per the protocol described by Presler-Jur et al.[37] The BC filter mass, concentrations and daily inhaled mass were calculated using Equation B1, Equation B2, and Equation B3. An inhalation rate of 16.3 $m^3\ day^{-1}$ determined by the U.S. Environmental Protection Agency for 16 to 21 year olds[46] was used in Equation B3 to determine the daily inhaled BC mass for each participant by microenvironment. Laboratory filter blanks (15 mm and 25 mm)

were stored in filter keepers and measured at least once each day that filters were analyzed. These laboratory blanks were used to determine the limit of detection (3× blank standard deviation) for the optical method. For the 15 AMAS/backpack pairs, the cumulative AMAS BC concentration (μg m^{-3}) of the three 15 mm filters (Equation B4) was compared to the corresponding 25mm backpack filter concentration estimate.

Ambient BC measurements were recorded using the 880 nm channel of a Magee Scientific Aethalometer (AE33, Berkeley, CA, USA), which was installed, maintained and monitored by the UCBerkeley-Stanford Children's Environmental Health Center at the California Air Resources Board (CARB) Fresno-Garland monitoring station (Air Quality System [AQS] site 060190011). Hourly BC concentrations reported by the AE33 instrument were used to estimate the mass of BC that would be captured on the AMAS filter if the AMAS had been located at the central site location operating at flow of 1.5 L min^{-1}. Ambient $PM_{2.5}$ concentrations (hourly averages) were also obtained from the AQS website for the month of November, 2016. Data were aggregated to 24-hr averages and compared to the AE33 BC data to determine the mean ambient BC:$PM_{2.5}$ ratio during the study.

Oxidative Potential Analysis

Oxidative potential (OP) is an indicator of increased human health risks from exposure to PM containing reactive oxygen species.[47, 48] The oxidative potential of $PM_{2.5}$ collected on sampling filters was estimated using a dithiothreitol (DTT) assay. The 15 mm filters were first cut in half and the 25 mm filters were quartered with ceramic scissors; the filter half or quarter were used for the DTT analysis. A DTT analysis method (Chapter 3 Appendix for details) similar to the traditional method[49] was used to determine the OP. The four absorbance measurements for each filter sample were used to calculate the consumption rate of DTT. Additionally, laboratory filter blanks were analyzed with this method, and the OP results were adjusted by the mean DTT consumption rate of the laboratory blanks to account for the reactivity contribution of the filter substrate. The OP for the mass collected on the filters, adjusted for air sample volume, and daily inhaled $PM_{2.5}$ were calculated for each microenvironment using Equation B5, Equation B6, Equation B7, and Equation B8. For the 15 AMAS/backpack pairs, the cumulative AMAS OP

concentration (pmol min^{-1} m^{-3}) of the three 15 mm filters (Equation B9) was compared to the corresponding 25mm backpack estimates.

Data Analysis

The Kruskal-Wallis test and pairwise Wilcoxon sign rank were used to test for significant differences between microenvironments for the BC and OP analyses. Deming regressions and root mean square errors were used to evaluate AMAS accuracy. The relative standard deviation of the black carbon analysis for the five collocated AMAS was used to evaluate precision. All data processing and analyses were conducted using R 3.4.1 (R Core Team, Vienna, Austria).

Results and Discussion

AMAS Performance

The AMAS devices were deployed a total of 37 times over the course of the pilot study (15 of which were paired with a reference sampler). An additional five AMAS were collocated on a single backpack by a member of the research team, resulting in 42 AMAS deployments in total (n=126 microenvironmental filters; 15 reference filters). On average, the AMAS battery lasted 14 hours at 1.5 L min^{-1}; however, asking participants to charge the device overnight resulted in most deployments meeting the target run time (48 hours). A total of 88% of AMAS (37 of the 42) logged data for at least 90% of the time (>43.2 hours) and all 37 of those logged for the entire 48-hour period; however, only 71% (30 of the 42) of the AMAS logged and sampled for greater than 90% of the 48-hour period (43.2 hours). Of these, 64% (27 of the 42) sampled and logged for the entire 48-hour period. Two additional deployments had incorrect microenvironment GPS coordinates programmed into the AMAS (the incorrect GPS coordinates were due to user error). Thus 20 deployments (54%) with student participants and the test with five AMAS collocated by a researcher were available for the complete analysis.

All 141 filters (15 reference + 126 AMAS) were analyzed for BC and OP; however, our data analyses for exposures were restricted to AMAS filter samples that were collected by student participants, collected $PM_{2.5}$ and logged data for the entire 48-hr period, had valid microenvironment GPS coordinates, and collected $PM_{2.5}$ for more than an hour (i.e., a sample volume > 0.1 m^3) in each microenvironment (59 of

126). For these 59 valid AMAS filters, the median (25^{th}, 75^{th}%) amount of time spent in the school, home, and other microenvironments as determined by the algorithm were 4.9 (3.9, 5.6) hrs day^{-1}, 15.5 (13.5, 16.4) hrs day^{-1}, and 4.4 (3.4, 5.8) hrs day^{-1}, respectively (

A).

The time sampled in each microenvironment was checked against the raw GPS data to evaluate the performance of the AMAS algorithm. The use of a pre-determined radius about the centroids of the home and school microenvironments (75 and 100 m, respectively) successfully detected the majority of the time when participants were present in these two locations. However, this approach struggled when GPS signal drift was high, when the home microenvironment consisted of larger multi-family dwellings, and because of the large footprint and open-building design (lack of internal hallways) of California high schools. A hypothesis is that the latter reason is why the estimated time spent at school seems lower than anticipated (7-8 hrs per day) and the estimated time spent in the 'other' microenvironment was higher than anticipated. Additionally, the time to acquire a GPS signal (distance from the home and school microenvironments) was another infrequent, but key issue that was observed. An empirical cumulative distribution of the distance (in meters) from the prior microenvironment when the AMAS transitioned to a new microenvironment is shown in Figure B6. This analysis reveals a key issue when relying on GPS data as the primary determinant of microenvironment transition: limited or no satellite connection results in error due to a delayed transition. The limitations of relying solely on the GPS to detect microenvironments was anticipated as this challenge has been discussed in previous studies that have used GPS for microenvironment classification.[19, 27, 28, 50] The reliance of only GPS location for microenvironment classification was merely a starting point for the AMAS development, and improvement of the microenvironment detection algorithm is the subject of ongoing work. For example, further refinement of the GPS settings and the use of other environmental sensors (e.g., ultraviolet light intensity, acceleration, temperature etc.) may help improve the ability to detect a chance in microenvironment when GPS signals are weak.

Black Carbon (BC)

Inhaled BC mass is shown in Figure 3-4B for each of the three microenvironments (BC exposure concentrations are provided in Figure B7). Median (25th, 75th%) levels of inhaled BC mass were 1.6 (1.1, 2.4) µg day^{-1} for school, 5.4 (2.9, 8.2) µg day^{-1} for home, and 2.2 (1.3, 3.1) µg day^{-1} for 'other'. Inhaled BC mass was significantly higher in home versus both school and 'other' microenvironments (pairwise Wilcoxon sign rank; $p<0.001$), even though

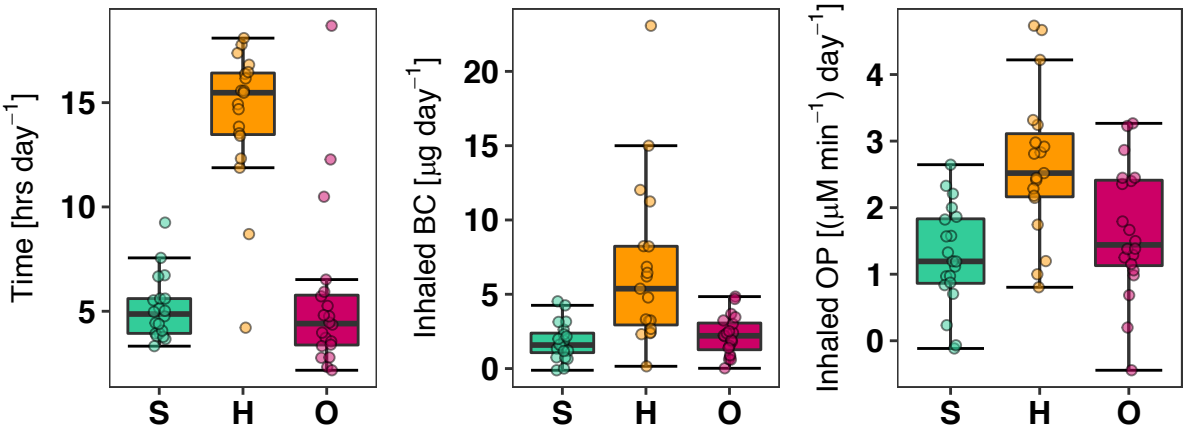

Figure 3-4: Microenvironment exposure results (school = S; home = H; other =O). Data are shown only for AMAS that were collected by participants, sampled the entire 48-hr period, had valid GPS coordinates, and collected PM2.5 for more than an hour (0.1 m3) in each microenvironment (n = 20, 19, 20 for S, H, and O). A) Daily time spent in microenvironments as detected by the algorithm. B) Daily inhaled black carbon mass. C) Daily oxidative potential reactivity of the inhaled PM2.5.

BC exposure concentrations tended to be similar across microenvironments (Kruskal-Wallis Test; $p=0.5$), as shown in Figure B7. This discrepancy is explained by the fact that participants spent the majority of their time (~65%) at home. Accordingly, most home filter samples (18 of 19) exceeded the method limit of detection (LOD) for BC (0.49 µg) as compared to fewer school (9 of 20) and other (12 of 20) filter samples. In addition to reducing algorithm misclassification of the school and other microenvironments (discussed above), another option for increasing sample mass on the school and other filters is to increase the flow through these channels.

Oxidative Potential (OP)

The OP for inhaled $PM_{2.5}$ is shown by microenvironment in

C. Similar to BC, the OP home filters (17 of 19) had the greatest number of filter samples with a measured response, within error, above the blank (0.34 μM min^{-1}) compared to the school (11 of 20) and 'other' filters (15 of 20). Measured OP (25^{th}, 75^{th}%) values were 1.2 (0.8, 1.8) [(μM min^{-1}) day^{-1}] for school, 2.5 (2.2, 3.1) [(μM min^{-1}) day^{-1}] for home, and 1.4 (1.1, 2.4) [(μM min^{-1}) day^{-1}] for other. When normalized to sampled air volume (Figure B14), these OP values are similar to those previously reported for urban, rural, or roadside PM (50-1500 pmol min^{-1} m^{-3}).[40] The inhaled OP for the home microenvironment was significantly greater than the exposure in the school microenvironment (pairwise Wilcoxon sign rank; $p< 0.001$), while there was no significant difference for OP per air sampled volume (Kruskal-Wallis Test; $p=0.07$). Variability in the OP measurement was relatively high, especially for filters that sampled lower air volumes, as shown in Figure B15. Future work should aim to increase the minimum sampled air volume and/or increase assay sensitivity to reduce error in the DTT assay. If future sample collection aimed to collect a minimum sampled mass equal to the BC LOD (0.49 μg), this would equate to 11.2 μg PM mL^{-1} in the DTT assay (based on an estimated ambient BC:PM ratio of 0.04 and a 500 μL dilution volume for the DTT assay), near 10 μg mL^{-1} previously recommended for the DTT assay.[39]

Instrumentation Exposure Comparisons

The BC results for the 15 deployments that had an AMAS paired with a backpack containing a reference sampler are shown in Figure 3-5. The gray bars represent the 48-hour average BC concentration of the 25mm backpack filters. The multi-colored bars represent the BC concentration fraction on each of the three AMAS filters (shown as a summation of the three microenvironments BC mass in μg divided by the total sampled volume for the 48-hour period). The relative difference between the backpack and cumulative AMAS BC concentrations are shown above each paired filter set. A Deming regression (Figure B8) was used to evaluate the 12 pairs with complete 48-hr deployments (excluding three pairs [2, 11, 15] which had backpack pump failures) and demonstrates a moderate correlation ($r = 0.67$) with low bias (22% mean absolute error). In addition, the five filter samples collected for the home microenvironment by the five

collocated AMAS were above the BC LOD and demonstrated a good agreement (Figure B9, Figure B10) for microenvironment BC mass and concentration estimates (relative standard deviation of 8.7 and 8.8% respectively) between AMAS, thus demonstrating AMAS precision. These results suggest that the AMAS can provide similar BC results as a traditional personal aerosol sampler.

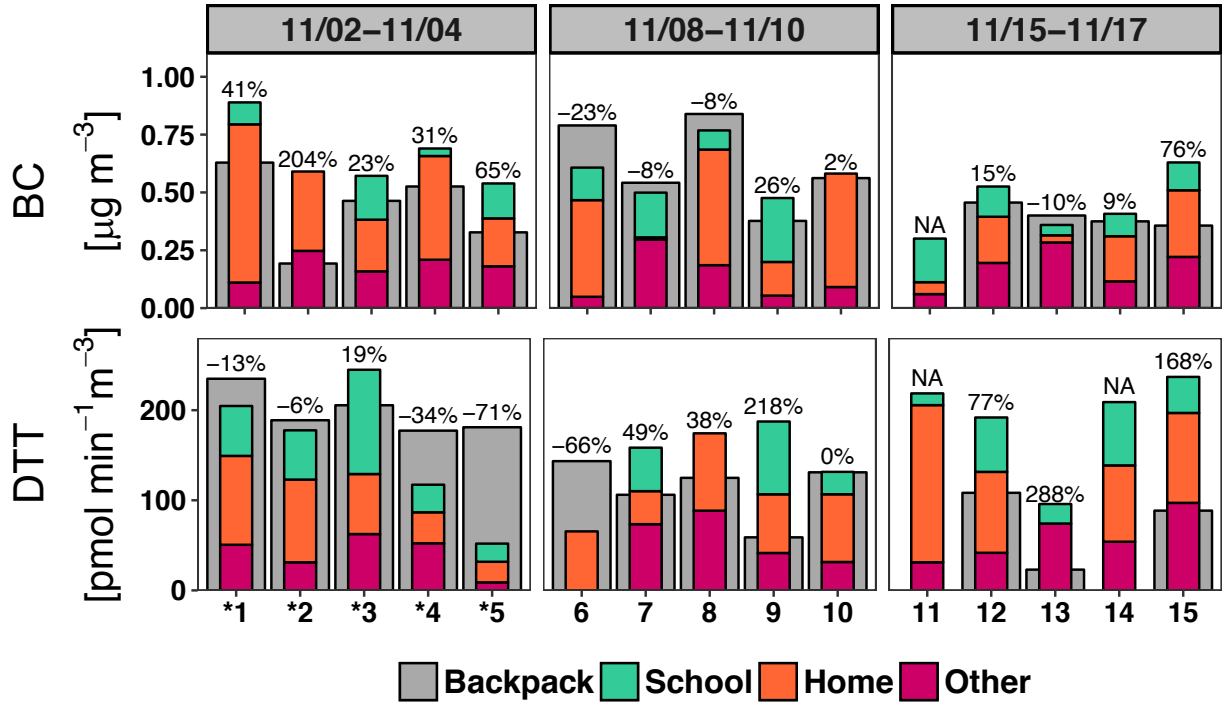

Figure 3-5: Comparison of backpack and AMAS 48-hour concentrations for BC and OP. The percent error between the AMAS cumulative concentration and the backpack concentrations for the 48-hour periods is listed above each bar. Filter pairs 1-5 had MTL Teflon filters for the backpack. All other backpack filters and all AMAS filters were Pallflex® FiberfilmTM.

Following the BC analysis, the OP for the 15 AMAS/backpack pairs were compared (Figure 3-5, Figure B16). The gray bars represent the 48-hour OP of the 25mm backpack filters. The multi-colored bars represent the OP fraction on the AMAS filters (shown as a summation of the three microenvironments OP in μM min^{-1} divided by the total sampled volume for the 48-hour period). In addition to the three backpack deployments that had pump failures, any AMAS or backpack deployment (5, 6, 9, 13, 14) that had a filter with a low OP (< 100 pmol min^{-1} m^{-3}) were excluded from the OP comparisons. The low OP measurements

were removed due to the high variability observed in the DTT assay (see Figure B15) at low levels of OP. The percent difference between the backpack and cumulative AMAS OP concentrations are shown above each set of paired filter data; a mean absolute difference of 33% between the seven backpack and filter pairs was found. A Deming regression (Figure B16) suggested a moderate correlation (r = 0.42) and more bias in the OP measurements as compared to the BC evaluations.

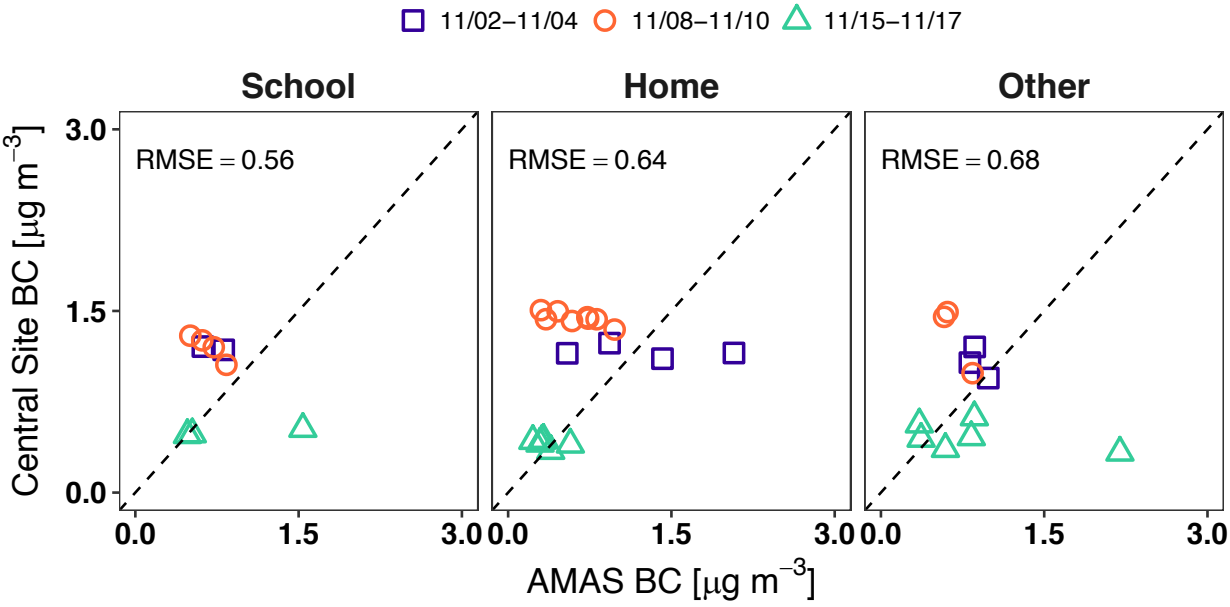

Figure 3-6: Central site BC concentrations compared to AMAS filter BC concentrations by microenvironment. The data shown in the plots include only filter samples from deployments which collected $PM_{2.5}$ and AMAS data for the entire 48-hr period, had valid GPS coordinates, collected $PM_{2.5}$ for more than an hour (0.1 m^3) in each microenvironment, and the BC measurement was above the LOD (0.49 μg) of the Magee Scientific Sootscan measurement (school, n = 9; home, n = 18; other, n = 12). The RMSE is shown in each microenvironment panel and the dashed line is the 1:1 reference line.

We also compared the AMAS BC data to the central site AE33 BC concentration (Figure 3-6) and mass (Figure B11) estimates by microenvironment for each filter from the 20 valid 48-hour deployments with BC measurements above the LOD (0.49 μg). One key item worth noting, particularly in the home microenvironment, is the variability in BC exposures between different participants on a given day. The variability of BC concentration (Figure 3-6, Figure B12) and mass (Figure B11) is accentuated on days with

higher ambient BC. These nuances in the data could indicate exceptional exposure events for some of the participants. An additional item to note, is that a consistent bias between the central site measurements and both the backpack and AMAS filters (Figure B13) was found on the days with higher ambient BC (11/2-1104 and 11/05-11/07). This finding agrees with previous studies that suggests indoor microenvironments generally provide some filtration and thus protection from elevated ambient air pollution exposures[51]. While there is a chance that this finding could be the result of measurement bias, the personal sampling comparison results (Figure 3-6) suggest this is not the case.

Strengths and Limitations

Overall the AMAS showed reasonable agreement with a collocated backpack reference sampler and provided valid BC and OP data by microenvironment for many of the collected filter samples. The participants, in general, were positive about their experience and preferred the AMAS over the backpack reference monitors (based on a user-satisfaction survey; data not shown). Most importantly the AMAS provided the subtle but important differences in personal exposures that would otherwise be ambiguous if an ambient central-site monitors was the only source of exposure information.

There are several limitations worth noting. First, the microenvironment classification tended to perform poorly when the transition distance thresholds were on the same order as the GPS signal drift (~200 m). The GPS signal was often slow to connect after long periods (overnight) of having a low quality or null GPS signal. We plan to modify the GPS settings and incorporate additional algorithm logic to determine if the sampler was in motion and assist in the detection of microenvironment transitions. Second, the battery life was relatively short, lasting only 14 hrs before additional charging was needed. Although compliant participants were often able to maintain the AMAS power for the entire 48-hour sampling period, we plan to add an additional battery to the AMAS to extend operating time between charges. An alternative strategy to extend operating lifetime is to reduce sample flow (i.e., pump power requirements) to 1 L min^{-1} for the home microenvironment; this change, however, may lead to more filter samples below analytic detection limits. Third, the DTT assay would benefit from using a smaller dilution volume than used in this study (500 μL), which may require alternative methods such as a small volume electrochemical assay.[52]

The AMAS has been developed and demonstrated the ability to evaluate an individual's BC and OP within individual microenvironments in Fresno, CA. The AMAS is capable of sampling PM onto filter media in distinct microenvironments, and to our knowledge there is no personal sampler with this capability. The ability of this novel personal sampler to collect PM from microenvironments onto filter media permits speciation of PM by microenvironment; thus, providing a new capability for further investigating the impacts of PM composition on health outcomes. An aerosol monitor capable of sampling in distinct microenvironments will allow exposure scientists and epidemiologists to collect more samples and thus provide better insight into the effect of PM composition on human health.

REFERENCES

1. Cohen, A. J.; Brauer, M.; Burnett, R.; Anderson, H. R.; Frostad, J.; Estep, K.; Balakrishnan, K.; Brunekreef, B.; Dandona, L.; Dandona, R., Estimates and 25-year trends of the global burden of disease attributable to ambient air pollution: an analysis of data from the Global Burden of Diseases Study 2015. *The Lancet* **2017,** *389*, (10082), 1907-1918.
2. Pope III, C. A.; Dockery, D. W., Health effects of fine particulate air pollution: lines that connect. *Journal of the air & waste management association* **2006,** *56*, (6), 709-742.
3. Brook, R. D.; Rajagopalan, S.; Pope, C. A.; Brook, J. R.; Bhatnagar, A.; Diez-Roux, A. V.; Holguin, F.; Hong, Y.; Luepker, R. V.; Mittleman, M. A., Particulate matter air pollution and cardiovascular disease: an update to the scientific statement from the American Heart Association. *Circulation* **2010,** *121*, (21), 2331-2378.
4. Mann, J. K.; Balmes, J. R.; Bruckner, T. A.; Mortimer, K. M.; Margolis, H. G.; Pratt, B.; Hammond, S. K.; Lurmann, F. W.; Tager, I. B., Short-term effects of air pollution on wheeze in asthmatic children in Fresno, California. *Environmental health perspectives* **2010,** *118*, (10), 1497.
5. Peel, J. L.; Tolbert, P. E.; Klein, M.; Metzger, K. B.; Flanders, W. D.; Todd, K.; Mulholland, J. A.; Ryan, P. B.; Frumkin, H., Ambient air pollution and respiratory emergency department visits. *Epidemiology* **2005,** *16*, (2), 164-174.
6. Wilson, J. G.; Kingham, S.; Pearce, J.; Sturman, A. P., A review of intraurban variations in particulate air pollution: Implications for epidemiological research. *Atmospheric Environment* **2005,** *39*, (34), 6444-6462.
7. Branco, P.; Alvim-Ferraz, M.; Martins, F.; Sousa, S., The microenvironmental modelling approach to assess children's exposure to air pollution–A review. *Environmental research* **2014,** *135*, 317-332.
8. Dons, E.; Panis, L. I.; Van Poppel, M.; Theunis, J.; Willems, H.; Torfs, R.; Wets, G., Impact of time–activity patterns on personal exposure to black carbon. *Atmospheric Environment* **2011,** *45*, (21), 3594-3602.
9. Lim, S.; Kim, J.; Kim, T.; Lee, K.; Yang, W.; Jun, S.; Yu, S., Personal exposures to PM 2.5 and their relationships with microenvironmental concentrations. *Atmospheric environment* **2012,** *47*, 407-412.
10. Van Ryswyk, K.; Wheeler, A. J.; Wallace, L.; Kearney, J.; You, H.; Kulka, R.; Xu, X., Impact of microenvironments and personal activities on personal PM 2.5 exposures among asthmatic children. *Journal of Exposure Science and Environmental Epidemiology* **2014,** *24*, (3), 260.
11. Health Effects Institute, *Traffic-related air pollution: a critical review of the literature on emissions, exposure, and health effects*; Special Report 17; Health Effects Institute: **2010**.
12. Hoek, G.; Beelen, R.; De Hoogh, K.; Vienneau, D.; Gulliver, J.; Fischer, P.; Briggs, D., A review of land-use regression models to assess spatial variation of outdoor air pollution. *Atmospheric environment* **2008,** *42*, (33), 7561-7578.
13. Jedynska, A.; Hoek, G.; Wang, M.; Yang, A.; Eeftens, M.; Cyrys, J.; Keuken, M.; Ampe, C.; Beelen, R.; Cesaroni, G., Spatial variations and development of land use regression models of oxidative potential in ten European study areas. *Atmospheric Environment* **2017,** *150*, 24-32.
14. Dons, E.; Van Poppel, M.; Kochan, B.; Wets, G.; Panis, L. I., Modeling temporal and spatial variability of traffic-related air pollution: Hourly land use regression models for black carbon. *Atmospheric environment* **2013,** *74*, 237-246.
15. Michanowicz, D. R.; Shmool, J. L.; Tunno, B. J.; Tripathy, S.; Gillooly, S.; Kinnee, E.; Clougherty, J. E., A hybrid land use regression/AERMOD model for predicting intra-urban variation in PM2. 5. *Atmospheric environment* **2016,** *131*, 307-315.
16. Schulte, J. K.; Fox, J. R.; Oron, A. P.; Larson, T. V.; Simpson, C. D.; Paulsen, M.; Beaudet, N.; Kaufman, J. D.; Magzamen, S., Neighborhood-scale spatial models of diesel exhaust concentration profile using 1-nitropyrene and other nitroarenes. *Environmental science & technology* **2015,** *49*, (22), 13422-13430.

17. Good, N.; Mölter, A.; Ackerson, C.; Bachand, A.; Carpenter, T.; Clark, M. L.; Fedak, K. M.; Kayne, A.; Koehler, K.; Moore, B., The Fort Collins Commuter Study: Impact of route type and transport mode on personal exposure to multiple air pollutants. *Journal of exposure science and environmental epidemiology* **2016,** *26*, (4), 397-404.
18. Ham, W.; Vijayan, A.; Schulte, N.; Herner, J. D., Commuter exposure to PM2. 5, BC, and UFP in six common transport microenvironments in Sacramento, California. *Atmospheric Environment* **2017,** *167*, 335-345.
19. Steinle, S.; Reis, S.; Sabel, C. E., Quantifying human exposure to air pollution—moving from static monitoring to spatio-temporally resolved personal exposure assessment. *Science of the Total Environment* **2013,** *443*, 184-193.
20. Larkin, A.; Hystad, P., Towards personal exposures: how technology is changing air pollution and health research. *Current Environmental Health Reports* **2017**, 1-9.
21. Koehler, K. A.; Peters, T. M., New methods for personal exposure monitoring for airborne particles. *Current environmental health reports* **2015,** *2*, (4), 399-411.
22. Bell, M. L.; Ebisu, K.; Leaderer, B. P.; Gent, J. F.; Lee, H. J.; Koutrakis, P.; Wang, Y.; Dominici, F.; Peng, R. D., Associations of PM2. 5 constituents and sources with hospital admissions: analysis of four counties in Connecticut and Massachusetts (USA) for persons≥ 65 years of age. *Environmental health perspectives* **2014,** *122*, (2), 138.
23. Secrest, M. H.; Schauer, J. J.; Carter, E. M.; Lai, A. M.; Wang, Y.; Shan, M.; Yang, X.; Zhang, Y.; Baumgartner, J., The oxidative potential of PM 2.5 exposures from indoor and outdoor sources in rural China. *Science of The Total Environment* **2016,** *571*, 1477-1489.
24. Charrier, J. G.; Anastasio, C., Rates of hydroxyl radical production from transition metals and quinones in a surrogate lung fluid. *Environmental science & technology* **2015,** *49*, (15), 9317-9325.
25. Arku, R. E.; Birch, A.; Shupler, M.; Yusuf, S.; Hystad, P.; Brauer, M., Characterizing exposure to household air pollution within the Prospective Urban Rural Epidemiology (PURE) study. *Environment international* **2018,** *114*, 307-317.
26. Carter, E.; Norris, C.; Dionisio, K. L.; Balakrishnan, K.; Checkley, W.; Clark, M. L.; Ghosh, S.; Jack, D. W.; Kinney, P. L.; Marshall, J. D., Assessing exposure to household air pollution: a systematic review and pooled analysis of carbon monoxide as a surrogate measure of particulate matter. *Environmental health perspectives* **2017,** *125*, (7).
27. Adams, C.; Riggs, P.; Volckens, J., Development of a method for personal, spatiotemporal exposure assessment. *Journal of Environmental Monitoring* **2009,** *11*, (7), 1331-1339.
28. Rabinovitch, N.; Adams, C. D.; Strand, M.; Koehler, K.; Volckens, J., Within-microenvironment exposure to particulate matter and health effects in children with asthma: a pilot study utilizing real-time personal monitoring with GPS interface. *Environmental Health* **2016,** *15*, (1), 96.
29. Steinle, S.; Reis, S.; Sabel, C. E.; Semple, S.; Twigg, M. M.; Braban, C. F.; Leeson, S. R.; Heal, M. R.; Harrison, D.; Lin, C., Personal exposure monitoring of PM 2.5 in indoor and outdoor microenvironments. *Science of the Total Environment* **2015,** *508*, 383-394.
30. Carvlin, G. N.; Lugo, H.; Olmedo, L.; Bejarano, E.; Wilkie, A.; Meltzer, D.; Wong, M.; King, G.; Northcross, A.; Jerrett, M., Development and field validation of a community-engaged particulate matter air quality monitoring network in Imperial, California, USA. *Journal of the Air & Waste Management Association* **2017,** *67*, (12), 1342-1352.
31. Northcross, A. L.; Edwards, R. J.; Johnson, M. A.; Wang, Z.-M.; Zhu, K.; Allen, T.; Smith, K. R., A low-cost particle counter as a realtime fine-particle mass monitor. *Environmental Science: Processes & Impacts* **2013,** *15*, (2), 433-439.
32. Ryan, P. H.; Son, S. Y.; Wolfe, C.; Lockey, J.; Brokamp, C.; LeMasters, G., A field application of a personal sensor for ultrafine particle exposure in children. *Science of the total environment* **2015,** *508*, 366-373.
33. Rivas, I.; Donaire-Gonzalez, D.; Bouso, L.; Esnaola, M.; Pandolfi, M.; Castro, M.; Viana, M.; Àlvarez-Pedrerol, M.; Nieuwenhuijsen, M.; Alastuey, A., Spatiotemporally resolved black carbon concentration, schoolchildren's exposure and dose in Barcelona. *Indoor air* **2016,** *26*, (3), 391-402.

34. Chartier, R.; Phillips, M.; Mosquin, P.; Elledge, M.; Bronstein, K.; Nandasena, S.; Thornburg, V.; Thornburg, J.; Rodes, C., A comparative study of human exposures to household air pollution from commonly used cookstoves in Sri Lanka. *Indoor air* **2017,** *27*, (1), 147-159.
35. Chow, J. C.; Watson, J. G.; Green, M. C.; Frank, N. H., Filter light attenuation as a surrogate for elemental carbon. *Journal of the Air & Waste Management Association* **2010,** *60*, (11), 1365-1375.
36. Künzli, N.; Mudway, I. S.; Götschi, T.; Shi, T.; Kelly, F. J.; Cook, S.; Burney, P.; Forsberg, B.; Gauderman, J. W.; Hazenkamp, M. E., Comparison of oxidative properties, light absorbance, and total and elemental mass concentration of ambient PM2. 5 collected at 20 European sites. *Environmental health perspectives* **2006,** *114*, (5), 684.
37. Presler-Jur, P.; Doraiswamy, P.; Hammond, O.; Rice, J., An Evaluation of Mass Absorption Cross-Section for Optical Carbon Analysis on Teflon Filter Media. *Journal of the Air & Waste Management Association* **2017**, (just-accepted).
38. Sameenoi, Y.; Panymeesamer, P.; Supalakorn, N.; Koehler, K.; Chailapakul, O.; Henry, C. S.; Volckens, J., Microfluidic paper-based analytical device for aerosol oxidative activity. *Environmental science & technology* **2012,** *47*, (2), 932-940.
39. Charrier, J. G.; McFall, A. S.; Vu, K. K.; Baroi, J.; Olea, C.; Hasson, A.; Anastasio, C., A bias in the "mass-normalized" DTT response–An effect of non-linear concentration-response curves for copper and manganese. *Atmospheric Environment* **2016,** *144*, 325-334.
40. Fang, T.; Verma, V.; Guo, H.; King, L.; Edgerton, E.; Weber, R., A semi-automated system for quantifying the oxidative potential of ambient particles in aqueous extracts using the dithiothreitol (DTT) assay: results from the Southeastern Center for Air Pollution and Epidemiology (SCAPE). *Atmospheric Measurement Techniques* **2015,** *8*, (1), 471-482.
41. Volckens, J.; Quinn, C.; Leith, D.; Mehaffy, J.; Henry, C. S.; Miller-Lionberg, D., Development and evaluation of an ultrasonic personal aerosol sampler. *Indoor air* **2017,** *27*, (2), 409-416.
42. Colorado State University, CSU UPAS Android App. https://play.google.com/store/apps/details?id=app.volckensgroup.UPASv2&hl=en (Nov 2017).
43. Colorado State University, CSU UPAS iOS App. https://itunes.apple.com/us/app/csu-upas/id1126067765?mt=8 (Nov 2017).
44. Kahle, D.; Wickham, H., ggmap: Spatial Visualization with ggplot2. *R Journal* **2013,** *5*, (1).
45. Drinovec, L.; Močnik, G.; Zotter, P.; Prévôt, A.; Ruckstuhl, C.; Coz, E.; Rupakheti, M.; Sciare, J.; Müller, T.; Wiedensohler, A., The" dual-spot" Aethalometer: an improved measurement of aerosol black carbon with real-time loading compensation. *Atmospheric Measurement Techniques* **2015,** *8*, (5), 1965-1979.
46. *Exposure Factors Handbook 2011 Edition (Final Report)*; EPA/600/R-09/052F; United States Environmental Protection Agency: Washington D.C., **2011**.
47. Abrams, J. Y.; Weber, R. J.; Klein, M.; Samat, S. E.; Chang, H. H.; Strickland, M. J.; Verma, V.; Fang, T.; Bates, J. T.; Mulholland, J. A., Associations between Ambient Fine Particulate Oxidative Potential and Cardiorespiratory Emergency Department Visits. *Environmental health perspectives* **2017,** *125*.
48. Weichenthal, S. A.; Lavigne, E.; Evans, G. J.; Godri Pollitt, K. J.; Burnett, R. T., Fine particulate matter and emergency room visits for respiratory illness. Effect modification by oxidative potential. *American journal of respiratory and critical care medicine* **2016,** *194*, (5), 577-586.
49. Cho, A. K.; Sioutas, C.; Miguel, A. H.; Kumagai, Y.; Schmitz, D. A.; Singh, M.; Eiguren-Fernandez, A.; Froines, J. R., Redox activity of airborne particulate matter at different sites in the Los Angeles Basin. *Environmental Research* **2005,** *99*, (1), 40-47.
50. Breen, M. S.; Long, T. C.; Schultz, B. D.; Crooks, J.; Breen, M.; Langstaff, J. E.; Isaacs, K. K.; Tan, Y.-M.; Williams, R. W.; Cao, Y., GPS-based microenvironment tracker (MicroTrac) model to estimate time–location of individuals for air pollution exposure assessments: Model evaluation in central North Carolina. *Journal of Exposure Science and Environmental Epidemiology* **2014,** *24*, (4), 412.
51. Guarnieri, M.; Balmes, J. R., Outdoor air pollution and asthma. *The Lancet* **2014,** *383*, (9928), 1581-1592.

52. Koehler, K. A.; Shapiro, J.; Sameenoi, Y.; Henry, C.; Volckens, J., Laboratory Evaluation of a Microfluidic Electrochemical Sensor for Aerosol Oxidative Load. *Aerosol Science and Technology* **2014,** *48*, (5), 489-497.

CHAPTER 4: DYNAMIC CLASSIFICATION OF MICROENVIRONMENTS USING A SUITE OF LOW-COST SENSORS

Chapter Overview

Exposure to air pollution is associated with increased mortality and morbidity, and exposures for individuals can vary significantly depending on their personal habits, daily routines, and where they travel each day. To develop and validate the AMAS algorithm; an algorithm capable of dynamically classifying predefined microenvironments using global positioning satellite (GPS), motion, and light sensor data. Twenty-three volunteers in Fort Collins, CO were recruited to carry an ultrasonic personal aerosol sampler (UPAS) for a 48-hour period. The UPAS was retrofitted with a GPS and a pushbutton to complement the existing sensor measurements (temperature, pressure, relative humidity, motion, light). The pushbutton was used in conjunction with a traditional time-activity diary to note when the volunteer was located in their home, work, or 'other' microenvironment. The AMAS algorithm predicted the amount of time spent in each microenvironment with a mean accuracy of 96% for each microenvironment and a mean precision for each microenvironment (94%, 99%, and 77% for Work, Home, and 'Other'). The ability to classify microenvironments dynamically, in real-time can enable the development of new sampling and measurement technologies that classify exposure by microenvironment.

Introduction

Exposure to air pollution has deleterious effects on human health.[1-5] Accurate human exposure data is necessary to fully evaluate the wide-ranging health impacts. To assess the health effects of air pollution, studies have traditionally relied on ambient concentrations reported by a central-site monitor. However, air pollution exposures are spatially and temporally heterogeneous and ambient air quality concentrations aren't necessarily representative of the air quality for an individual, particularly indoors.[6-10] Recent research has focused on collecting real-time, spatially-resolved exposure data, coupled with post-hoc quantification of air pollution levels within distinct microenvironments (e.g. home, work, transit, etc.).[11-14] These post-hoc evaluations have helped determine when and where exposures are occurring.[15]

To estimate microenvironment exposures, studies have traditionally used surveys and diary methods. These methods are burdensome for study participants (particularly for children) and are subject to reporting bias and/or missing data.[13, 16] To alleviate the burden of self-reporting, some studies have used handheld[11, 12, 14, 17] or smartphone-based Global Positioning Systems (GPS)[18-21] to monitor where participants spend their time. These studies have demonstrated that GPS sensors tend to provide accurate location data when outdoors, however, the accuracy is compromised by signal loss and drift in and around buildings. These GPS limitations can reduce positional accuracy and complicate exposure characterization by misclassifying indoor microenvironments. Therefore, recent studies have included a buffer around microenvironments to account for positional inaccuracies rather than solely rely on geographic information system (GIS) geocoded building boundaries.[11, 12] Breen et al.[12], used geocoded building boundaries when the GPS accuracy was high, but used a circular buffer (1 km radius) when the GPS accuracy was low. Other studies have combined a single static buffer with temperature[11, 22, 23], light[24-27], or motion[28, 29] data to augment GPS measurements and help detect a transition between microenvironments. The algorithms developed to date have relied on data collection from multiple sources to collect the exposure (e.g. central site monitors or continuous personal sampling devices) and microenvironment detection data (e.g. GPS, temperature, motion, light, etc.). This approach has been acceptable for post-hoc microenvironment exposure analysis, however, there are potential advantages to using a single device that can collect filter samples by microenvironment to evaluate exposures by particulate matter composition.[30-33] For example, the Automated Microenvironment Aerosol Sampler (AMAS)[34] is a wearable device containing four separate filter channels for collecting fine particulate matter ($PM_{2.5}$) with integrated GPS, motion, light, and temperature sensors. Devices such as the AMAS can use microenvironment-detection algorithms to

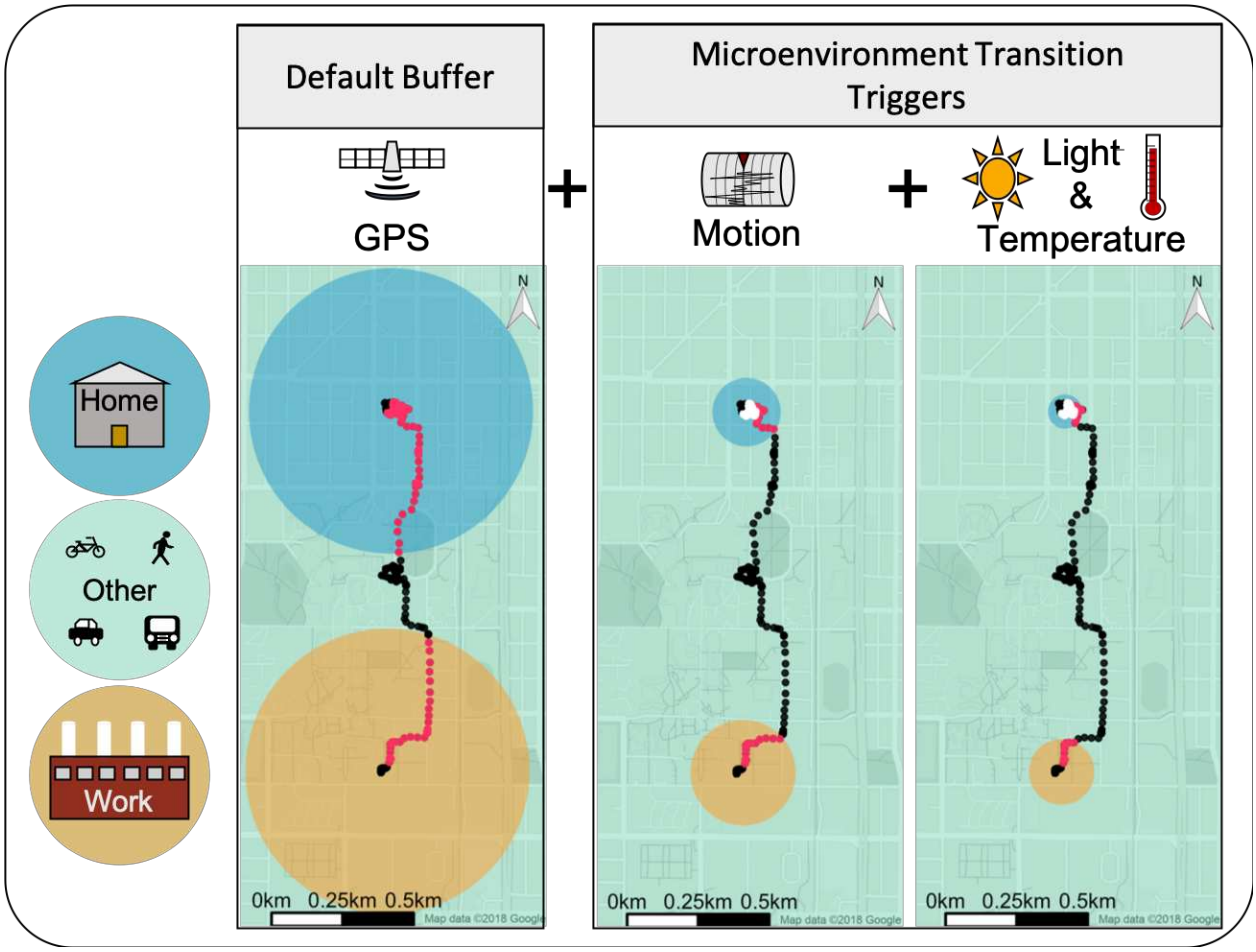

Figure 4-1: A general overview for how the adaptive buffer size (ABS) algorithm uses sensor data to modify the size of the coordinate buffer and classifies when an individual is present in a given microenvironment. When only GPS location data are available, a large buffer is used to account for potential GPS signal drift. As more motion and environmental triggers are detected, buffer radii are reduced as there is increased certainty that a microenvironment transition has occurred. The black dots represent when an algorithm correctly classifies the microenvironment. The red dots demonstrate points that were incorrectly classified. The white dots represent points when the GPS accuracy had drifted, but since there was no motion detected the points were correctly classified within the microenvironment.

dynamically adjust the flow of air through individual filters and collect $PM_{2.5}$ samples specific to a microenvironment.

The goal of this work was to develop an adaptive buffer size (ABS) algorithm capable of dynamically classifying an individual's location into one of three microenvironments: home, work, and 'other' (a miscellaneous category encompassing all non-home and non-workplace activities). The ABS algorithm (Figure 4-1, Figure C1) uses GPS, motion, temperature, and light sensor data to determine a transition between microenvironments. Rather than relying on fixed buffers around each location, the algorithm employs a dynamic buffer around each microenvironment that is adjusted based on GPS signal quality and additional sensor data. The algorithm identifies transitions between microenvironments by detecting changes in motion, temperature, light and GPS signal strength. Performance of the ABS algorithm was evaluated via simulation using data collected by participants in Fort Collins, CO and verified using a traditional diary method combined with a user pushbutton method for digital logging. Results from this work demonstrate that the ABS algorithm can successfully classify microenvironments and provides the opportunity to further advance personal exposure monitoring.

Methods

The development and evaluation of the ABS algorithm involved four steps: 1) collection of a "reference" dataset of spatially and temporally resolved microenvironment transitions using a panel of volunteers, 2) the dataset was curated to resolve any errors made by the participants or gaps in the sensor data, 3) formulation of the ABS algorithm, and 4) evaluation of the ABS algorithm (and other, simpler algorithms) relative to the reference dataset.

Data Collection

Adult participants were recruited from Colorado State University in Fort Collins, CO over the course of a four-month period (Dec. 2015 – Mar. 2016). The only requirements were that participants were working adults that did not live in the same residence as any of the other participants. Each participant provided their home and work addresses, which were used to determine a coordinate centroid (latitude, longitude) for these microenvironments. Participants were asked to note the timing of each microenvironment transition (i.e., the times when they left or entered their home and work microenvironments) using a traditional diary method. In addition, participants were asked to carry an Ultrasonic Personal Aerosol Sampler (UPAS)[35] for

approximately 48 hours. The UPAS measured and recorded ultraviolet light intensity (Silicon Labs, SI1145), temperature, pressure, relative humidity (Bosch Sensortech, BME280), and motion (ST Microelectronics, LSM303). The UPAS was further modified (Figure 4-2, Table C1) by adding a GPS sensor (Adafuit, 746) and a pushbutton recorder (Switchcraft Inc., ED913). The modified UPAS will be referred to as the personal monitor throughout the remainder of the manuscript. Due to the known limitations of the traditional diary method, participants were asked to use the pushbutton during each microenvironment transition to serve as an additional source of reference data. The personal monitor logged all sensor data, including the pushbutton status, to non-volatile memory at a frequency of 0.2 Hz (every 5 sec). The number of satellites tracked by the GPS was logged, in addition to the latitude and longitude, in degrees decimal minutes (DDM). Linear acceleration was measured on a ±2g full scale for all three primary axes and the total acceleration was calculated using Eqn. C1. Light intensity data were collected as 100× the ultraviolet (UV) index. Temperature data were logged in Celsius. Battery voltage was logged in volts.

Data Curating

The data collected by the participants were curated to provide a reference dataset to use for the development and evaluation of the ABS algorithm. The GPS latitude and longitude data were converted to decimal degree (DD) formatting and used to calculate the distances from the home and work centroid coordinates using the Haversine formula.[36] The pushbutton and diary data were used to determine the duration that each participant spent within each microenvironment and the precise timing of when they transitioned between microenvironments (e.g., when the participant left “home” and entered the “other” microenvironment). If the transition time recorded by the pushbutton and diary methods coincided, the pushbutton event was used unless there was a diary entry that specifically noted an error in the pushbutton transition time. The pushbutton data were also used to estimate time spent in each microenvironment as participants tended to record rounded times in their diaries or had discrepancies between the clock on the personal monitor and the clock or watch they were using. Some participants pressed the pushbutton on the personal monitor multiple times upon entering or exiting a microenvironment. In these instances, only one

(the first) button press was counted as a microenvironment transition. In the event that there were button presses in the personal monitor data log but no corresponding entry in the participant's diary, the data were manually evaluated to determine the GPS distance from both microenvironment centroids. If the GPS distance was less than 500 m from a home or work microenvironment when the button was pressed, the event was included and coded appropriately; otherwise it was assumed that the button press was accidental and discarded. If the participant's diary included events that didn't have a corresponding pushbutton event, it was assumed that the participant made the microenvironment transition but forgot to press the button. Infrequently, participants failed to note a transition that caused an impossible result (i.e. a direct home to work transition). To estimate the time spent in each microenvironment for those datasets, the data were manually evaluated in an attempt to code the data based on GPS distances. Once the diary and pushbutton time-location data were compiled they were manually validated against the GPS data. For the reminder of the manuscript, the combined diary and pushbutton data are referred to as the reference dataset.

Adaptive Buffer Size (ABS) Algorithm

The ABS algorithm dynamically adjusts the buffer size around both the home and work microenvironments to account for uncertainty in GPS positional accuracy. The use of variable buffer sizes for microenvironment classification has been reported previously[12]. However, the previous work relied on geocoded building boundaries and only used GPS data. Building on this work, the ABS algorithm was formulated from the hypothesis that acute changes in GPS signal quality, acceleration, UV light intensity, and temperature are indicative of a transition between microenvironments (e.g., moving from an indoors to outdoors). The ABS algorithm uses these triggers to adjust the buffer sizes in an attempt to optimize microenvironment classification (i.e., to maximize accuracy, sensitivity, and specificity as defined below). A detailed flow chart depicting ABS algorithm operation is shown in Figure C1.

The ABS algorithm defines three circular buffers with varying radial distances from the centroid of the work and home microenvironments; 1) large buffer: 500 m for both the home and work microenvironment, 2) medium buffer: 185 m and 120 m for the work and home microenvironment respectively, and 3) small buffer: 115 m and 60 m for the work and home microenvironment respectively. Breen et al.[12] used a large

buffer with a 1000 m radius to account for GPS signal drift; however, they acknowledged this as one of the limitations of their work. The limitation of using a large buffer is demonstrated in Figure 4-1 shown with a 500 m buffer, if the buffer was 1000 m there would be an overlap of the work and home microenvironments. Therefore, this work reduced the largest buffer radius by half (to 500 m) to improve outdoor microenvironment classification and to accommodate microenvironments that are located near each other. For the other two buffer sizes, the reference dataset was used to evaluate how far the participants were from the center of the home or work when a microenvironment transition was noted. These data were analyzed to determine the 75^{th} and 85^{th} percentile distances (Figure C3) for the all of the microenvironmental transitions in the reference dataset. The medium and small buffers were set to the 85^{th} (185 m and 120 m for work and home respectively) and 75^{th} (115 m and 60 m for work and home respectively) percentile distances.

The ABS algorithm uses a combination of categorical and continuous variables as triggers for detecting microenvironment transitions: 1) GPS signal status, 2) motion and environmental triggers, and 3) personal monitor charging status. The first step was to determine if there was a GPS signal available. If no GPS signal was available the last known location and the large buffer was used, otherwise motion and environmental triggers were used to check for microenvironment transitions. Motion and environmental triggers are acute changes in acceleration, temperature, and light data that can help predict a transition between two microenvironments. To invoke a motion trigger, the absolute value of the change in total acceleration between each time step had to be greater than 0.37 g. A temperature trigger was defined as when the absolute value temperature change for a five second period was greater than 0.02 °C and the current change in temperature had a sign change (negative, positive, or zero) as compared to the prior temperature change measurement. A UV light trigger occurs when there is a UV index[37] greater than 0.03. These trigger levels represent the 95^{th} percentile values of the reference dataset. Once a motion, UV light, or temperature trigger is detected, an individual timer for each trigger is reset and continues to increment once every second until the next trigger of that type is detected. The personal monitor had to be charged

overnight, therefore, the ABS algorithm described here also used the battery voltage to determine when the personal monitor was plugged into a wall outlet and thus no microenvironment transition could occur.

The ABS algorithm uses the status of the triggers to select one of the three radial buffers. If no transition triggers are active, the default buffer with a radius of 500 m is used around each microenvironment. If motion and one of the environmental triggers is activated, the medium buffer is used. If triggers for motion, light, and temperature are all detected then the small buffer is used. This method allows the buffer size to be evaluated every 5 s and the radii to be reduced if the probability of a microenvironment transition increases.

ABS Algorithm Evaluation

To test our hypothesis that environmental and motion triggers provide key data for enhancing microenvironment classification, reference algorithms were used to determine if the ABS algorithm can provide improved performance as compared to algorithms that use a static buffer. Three of the algorithms had a single static buffer set for the home and work microenvironments equal to one of the three buffer sets used in the ABS algorithm. These static buffer algorithms are referred to as "GPS-S" (115 m and 60 m, work and home buffers), "GPS-M" (185 m and 120 m, work and home buffers), and "GPS-L" (500 m and 500 m, work and home buffers). The fourth algorithm, referred to as the "Motion" algorithm, was identical to the ABS algorithm except only motion triggers were used (light and temperature data were excluded) to determine if the environmental sensor data enhances microenvironment classification

All five of the algorithms were evaluated through simulation by applying them to the reference dataset. Performance of each algorithm was calculated by comparing each five-second simulated point to the participant's reference dataset to estimate the true positive, false positive, true negative, and false negative classifications for each algorithm by microenvironment. For example, for the home microenvironment, a true positive indicates that an algorithm predicted the home microenvironment when the person was truly at home. A false negative indicates that an algorithm incorrectly predicted the work or other microenvironment when the person was actually at home. With these data, the sensitivity (Eqn.C2), specificity (Eqn. C3), and accuracy (Eqn. C4) of each algorithm were calculated by microenvironment. The

sensitivity characterizes the degree to which an algorithm underestimates the amount time spent in each microenvironment. The specificity indicates how much an algorithm overestimated time in each microenvironment. Finally, the total algorithm accuracy was also evaluated to determine the effectiveness of each algorithm across all microenvironments. The Friedman and pairwise post-hoc Nemenyi tests (PMCMR package) were used to test for significant differences between the ABS and reference algorithms. All analyses and simulations were performed using R 3.5.0 (R Core Team, Vienna, Austria).

Results

A total of 22 participants were recruited into the study and provided a total of 25 microenvironment transition datasets (three participants collected data twice) from December 2015 through March 2016. All 25 participant datasets spanned at least 24 hours of data with median, standard deviation, minimum and maximum data collection times of 47.8, 7.7, 30.9, and 71.9 hours respectively. These 25 datasets provided 274 microenvironment transitions (90 defined only by the traditional diary method, 5 required manual assignment using GPS coordinate data, and the remaining 186 were defined by the pushbutton or both the pushbutton and traditional diary method) into or out of 22 unique home and 4 work microenvironments (campus buildings at Colorado State University). Four of the participants failed to use the traditional diary method, but those participants did use the pushbutton to indicate their microenvironment transitions. The median (25^{th}, 75^{th} percentile) amount of time that participants spent in the home, work, and 'other' microenvironments based on the reference dataset were 27.8 (24.3, 30.8), 11.5 (8.4, 14.9), and 4.6 (3.1, 9.2) hours. These results are also shown in Figure C4.

The number of predicted microenvironment transitions (Table C2) and median (25^{th}, 75^{th} percentile) amounts of time spent in the home, work, and other microenvironments (Figure C4, Table C3) were determined for each of the five algorithms. The ABS algorithm predicted 483 microenvironment transitions and the median (25^{th}, 75^{th} percentile) amounts of time spent in the home, work, and other microenvironments were 28.1 (24.6, 30.0), 12.1 (9.2, 14.4), and 4.0 (2.8, 8.2) hours respectively.

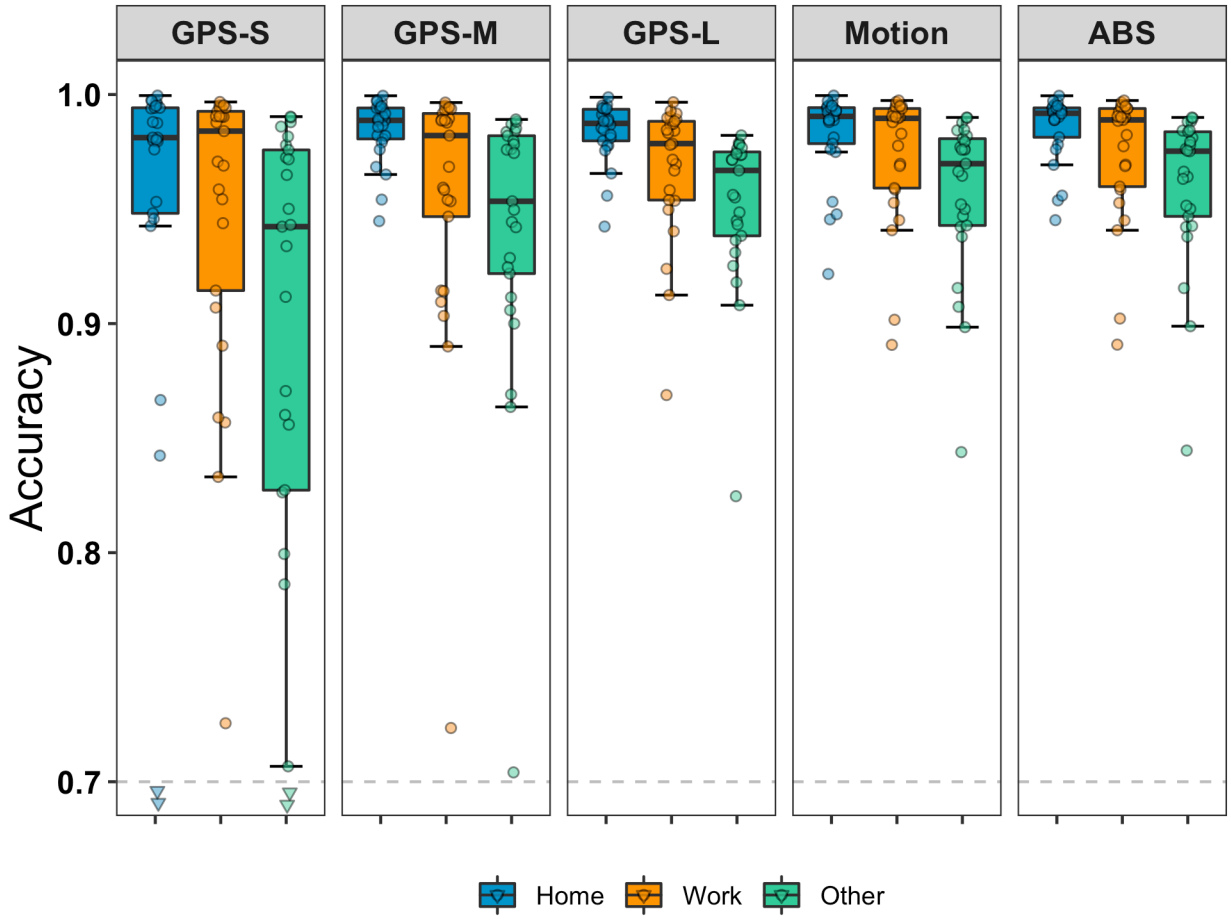

Figure 4-2: The accuracy for each of the five algorithms by microenvironment based on the five-second simulated data compared against the participant reference dataset. Each point represents the accuracy for a volunteer (n = 25) The triangle points represent outliers that fall below the 0.7 cutoff indicated by the dashed grey line.

The accuracy, sensitivity, and specificity were calculated for all five algorithms by microenvironment using all 25 datasets. The accuracy comparisons by microenvironment are shown in Figure 4-2 and the total accuracy for the microenvironments combined are shown in Figure C5. The median (25^{th}, 75^{th} percentile) accuracy values are summarized in Table C4 and the pairwise post-hoc Nemenyi results are shown in Table C5 and C6. The sensitivity and specificity by microenvironment are shown in Figure 4-3. A summary of the median (25^{th}, 75^{th} percentile) data shown in Table C7, and the pairwise post-hoc Nemenyi results are shown in Table C8 (Sensitivity) and Table C9 (Specificity).

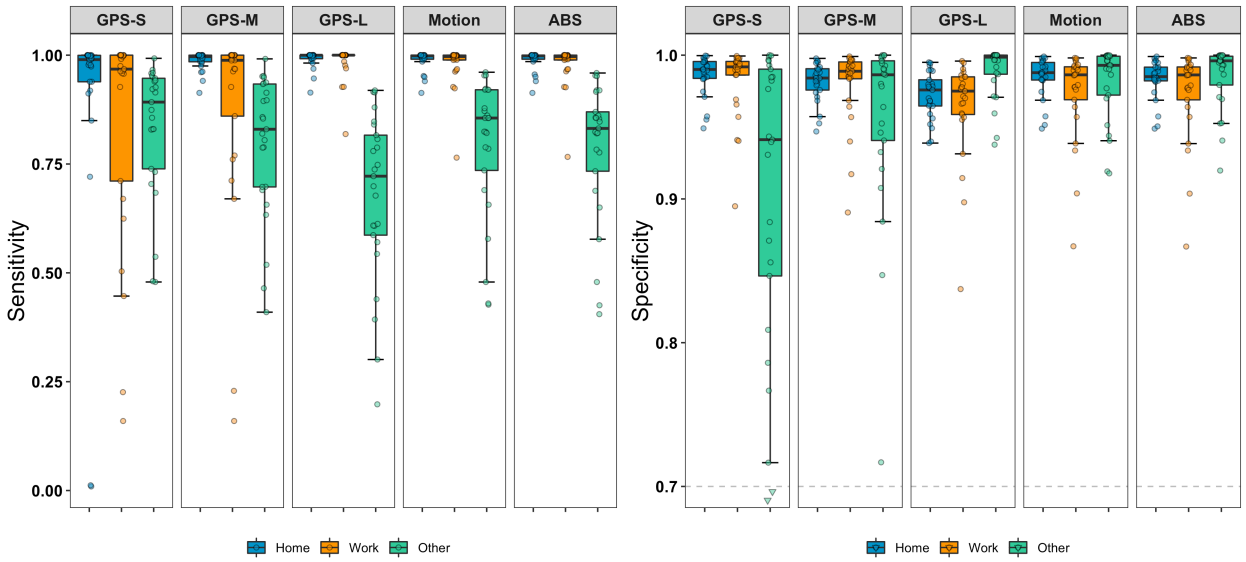

Figure 4-3: The sensitivity and specificity for each of the five algorithms by microenvironment based on the five second simulated data compared against the participant reference dataset. Each point represents the accuracy for a volunteer (n = 25). The triangle points in the specificity plot represent outliers that fall below the 0.7 cutoff indicated by the dashed grey line.

Discussion

For microenvironments that are defined with buffers, the GPS-only algorithms show a positive trend between the size of the buffer and the classification accuracy for a given microenvironment (Figure 4-2). However, there is a distinct tradeoff that occurs for the GPS-only algorithms; as the buffer size increases the increased accuracy for the home and work is gained through a loss of accuracy for the other microenvironment (i.e., the home and work buffers infringe upon the other microenvironment). The same tradeoff is also apparent with sensitivity: the sensitivity for the home and work classifications also increase, but the sensitivity for the 'other' classifications are negatively impacted leading to an underestimation of the amount of time spent outside of the home and work microenvironments. Inverse tradeoffs are also apparent for the specificity of the three GPS-only algorithms; the specificity for the 'other' classifications increases as the buffer size increases, however, these increases are offset with decreases in the specificity for the home and work classifications (Figure 4-3). These tradeoffs can be seen in Figure 4-1 where the

larger buffer encompasses the entire area around the home and work microenvironment. However, the large boundary also encompasses the majority of points that are logged during the transition between the home and work microenvironments leading to an underestimate of the time spent in the 'other' microenvironment. Proper classification of the 'other' microenvironment is critical; while the amount of time spent in the 'other' microenvironment is typically lower, air pollution concentrations in the 'other' microenvironment tend to be elevated (e.g., while in transit on roadways). Thus, exposures in the 'other' microenvironment and can account for a substantial portion of a person's daily cumulative exposure.[38, 39]

Using the trigger data to adjust the buffer size can help to retain classification accuracy (Figure 4-2) without loss of sensitivity and specificity (Figure 4-3). Overall, the ABS and Motion algorithms outperformed the three GPS-only algorithms as demonstrated by improved total and microenvironment accuracies that were statistically significant when compared to the most accurate GPS-only (GPS-L) algorithm (Table C5 and C6). Additionally, unlike the GPS-only algorithms, both the ABS and Motion algorithms were able to reduce the tradeoffs between the sensitivity and specificity; the sensitivity for the 'other' classifications and the specificity for the home (with the exception of the ABS algorithm) and work classifications were improved and were statistically significant as compared to the GPS-L algorithm. While the ABS algorithm only slightly outperformed the Motion algorithm in both the total and microenvironment accuracies as seen in Table C4, there are slight differences for the 'other' sensitivity and in the specificities (Table C7). One key difference worth noting is that the Motion algorithm has a substantial increase in number of detected transitions (659) as compared to the ABS algorithm (483). For post-hoc data analysis or continuous personal sampling devices, the increased number of transitions won't likely lead to any adverse issues. However, for air sampling devices that can collect unique filter samples by microenvironment such as the AMAS[34], all of these unnecessary detected changes in microenvironment can led to mechanical degradation of the sampler.

Previous work by Breen et al.[12] developed a microenvironment algorithm that used a combination of geocoded building boundaries and a 1 km buffer depending on GPS signal strength to classify eight different microenvironments (inside and outside of the home, work, school; inside vehicles; other

locations). They evaluated their algorithm and determined the sensitivity and accuracy for the Work (99.9% & 99.6%), Work-Out (60.4% & 99.7%), School (93.1% & 99.9%), School-Out (73.5% & 99.9%), Home (98.8% & 98.9%), and Home-out (81.4% & 98.9%) microenvironments. The 'other' microenvironment described herein would encompass all of the microenvironments aside from the work, home, and school. Thus, a direct comparison is not easily made to the sensitivity and accuracy results published by Breen et al., but we can see the ABS algorithm provides similar results. Both algorithms provide a high accuracy and sensitivity for detecting the home and work microenvironments, but both have reduced sensitivity values for detecting when an individual is outside the home and work microenvironment. This comparison is notable as the performance of the ABS algorithm in detecting microenvironments in real time is comparable to the performance of a post-hoc analysis.

Strengths, Limitations, and Future Work

There are several strengths worth noting: 1) The reference dataset was collected by 22 volunteers who were not asked to change their daily routines and allowed for the evaluation of microenvironment transitions that occurring at random throughout the day over two seasons (Winter and Spring). 2) This work reports the accuracy, sensitivity, and specificity of the algorithms to demonstrate the tradeoffs that can be associated with microenvironment classification. The primary concern is that a high accuracy for an algorithm can be achieved but at the cost of underestimating time spent in certain microenvironments. This tradeoff can have dramatic impacts for health assessments if large exposures occur in microenvironments where people only spend a short amount of time during the day. 3) The ability to detect microenvironments accurately and in real time enables the use novel devices such as the AMAS that can collect filter-based air quality samples by microenvironment. Filter-based air quality samples collected by microenvironment provide spatially- and temporally- resolved particulate matter samples that can be speciated and used for health exposure assessments.

There are several limitations worth noting. Circular buffers were used to define the home and work microenvironments rather than polygons or the actual building boundaries. This simplified approach was used (1) to accommodate memory limitations within the UPAS microcontroller and (2) to simplify the

implementation of the algorithm (i.e., requiring no prior knowledge of each microenvironment except the coordinate location). Future work could allow for adjustable radial buffer sizes for each microenvironment or could use a rectangular rather than circular buffer, as most building footprints tend to be rectangular. Defining a microenvironment with a circular buffer and a centroid point rather than the building boundary can result in defining a portion of a work or home microenvironment as 'other'. The use of a rectangular buffer, however, would require additional coordinate data.

To better account for GPS signal issues that result in poor signal quality or complete signal loss, future work should monitor GPS signal quality parameters such as horizontal dilution of precision (HDOP). Another option that is becoming more cost-effective would be to incorporate advanced spatial tracking techniques such as dead reckoning that integrate motion and GPS sensors to account for GPS signal degradation.[21] While leveraging light detection and temperature data didn't provide a substantial benefit to the performance of ABS algorithm (beyond the motion data), future work that combines these environmental data with enhanced motion data could lead to the development of algorithms that could potentially "learn" microenvironment boundaries.

The light sensor used for this work could only measure UV light and thus could only help detect transitions during daylight hours. Also, UV light can be detected indoors, that is why the algorithm developed in this work required UV motion to be coupled with either temperature or acceleration motion. Future work should either replace the UV sensor with or add an additional light sensor capable of measuring both indoor low-level light and outdoor light.

Finally, this work included only four work locations within a single city (Fort Collins, CO) and during two seasons (Winter and Spring). Future improvements to the algorithm, such as those described above, should be validated with more extensive testing that spans a variety of locations and climates.

Conclusions

This work describes an algorithm that is capable of detecting pre-determined microenvironments in real-time using minimal user input. The ability to dynamically classify microenvironments in real-time can aid researchers by reducing the amount of post-processing work required to classify exposure by

microenvironment, ease the integration of exposure data into spatial models, and potentially provide air quality notifications in real-time. Improvements to all of these areas will help researchers better understand the links between air pollution exposure and health.

REFERENCES

1. Brook, R. D.; Rajagopalan, S.; Pope, C. A.; Brook, J. R.; Bhatnagar, A.; Diez-Roux, A. V.; Holguin, F.; Hong, Y.; Luepker, R. V.; Mittleman, M. A., Particulate matter air pollution and cardiovascular disease: an update to the scientific statement from the American Heart Association. *Circulation* **2010,** *121*, (21), 2331-2378.
2. Cohen, A. J.; Brauer, M.; Burnett, R.; Anderson, H. R.; Frostad, J.; Estep, K.; Balakrishnan, K.; Brunekreef, B.; Dandona, L.; Dandona, R., Estimates and 25-year trends of the global burden of disease attributable to ambient air pollution: an analysis of data from the Global Burden of Diseases Study 2015. *The Lancet* **2017,** *389*, (10082), 1907-1918.
3. Mann, J. K.; Balmes, J. R.; Bruckner, T. A.; Mortimer, K. M.; Margolis, H. G.; Pratt, B.; Hammond, S. K.; Lurmann, F. W.; Tager, I. B., Short-term effects of air pollution on wheeze in asthmatic children in Fresno, California. *Environmental health perspectives* **2010,** *118*, (10), 1497.
4. Peel, J. L.; Tolbert, P. E.; Klein, M.; Metzger, K. B.; Flanders, W. D.; Todd, K.; Mulholland, J. A.; Ryan, P. B.; Frumkin, H., Ambient air pollution and respiratory emergency department visits. *Epidemiology* **2005,** *16*, (2), 164-174.
5. Pope III, C. A.; Dockery, D. W., Health effects of fine particulate air pollution: lines that connect. *Journal of the air & waste management association* **2006,** *56*, (6), 709-742.
6. Branco, P.; Alvim-Ferraz, M.; Martins, F.; Sousa, S., The microenvironmental modelling approach to assess children's exposure to air pollution–A review. *Environmental research* **2014,** *135*, 317-332.
7. Lim, S.; Kim, J.; Kim, T.; Lee, K.; Yang, W.; Jun, S.; Yu, S., Personal exposures to PM 2.5 and their relationships with microenvironmental concentrations. *Atmospheric environment* **2012,** *47*, 407-412.
8. Van Ryswyk, K.; Wheeler, A. J.; Wallace, L.; Kearney, J.; You, H.; Kulka, R.; Xu, X., Impact of microenvironments and personal activities on personal PM 2.5 exposures among asthmatic children. *Journal of Exposure Science and Environmental Epidemiology* **2014,** *24*, (3), 260.
9. Baxter, L. K.; Dionisio, K. L.; Burke, J.; Sarnat, S. E.; Sarnat, J. A.; Hodas, N.; Rich, D. Q.; Turpin, B. J.; Jones, R. R.; Mannshardt, E. J. J. o. E. S.; Epidemiology, E., Exposure prediction approaches used in air pollution epidemiology studies: key findings and future recommendations. **2013,** *23*, (6), 654.
10. Özkaynak, H.; Baxter, L. K.; Dionisio, K. L.; Burke, J. J. J. o. E. S.; Epidemiology, E., Air pollution exposure prediction approaches used in air pollution epidemiology studies. **2013,** *23*, (6), 566.
11. Adams, C.; Riggs, P.; Volckens, J., Development of a method for personal, spatiotemporal exposure assessment. *Journal of Environmental Monitoring* **2009,** *11*, (7), 1331-1339.
12. Breen, M. S.; Long, T. C.; Schultz, B. D.; Crooks, J.; Breen, M.; Langstaff, J. E.; Isaacs, K. K.; Tan, Y.-M.; Williams, R. W.; Cao, Y., GPS-based microenvironment tracker (MicroTrac) model to estimate time–location of individuals for air pollution exposure assessments: Model evaluation in central North Carolina. *Journal of Exposure Science and Environmental Epidemiology* **2014,** *24*, (4), 412.
13. Elgethun, K.; Yost, M. G.; Fitzpatrick, C. T. E.; Nyerges, T. L.; Fenske, R. A., Comparison of global positioning system (GPS) tracking and parent-report diaries to characterize children's time–location patterns. *Journal Of Exposure Science And Environmental Epidemiology* **2006,** *17*, 196.
14. Kim, T.; Lee, K.; Yang, W.; Do Yu, S., A new analytical method for the classification of time–location data obtained from the global positioning system (GPS). *Journal of Environmental Monitoring* **2012,** *14*, (8), 2270-2274.
15. Steinle, S.; Reis, S.; Sabel, C. E., Quantifying human exposure to air pollution—moving from static monitoring to spatio-temporally resolved personal exposure assessment. *Science of the Total Environment* **2013,** *443*, 184-193.
16. Kelly, P.; Krenn, P.; Titze, S.; Stopher, P.; Foster, C., Quantifying the difference between self-reported and global positioning systems-measured journey durations: a systematic review. *Transport Reviews* **2013,** *33*, (4), 443-459.

17. Wu, J.; Jiang, C.; Houston, D.; Baker, D.; Delfino, R., Automated time activity classification based on global positioning system (GPS) tracking data. *Environmental Health* **2011,** *10*, (1), 101.
18. Asimina, S.; Chapizanis, D.; Karakitsios, S.; Kontoroupis, P.; Asimakopoulos, D.; Maggos, T.; Sarigiannis, D., Assessing and enhancing the utility of low-cost activity and location sensors for exposure studies. *Environmental monitoring and assessment* **2018,** *190*, (3), 155.
19. Donaire-Gonzalez, D.; Valentín, A.; de Nazelle, A.; Ambros, A.; Carrasco-Turigas, G.; Seto, E.; Jerrett, M.; Nieuwenhuijsen, M. J., Benefits of mobile phone technology for personal environmental monitoring. *JMIR mHealth and uHealth* **2016,** *4*, (4).
20. Glasgow, M. L.; Rudra, C. B.; Yoo, E.-H.; Demirbas, M.; Merriman, J.; Nayak, P.; Crabtree-Ide, C.; Szpiro, A. A.; Rudra, A.; Wactawski-Wende, J., Using smartphones to collect time–activity data for long-term personal-level air pollution exposure assessment. *Journal of Exposure Science and Environmental Epidemiology* **2016,** *26*, (4), 356.
21. Langlois, C.; Tiku, S.; Pasricha, S., Indoor localization with smartphones. *to appear, IEEE Consumer Electronics* **2017**.
22. Nethery, E.; Mallach, G.; Rainham, D.; Goldberg, M. S.; Wheeler, A. J., Using Global Positioning Systems (GPS) and temperature data to generate time-activity classifications for estimating personal exposure in air monitoring studies: an automated method. *Environmental Health* **2014,** *13*, (1), 33.
23. Lee, B.; Lim, C.; Lee, K., Classification of indoor-outdoor location using combined global positioning system (GPS) and temperature data for personal exposure assessment. *Environmental health and preventive medicine* **2017,** *22*, (1), 29.
24. Flynn, J. I.; Coe, D. P.; Larsen, C. A.; Rider, B. C.; Conger, S. A.; Bassett, J. D., Detecting indoor and outdoor environments using the ActiGraph GT3X+ light sensor in children. *Medicine and science in sports and exercise* **2014,** *46*, (1), 201-206.
25. Hu, M.; Li, W.; Li, L.; Houston, D.; Wu, J., Refining time-activity classification of human subjects using the global positioning system. *PloS one* **2016,** *11*, (2), e0148875.
26. Tandon, P. S.; Saelens, B. E.; Zhou, C.; Kerr, J.; Christakis, D. A., Indoor versus outdoor time in preschoolers at child care. *American journal of preventive medicine* **2013,** *44*, (1), 85-88.
27. Pagels, P.; Raustorp, A.; Guban, P.; Fröberg, A.; Boldemann, C., Compulsory school in-and outdoors—Implications for school children's physical activity and health during one academic year. *International journal of environmental research and public health* **2016,** *13*, (7), 699.
28. Kestens, Y.; Thierry, B.; Chaix, B., Re-creating daily mobility histories for health research from raw GPS tracks: Validation of a kernel-based algorithm using real-life data. *Health & place* **2016,** *40*, 29-33.
29. Dewulf, B.; Neutens, T.; Van Dyck, D.; De Bourdeaudhuij, I.; Panis, L. I.; Beckx, C.; Van de Weghe, N., Dynamic assessment of inhaled air pollution using GPS and accelerometer data. *Journal of Transport & Health* **2016,** *3*, (1), 114-123.
30. Council, N. R., *Research priorities for airborne particulate matter: IV. Continuing research progress*. National Academies Press: 2004; Vol. 4.
31. Bell, M. L.; Dominici, F.; Ebisu, K.; Zeger, S. L.; Samet, J. M. J. E. h. p., Spatial and temporal variation in PM2. 5 chemical composition in the United States for health effects studies. **2007,** *115*, (7), 989.
32. Kelly, F. J.; Fussell, J. C. J. A. E., Size, source and chemical composition as determinants of toxicity attributable to ambient particulate matter. **2012,** *60*, 504-526.
33. Valavanidis, A.; Fiotakis, K.; Vlachogianni, T. J. J. o. E. S.; Health, P. C., Airborne particulate matter and human health: toxicological assessment and importance of size and composition of particles for oxidative damage and carcinogenic mechanisms. **2008,** *26*, (4), 339-362.
34. Quinn, C.; Miller-Lionberg, D. D.; Klunder, K. J.; Kwon, J.; Noth, E. M.; Mehaffy, J.; Leith, D.; Magzamen, S.; Hammond, S. K.; Henry, C. S.; Volckens, J., Personal Exposure to PM2.5 Black Carbon and Aerosol Oxidative Potential using an Automated Microenvironmental Aerosol Sampler (AMAS). *Environmental Science & Technology* **2018,** *52*, (19), 11267-11275.
35. Volckens, J.; Quinn, C.; Leith, D.; Mehaffy, J.; Henry, C. S.; Miller-Lionberg, D., Development and evaluation of an ultrasonic personal aerosol sampler. *Indoor air* **2017,** *27*, (2), 409-416.
36. Sinnott, R. W., Virtues of the haversine. *Sky Telesc.* **1984,** *68*, 159.

37. World Health Organization, Global Solar UV index: A Practical Guide. In 2002.
38. HEI. *Exposure Factors Handbook 2011 Edition (Final Report)*; EPA/600/R-09/052F; United States Environmental Protection Agency: Washington D.C., 2011.
39. Wilson, J. G.; Kingham, S.; Pearce, J.; Sturman, A. P., A review of intraurban variations in particulate air pollution: Implications for epidemiological research. *Atmospheric Environment* **2005,** *39*, (34), 6444-6462.

CHAPTER 5: CONCLUSIONS, LIMITATIONS, AND FUTURE WORK

Conclusions

Low-cost sample collection and analysis for contaminants will inevitably become part of our daily lives and be invaluable resources for traditional researchers, public health officials, citizen scientists, and activists. Improvement to sample collection and analysis methods with novel devices such as the AMAS and μPAD will help increase the frequency of sample collection and the throughput of sample analysis. Increased monitoring for environmental contaminants will help resolve exposure both spatially and temporally. The ability to collect more spatial-temporal exposure data provides researchers with more data that can be paired with public health data. Pairing health and exposure data will help provide a better understanding of the health associations between environmental contaminants and health outcomes and help combat methods such as manufactured uncertainty.

A summary of the work described here is split into two categories; air and water quality assessment.

Water Quality Assessment

- Tap water samples collected across Fort Collins, Colorado were tested with a method that coupled preconcentration and a distance-based μPAD. The method has the advantages of being hand-powered (instrument-free) and using a simple 'read by eye' quantification motif (based on color distance).
- The method was validated against ICP-MS to demonstrate the ability to quantify the copper content at levels ranging from 0.2-5000 ppb in tap-water within 30% of a reference technique.

Air Quality Assessment

- The AMAS, improves upon the previously developed UPAS and allows for sample collection by microenvironment (i.e. home, school, transit, etc.).
- The AMAS functionality was demonstrated with a pilot study in Fresno, California. During the study 25 students collected 48-hour samples (n = 37).

- The results from the pilot study found that the majority of black carbon and oxidative potential exposures for the high school students was at home where they spent most of their time.
- Validation of the AMAS demonstrated good relative precision (8.7% among collocated instruments; [n=5]) and a mean absolute error of 22% for BC and 33% for OP when compared to a traditional personal sampling instrument.
- In addition to the pilot study, an adaptive buffer size (ABS) algorithm that supplements GPS location data with motion, light, and temperature data was developed using samples collected by volunteers in Fort Collins, Colorado.
- The ABS algorithm improves the estimates for time spent at home, work, and in the 'other' microenvironments as compared to classification methods that only rely on GPS location and enables novel devices such as the AMAS to collect microenvironmental air quality samples.

Limitations and Future Work

Novel sample collection devices and methods are improving the spatial-temporal resolution of exposure data. However, the influx of these low-cost sample collection and analysis methods are creating some new concerns such as how to validate and manage all of the data collected. In response government agencies such as the Environmental Protection Agency (EPA) and the South Coast Air Quality Management District have begun creating programs to validate the performance of low-cost air quality monitors.[1, 2] The validation and certification of low-cost monitoring methods is crucial to ensuring that the data can be trusted. If the data from low-cost sensors can be deemed trustworthy, communities (such as the residents of Flint, Michigan) would have quantitative options to test for the presence of harmful contaminants (such as lead in drinking water).

Specific to the work described here, limitations and future work are detailed below and split into two categories; air and water quality assessment.

Water Quality Assessment

- The preconcentration method used in this work is a manual method that can be physically challenging. The development of a low-cost automated device would help aid in-field evaluation and improve sample throughput.
- The work described here only focus on the detection of one metal contaminant, copper. However, the Empore™ chelation disks used for preconcentration in this work can capture other heavy metals. Future work should evaluate preconcentration of other heavy metals.
- If preconcentration of other heavy metals was successful, evaluation or development of distance-based μPADs that could detect those metals would be needed. An ideal system would allow for the preconcentration of a number of heavy metals (i.e. lead and copper) and be coupled with a multiplexed μPAD.
- The distance-based μPAD device described here requires the user to manually read the distance of the color formation, note the distance or concentration conversion, and properly record the information in a database. Future work should consider the development of a smartphone application that can determine the contaminant concentrations via a photograph or scan and then automatically store the results with time, date, and location metadata in a digital database.

Air Quality Assessment

- Future work with the AMAS is already underway with additional sampling in Fresno, California. The current sampling campaign is collecting air quality data for an asthma cohort. In addition to the AMAS filter samples that will be used to evaluate black carbon and oxidative stress exposure, urine markers and health data are being collected. This additional data is being collected to evaluate the health associations between asthma and air exposures to black carbon and oxidative potential of particulate matter.
- The work described herein only evaluated the sample filters for black carbon and oxidative potential of the particulate matter. Future work should consider evaluating the filter samples for

other contaminants such as heavy metals using non-destructive measurement techniques such as X-ray fluorescence.

- The individual sample filters were not weighed to determine the total particulate matter collected on each filter. The filters weren't weighed as there wasn't enough particulate matter mass on each filter. Future work should consider modifying the flow rates for microenvironments such as the 'other' microenvironment where subjects spend very little time and thus increase the amount of particulate mass collected in those microenvironments. Another possible solution would be to increase the sample duration and as a result collect more particulate matter on each filter. Finally, another option worth considering is to integrate a sensor capable of continuously detecting particulate matter to complement the filter-based sample collection.
- The ABS algorithm used fixed circular boundaries for each microenvironment. Future work should consider using adjustable radial boundary sizes for each microenvironment or a rectangular rather than circular bounding box as most building footprints tend to be rectangular. The use of a rectangular boundary however, would require additional input and be more cumbersome.
- To better account for GPS signal issues that result in poor signal quality or complete signal loss, future work should monitor GPS signal quality parameters such as horizontal dilution of precision (HDOP).
- Future development of the AMAS and the ABS algorithm should consider incorporating advanced spatial tracking techniques such as dead reckoning that integrate motion and GPS sensors to account for GPS signal limitations. Leveraging light detection and temperature data combined with enhanced motion data could lead to the development of algorithms that could "learn" microenvironment boundaries.
- The ABS algorithm development only included four work locations and only took place in Fort Collins, Colorado during two seasons (Winter and Spring). Future work should include extensive testing in a variety of locations and climates for further validation.

REFERENCES

1. Air Sensor Toolbox. https://www.epa.gov/air-sensor-toolbox/ (June 2018).
2. Air Quality Sensor Performance Evaluation Center (AQ-SPEC). http://www.aqmd.gov/aq-spec (June 2018).

APPENDEX A

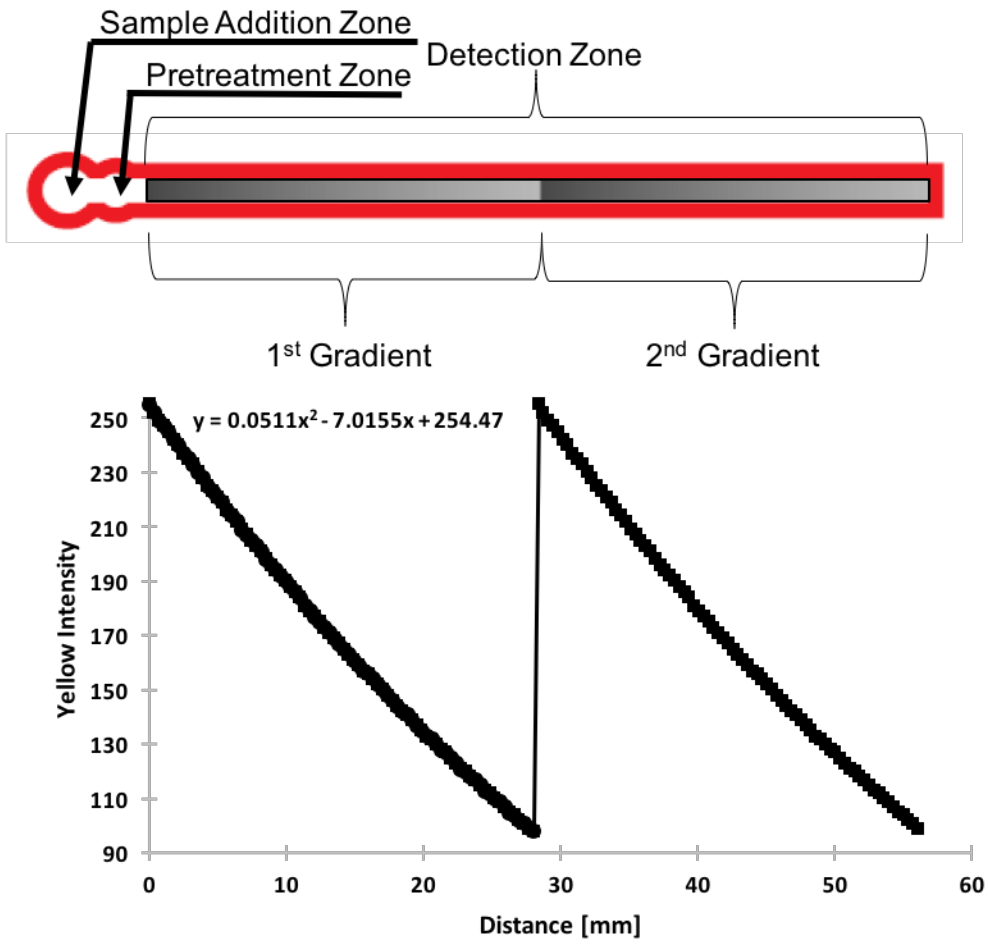

Figure A1: Distance-based µPAD design and locations of reagent gradients. The ink gradient was designed for the yellow channel on the Epson R280 printer. The yellow intensity can range from 0-255. This design starts at the maximum value of 255 and has a minimum value of 98.

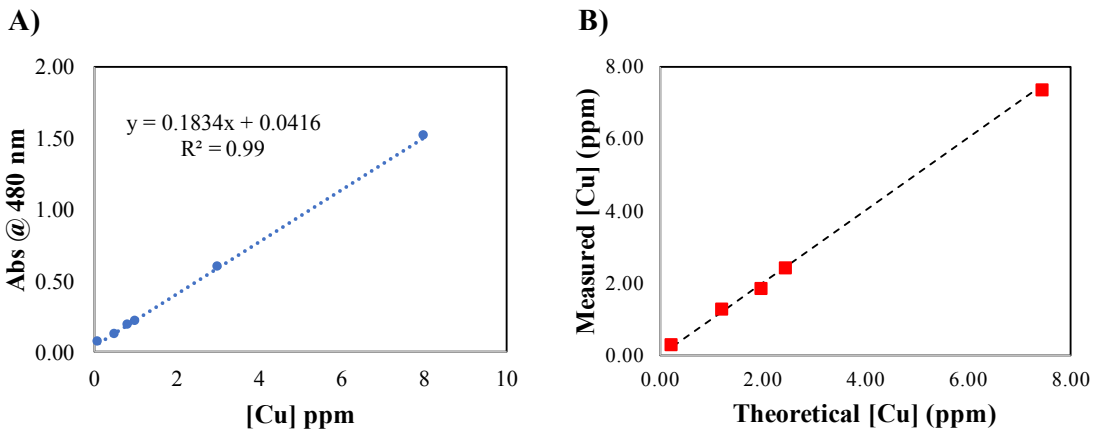

Figure A2: Validation of the efficiency of the preconcentration method. A) Calibration for a HACH TNT 860 kit, consisting of the measured absorbances (480 nm wavelength, Agilent UV-Vis spectrometer) for Cu standards in DI H20. Values are shown in Table S1. B) Observed Cu concentrations compared to theoretical Cu concentrations after preconcentration. The preconcentration method for this validation consisted of a 15 mL sample volume of Cu solution passed through a 8 mm Empore chelation disk, which was followed by a 0.1 mL 3M HNO3 acid wash into a falcon tube to remove the Cu ions from the chelation disk. Next 0.033 mL of 6.3M sodium acetate buffer was added for neutralization, and finally the sample was diluted with 5.867 DI H2O to ensure the sample concentration was in the HACH TNT kit range (0.1-8.0 ppm). Values are shown in Table A2-2.

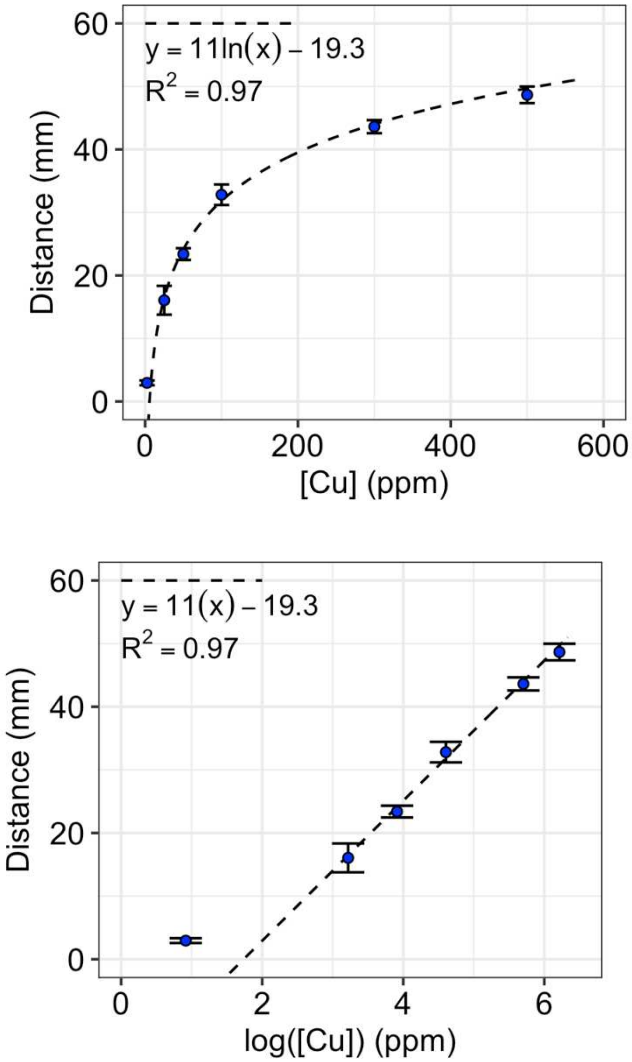

Figure A3: A) Double gradient calibration curve without preconcentration. B) Double gradient calibration curve without preconcentration and log transformed x-axis.

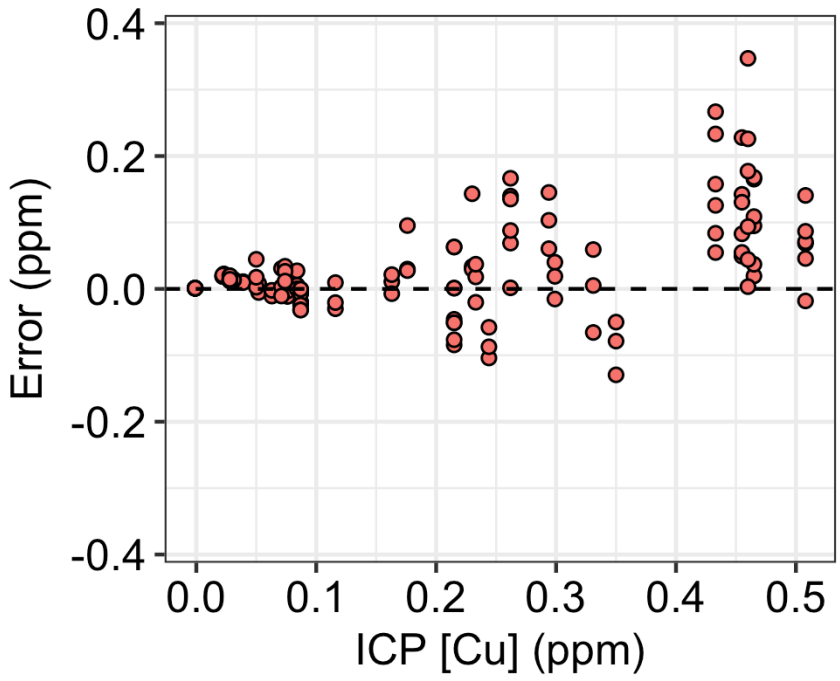

Figure A4: Error between mean µPAD and ICP Cu concentrations 20µLaliquot volumes for all 34 samples.

$$\boldsymbol{PF = (\eta_c * \eta_w)\left(\frac{V_S}{V_A + V_B + V_{Bu}}\right)\left(\frac{V_a}{V_\mu}\right)}$$

Equation A1: Preconcentration Factor.

Empore Disk Capture Efficiency (η_c); Acid Wash Metal Extraction Efficiency (η_w);

Sample Volume in mL(V_S); Acid Volume in mL (V_A); Base Volume in mL (V_B);

Buffer Volume in mL(V_{Bu}); Preconcentrate Aliquot Volume in mL (V_a); µPAD aliquot volume(V_μ)

Table A1: HACH TNT 860 absorbance calibration (480 nm) with Agilent UV-Vis for Cu solutions in DI H2O.

[Cu]	UV-Vis Abs @ 480 nm
ppm	abs
0.1	0.0644
0.5	0.1275
0.8	0.1951
1	0.2165
3	0.5954
8	1.5082

Table A2: Preconcentration efficiency validation. The preconcentration method for this validation consisted of a 15 mL sample volume of Cu solution passed through a 8 mm Empore chelation disk, which was followed by a 0.1 mL 3M HNO_3 acid wash into a falcon tube to remove the Cu ions from the chelation disk. Next 0.033 mL of 6.3M sodium acetate buffer was added for neutralization, and finally the sample was diluted with 5.867 DI H2O to ensure the sample concentration was in the HACH TNT kit range (0.1-8.0 ppm).

[Cu]	Sample Vol	Acid Vol (mL)	Base Vol (mL)	Final Vol (mL)	Measured Abs @ 480nm	Theoretical [Cu] (ppm)	Measured [Cu] (ppm)	Relative Percent Difference
ppm	mL	mL	mL	mL	Abs.	ppm	ppm	%
0.1	15	0.1	0.033	6	0.090	0.25	0.263	5%
0.5	15	0.1	0.033	6	0.270	1.25	1.243	-1%
0.8	15	0.1	0.033	6	0.374	2	1.810	-10%
1	15	0.1	0.033	6	0.480	2.5	2.390	-4%
3	15	0.1	0.033	6	1.380	7.5	7.296	-3%

Table A3: Calibration curve results (data shown for 20µL aliquots).

[Cu] (ppm)	Samples (n)	Distance mean±sd (mm)
2.5	9	3.0±0.4
25	26	16.1±2.3
50	5	23.4±0.9
100	26	32.8±1.6
300	8	43.6±1.0
500	8	48.7±1.3

Table A4: Preconcentrated μPAD results for the samples collected from taps located in buildings on Colorado State University Campus and from residencies of Fort Collins, Colorado (data shown for 20μL aliquots).

Sample	Samples	[Cu] ICP	[Cu] Estimate mean±sd	Distance mean±sd
iD	n	ppm	ppm	mm
C01	3	0.294	0.397±0.042	28.5±1.2
C02	3	0.230	0.299±0.065	25.1±2.3
C03	3	0.262	0.387±0.050	28.2±1.5
C04	6	0.433	0.587±0.083	32.9±1.6
C05	3	0.163	0.171±0.015	18.9±1.0
C06	3	0.233	0.245±0.029	23.0±1.4
C07	3	0.331	0.331±0.063	26.3±2.2
C08	3	0.039	0.049±0.001	4.8±0.2
C09	6	0.465	0.564±0.062	32.5±1.3
C10	6	0.455	0.570±0.067	32.6±1.3
C11	3	0.176	0.227±0.039	22.1±1.9
C12	3	0.080	0.084±0.003	10.9±0.4
C13	3	0.076	0.073±0.009	9.2±1.4
C14	3	0.244	0.161±0.023	18.2±1.6
C15	3	0.299	0.314±0.028	25.8±1.0
C16	6	0.508	0.574±0.052	32.7±1.1
C17	6	0.460	0.609±0.127	33.2±2.4
C18	3	0.350	0.264±0.040	23.8±1.8
C19	3	0.262	0.337±0.068	26.5±2.4
C20	3	0.023	0.045±0.000	3.8±0.1
P01	3	0.023	0.042±0.001	3.0±0.2
P02	9	0.215	0.195±0.056	20.0±3.2
P03	3	0.084	0.095±0.014	12.2±1.7
P04	3	0.052	0.052±0.007	5.2±1.6
P05	3	0.063	0.058±0.005	6.5±1.0
P06	3	0.022	0.041±0.001	2.8±0.3
P07	9	0.087	0.071±0.012	8.8±2.0
P08	3	0.050	0.072±0.021	8.7±3.4
P09	3	0.071	0.079±0.021	9.8±3.0
P10	3	0.074	0.098±0.011	12.6±1.3
P11	3	0.116	0.102±0.021	12.9±2.2
P13	3	0.031	0.045±0.001	3.7±0.2
P14	9	0.028	0.043±0.003	3.1±0.8
P15	9	-0.001	0.000±0.000	0.0±0.0

Table A5: Preconcentrated μPAD results for the samples collected from taps located in buildings on Colorado State University Campus in Fort Collins, Colorado (data shown for 10μL aliquots).

Sample	Samples	[Cu] ICP	[Cu] Estimate mean±sd	Distance mean±sd
ID	n	ppm	ppm	mm
C04	3	0.433	0.486±0.054	22.9±1.3
C09	3	0.465	0.430±0.062	21.5±1.6
C10	3	0.455	0.477±0.040	22.7±0.9
C16	3	0.508	0.535±0.042	24.0±0.9
C17	3	0.460	0.471±0.045	22.6±1.1

Table A6: Preconcentrated μPAD results for the samples collected from taps located in buildings on Colorado State University Campus in Fort Collins, Colorado (data shown for 5μL aliquots).

Sample	Samples	[Cu] ICP	[Cu] Estimate mean±sd	Distance mean±sd
iD	n	ppm	ppm	mm
C04	3	0.433	0.457±0.092	14.2±2.3
C09	3	0.465	0.410±0.070	13.0±1.9
C10	3	0.455	0.470±0.052	14.6±1.2
C16	3	0.508	0.498±0.046	15.3±1.1
C17	3	0.460	0.457±0.026	14.3±0.6

Table A7: ICP-MS results for the samples collected from taps located in buildings on Colorado State University Campus. All values in ppm.

	B	Ba	Be	Ca	Cd	Cd	**Cu**	Mg	Mn	Ni	Pb	Sr	Zn	As-1	Cu-1	Fe-1	K-1
LOQ	0.021	0.000	0.000	0.017	0.000	0.000	**0.001**	0.002	0.000	0.000	0.000	0.000	0.001	0.002	0.003	0.007	0.002
C01	0.010	0.014	-0.001	8.895	-0.001	-0.002	**0.294**	1.641	0.000	0.003	0.008	0.044	0.034	0.003	0.303	0.174	0.644
C02	0.006	0.018	-0.001	6.745	-0.001	-0.002	**0.230**	1.337	-0.001	0.006	0.001	0.032	0.157	0.003	0.223	0.139	0.451
C03	0.009	0.019	-0.001	6.497	-0.001	-0.002	**0.262**	1.620	-0.001	0.007	0.001	0.032	0.105	0.005	0.257	0.130	0.456
C04	0.006	0.018	-0.001	6.908	-0.001	-0.002	**0.433**	1.337	-0.001	0.003	0.000	0.033	0.077	0.003	0.419	0.136	0.458
C05	0.006	0.017	-0.001	6.883	-0.001	-0.002	**0.163**	1.419	0.000	0.002	0.000	0.035	0.080	0.005	0.170	0.145	0.507
C06	0.007	0.016	-0.001	7.586	-0.001	-0.002	**0.233**	1.503	0.000	0.005	0.000	0.039	0.049	0.003	0.227	0.163	0.520
C07	0.007	0.018	-0.001	7.353	-0.001	-0.002	**0.331**	1.448	-0.001	0.001	-0.001	0.035	0.021	0.003	0.293	0.145	0.450
C08	0.006	0.017	-0.001	6.904	-0.001	-0.002	**0.039**	1.357	0.000	0.001	-0.001	0.035	0.116	0.005	0.038	0.158	0.491
C09	0.007	0.016	-0.001	7.258	-0.001	-0.002	**0.465**	1.401	-0.001	0.047	-0.001	0.037	0.279	0.005	0.474	0.141	0.515
C10	0.006	0.017	-0.001	7.145	-0.001	-0.002	**0.455**	1.360	0.000	0.010	0.000	0.035	0.054	0.003	0.451	0.153	0.476
C11	0.046	0.020	-0.001	7.674	-0.001	-0.002	**0.176**	1.628	0.000	0.008	0.003	0.039	0.179	0.003	0.183	0.169	0.570
C12	0.006	0.018	-0.001	7.131	-0.001	-0.002	**0.080**	1.516	-0.001	0.018	-0.001	0.036	0.020	0.006	0.077	0.146	0.493
C13	0.008	0.017	-0.001	8.113	-0.001	-0.002	**0.076**	1.638	0.000	0.010	0.006	0.041	0.044	0.003	0.073	0.167	0.543
C14	0.010	0.017	-0.001	9.043	-0.001	-0.002	**0.244**	1.590	0.004	0.030	0.009	0.043	0.168	0.005	0.256	0.567	0.672
C15	0.009	0.015	-0.001	8.595	-0.001	-0.002	**0.299**	1.632	0.000	0.005	-0.001	0.043	0.126	0.003	0.298	0.167	0.600
C16	0.006	0.016	-0.001	6.976	-0.001	-0.002	**0.508**	1.385	0.000	0.001	-0.001	0.034	0.010	0.005	0.533	0.178	0.497
C17	0.006	0.016	-0.001	7.021	-0.001	-0.002	**0.460**	1.417	-0.001	0.008	0.000	0.035	0.041	0.002	0.445	0.141	0.471
C18	0.011	0.015	-0.001	9.855	-0.001	-0.002	**0.350**	1.806	-0.001	0.011	-0.001	0.048	0.075	0.006	0.359	0.181	0.707
C19	0.008	0.014	-0.001	8.136	-0.001	-0.002	**0.262**	1.505	-0.001	0.003	-0.001	0.040	0.184	0.005	0.269	0.153	0.587
C20	0.115	0.034	-0.001	5.169	-0.001	-0.002	**0.023**	3.850	-0.001	0.012	-0.001	0.032	0.036	0.004	0.022	0.096	0.483

Table A8: ICP-MS results for the samples collected from taps located in residencies of Fort Collins, Colorado. All values in ppm.

	Al	Ca	Cu	Mg	Mn	Ni	Pb	Sr	Zn	As-1	Cu-1	Fe-1	K-1
LOQ	0.001	0.017	**0.001**	0.002	0.000	0.000	0.000	0.000	0.001	0.002	0.003	0.007	0.002
P01	0.033	8.776	**0.023**	1.671	0.003	0.001	-0.001	0.043	0.002	0.003	0.024	0.198	0.664
P02	0.007	4.198	**0.215**	1.690	0.002	0.000	0.000	0.040	0.003	0.002	0.219	0.074	0.690
P03	0.011	6.523	**0.084**	1.344	-0.001	0.001	-0.001	0.031	0.010	0.006	0.083	0.129	0.455
P04	0.024	8.200	**0.052**	2.036	0.000	0.001	-0.001	0.043	0.079	0.003	0.054	0.153	0.683
P05	0.021	10.187	**0.063**	0.592	-0.001	0.004	-0.001	0.040	0.025	0.004	0.064	0.191	0.329
P06	0.014	5.814	**0.022**	1.428	-0.001	0.000	-0.001	0.034	0.010	0.002	0.021	0.119	0.484
P07	0.021	8.746	**0.087**	1.644	0.000	0.002	0.000	0.043	0.028	0.003	0.097	0.191	0.722
P08	0.020	7.649	**0.050**	1.474	-0.001	0.001	-0.001	0.041	0.032	0.005	0.050	0.147	0.573
P09	0.016	6.898	**0.071**	1.566	0.000	0.000	-0.001	0.041	0.019	0.005	0.072	0.126	0.634
P10	0.012	6.483	**0.074**	1.501	-0.001	0.001	-0.001	0.034	0.007	0.002	0.069	0.131	0.457
P11	0.019	6.707	**0.116**	1.699	0.000	0.001	-0.001	0.042	0.034	0.004	0.117	0.119	0.691
P13	0.012	6.956	**0.031**	1.365	0.005	0.001	0.001	0.035	0.114	0.003	0.030	0.353	0.477
P14	0.023	8.093	**0.028**	1.515	0.000	0.001	-0.001	0.041	0.051	0.005	0.029	0.154	0.679
P15	-0.002	5.973	**-0.001**	1.395	-0.001	0.000	-0.001	0.033	0.002	0.005	-0.001	0.119	0.488

ICP-MS Analysis Method

Elemental concentrations of Ag, Al, As, B, Ba, Be, Ca, Cd, Ce, Co, Cr, Cs, Cu, Dy, Er, Eu, Fe, Ga, Gd, Ho, K, La, Lu, Mg, Mn, Mo, Na, Nd, Ni, P, Pb, Pr, Rb, S, Se, Sm, Sr, Th, Tl, Tm, U, V, Yb, and Zn were measured using an Elan DRC (dynamic reaction cell) II mass spectrometer (PerkinElmer) connected to a Seaspray™ MEINHARD nebulizer and a quartz cyclonic spray chamber. Samples were introduced using an ASX-520 autosampler (CETAC Technologies). Ag, Al, B, Ba, Be, Ca, Cd, Ce, Co, Cs, Cu, Dy, Er, Eu, Ga, Gd, Ho, La, Lu, Mg, Mo, Na, Nd, Ni, P, Pb, Pr, Rb, S, Sm, Sr, Th, Tl, Tm, U, Yb, and Zn were measured in standard mode. As, Cr, Mn, Fe, K, Se, and V were measured in DRC mode using ammonia as the reactive gas. Before analysis the nebulizer gas flow and lens voltage were optimized for maximum Indium signal intensity. A daily performance check was also run which ensured that the instrument was operating properly and reduced the formation of oxides and doubly-charged species by monitoring CeO^{+}:Ce^{+} and Ba^{++}:Ba. A calibration curve was obtained by analyzing 7 dilutions of a multi-element stock solution (Inorganic Ventures). To correct for instrument drift Indium (In) was used as an internal standard at a concentration of 25 µg/L.

APPENDIX B

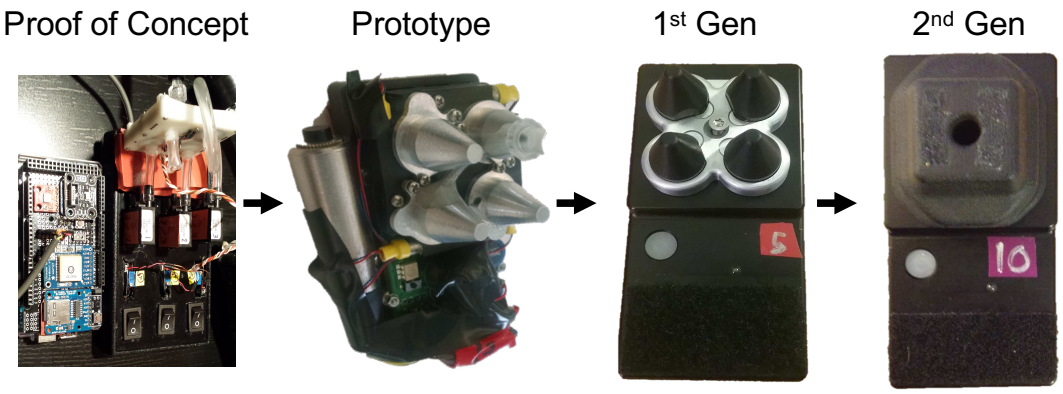

Figure B1: AMAS evolution. The AMAS originated as a proof of concept consisting of an Arduino with breakout boards (light sensing, GPS, SD card, temperature, pressure, and relative humidiy), three Omron flow sensors, three manual toggle vales, a rapid prototype filter holder, and a SKC personal air sampler. Following the proof of concept, the inlet of an Ultrasonic Personal Aerosol Sampler (UPAS) was modified to include four separate filter-valve flow channels with custom valves that were controlled by the UPAS microcontroller. After testing with the prototype, two generations of the PM2.5 inlets have been developed to date. Similar to the prototype, the first generation consisted of four individual plastic filter cartridges that fit into a separate PM2.5 cyclone inlet. The second generation replaced the individual filter cartridges with a single aluminum filter holder which holds all four filters. Additionally, the second-generation inlet integrated the cyclone inlets into a single inlet/cover to make the device more aesthetically pleasing. The second-generation AMAS also contains a multidirectional inlet to reduce the possibility of blocked air flow, which was a concern in the first-generation design. Cyclone designs have been developed for 1.0, 1.5, and 2.0 Lmin-1 operation and can be easily integrated into the AMAS design. The first-generation AMAS used four 2.0 Lmin-1 cyclones, and the second-generation AMAS used four 1.5 Lmin-1 cyclones; however, AMAS the inlet can be designed to incorporate a combination of 1.0, 1.5, and 2.0 min-1 cyclone design

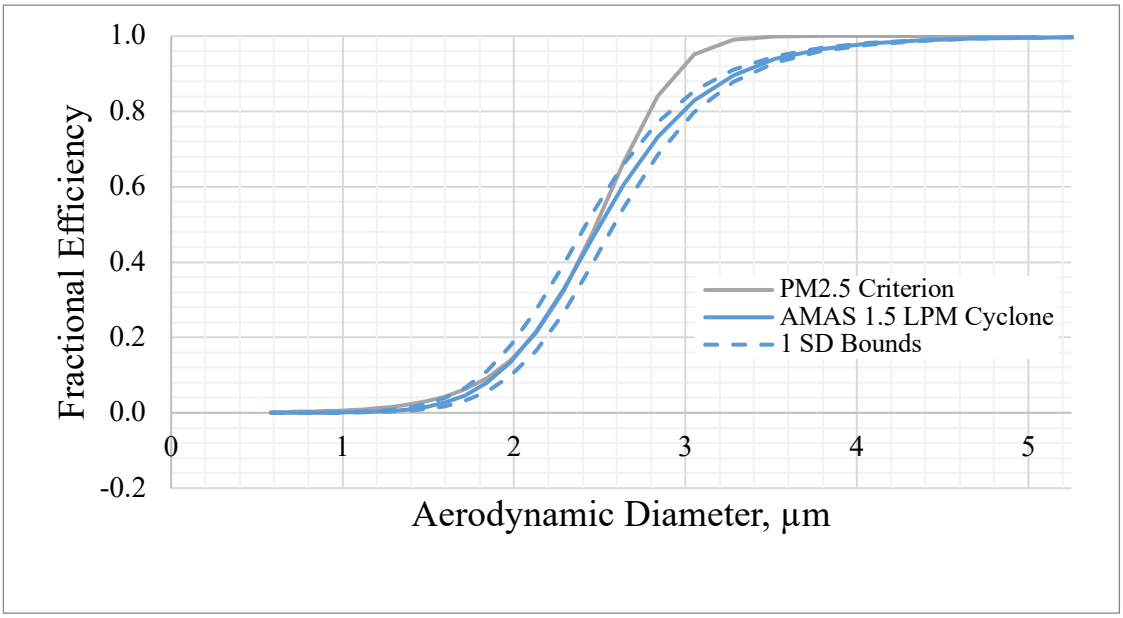

Figure B2: Cyclone performance. Collection efficiency for the 1.5 LPM cyclone design used in this study. The cyclone design was developed with the same methods detailed by Volckens et. al.[1] and use cyclone dimension nomenclature defined by Kenny and Gussman.[2,3] The cyclone dimensions in mm are as follows; D_c=9.43, D_{in}=2.212, D_e=2.546, B=2.358, H=4.055, Z=10.657, S=3.301. Laboratory testing of the cyclone provided a d_{50} (50% collection efficiency of particles with an aerodynamic diameter of 2.5µm) of 2.50±0.08 and a β (slope parameter) of 7.98±0.34 where the confidence intervals are one standard deviation.

[1] Volckens, J.; Quinn, C.; Leith, D.; Mehaffy, J.; Henry, C. S.; Miller-Lionberg, D., Development and evaluation of an ultrasonic personal aerosol sampler. *Indoor air* 2017, *27*, (2), 409-416.

[2] Kenny, L.; Gussman, R., A direct approach to the design of cyclones for aerosol-monitoring applications. *Journal of aerosol science* 2000, *31*, (12), 1407-1420.

[3] Kenny, L.; Gussman, R.; Meyer, M., Development of a sharp-cut cyclone for ambient aerosol monitoring applications. *Aerosol Science & Technology* 2000, *32*, (4), 338-358.

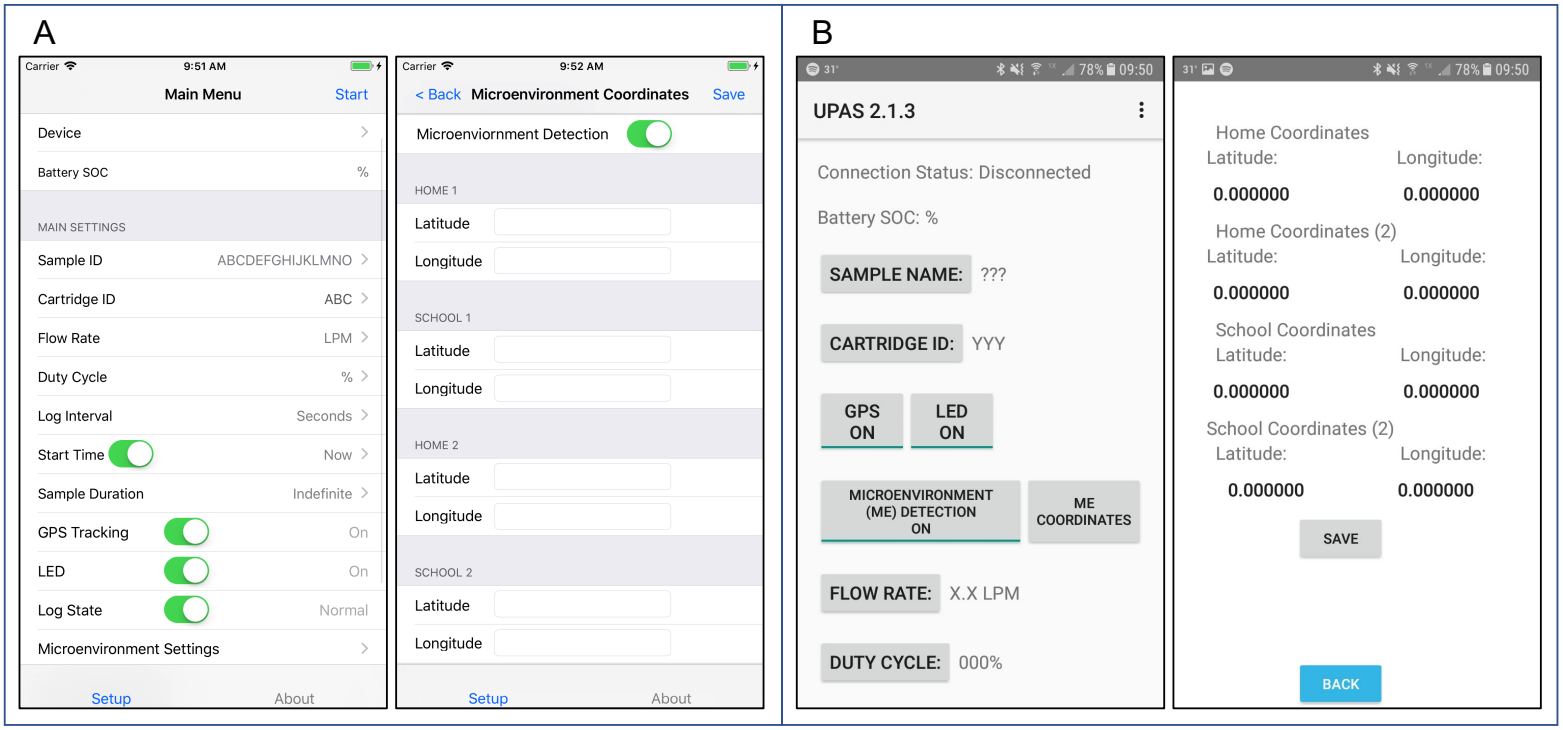

Figure B3: Phone application screenshots. A) iOS, B) Android.

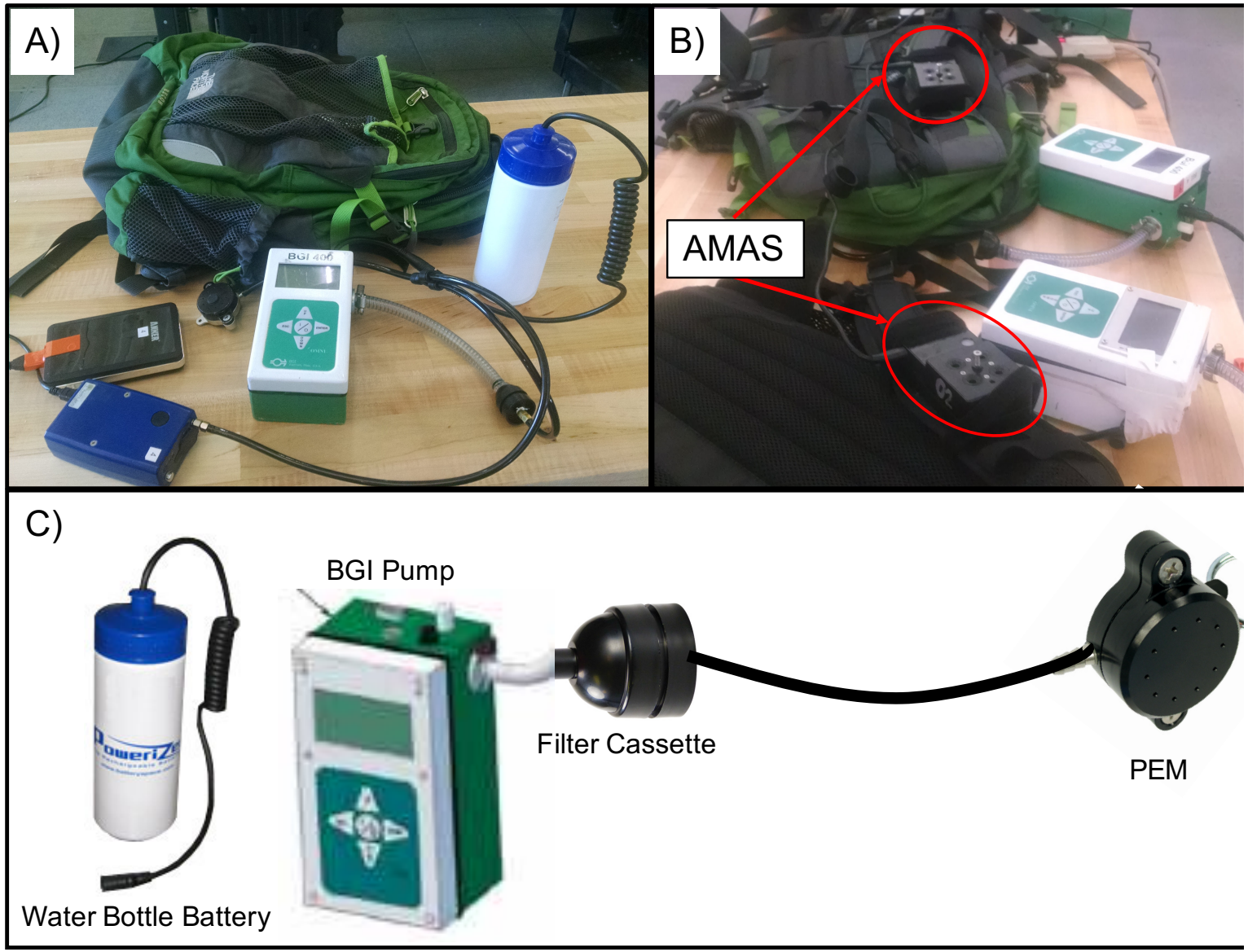

Figure B4: Reference sampler equipment.

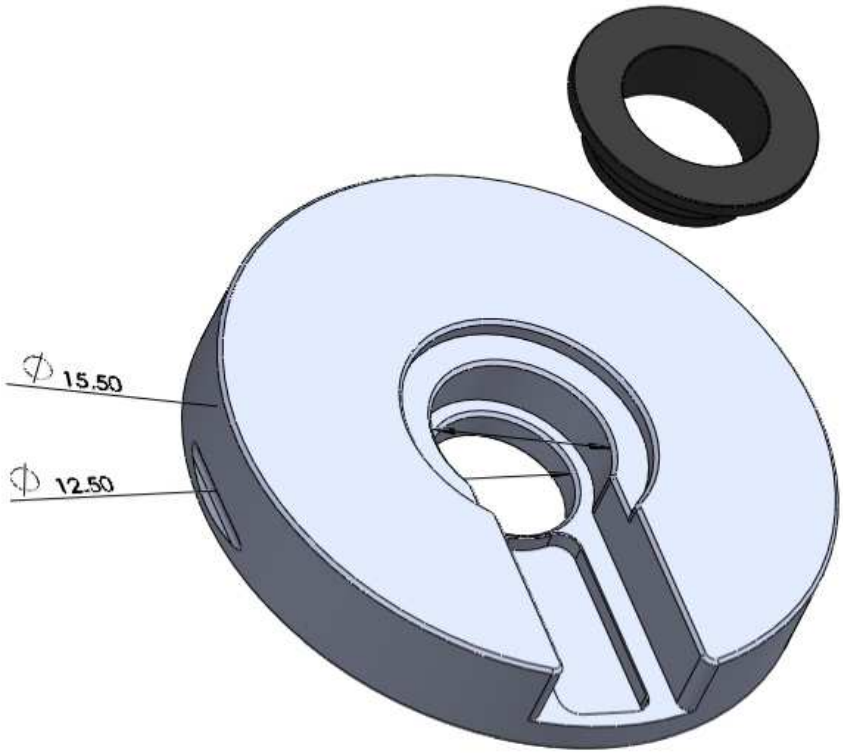

Figure B5: Custom 15mm Sootscan filter holder. Anodized aluminum lower filter holder with a 12.5 mm view diameter hole (identical to the standard 25 mm Magee Scientific Sootscan filter holder) and a 15.5 mm cavity to accommodate 15 mm filters. A plastic insert for securing the filter is also shown and has a 12.5 mm through hole as well.

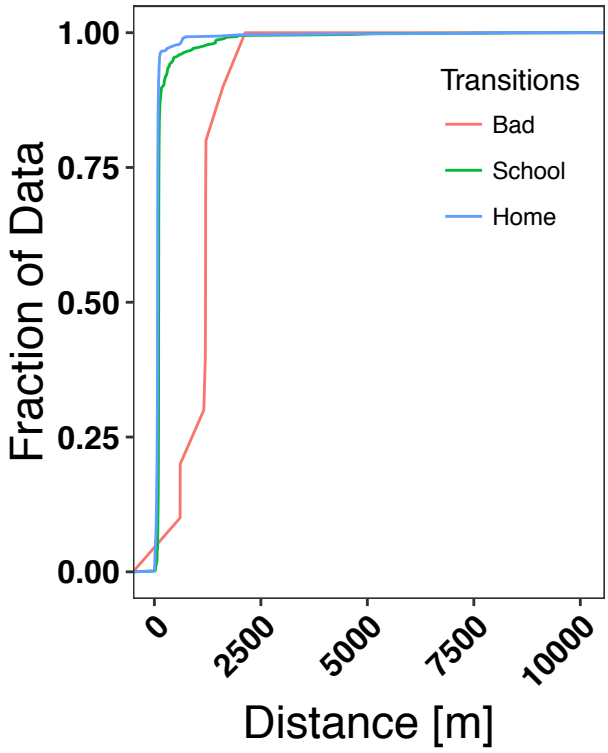

Figure B6: Distance from microenvironment at transition. The cumulative distributions for the distance from a microenvironment at the time of a transition for both entering and exiting the home and school microenvironments (Bad, n = 10; School, n = 585; Home, n = 780). Bad is defined as a transition that occurs between a school and a home microenvironment without detecting time in the other microenvironment.

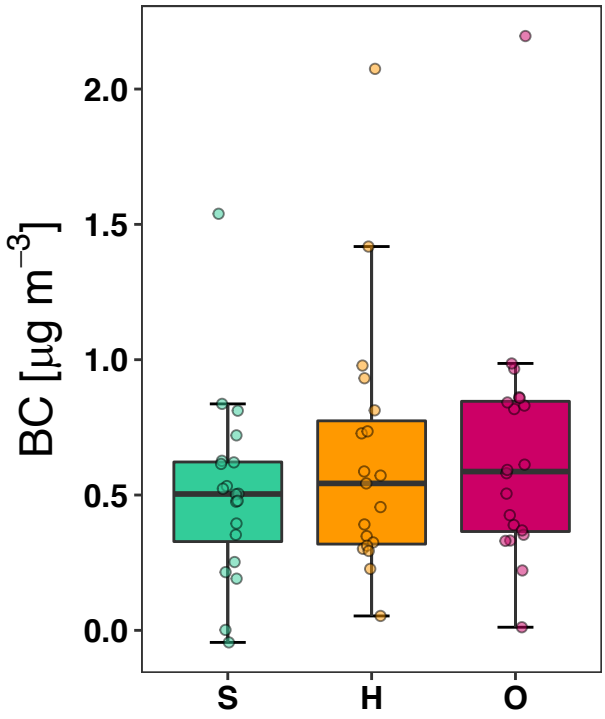

Figure B7: Black carbon concentration boxplot. The data shown in the plots include only samples that collected PM2.5 and AMAS data for the entire 48-hr period, had valid GPS coordinates, and collected PM2.5 for more than an hour (0.1 m3) in each microenvironment. (n = 20, 19, 20 for S = school, H = home, and O = other).

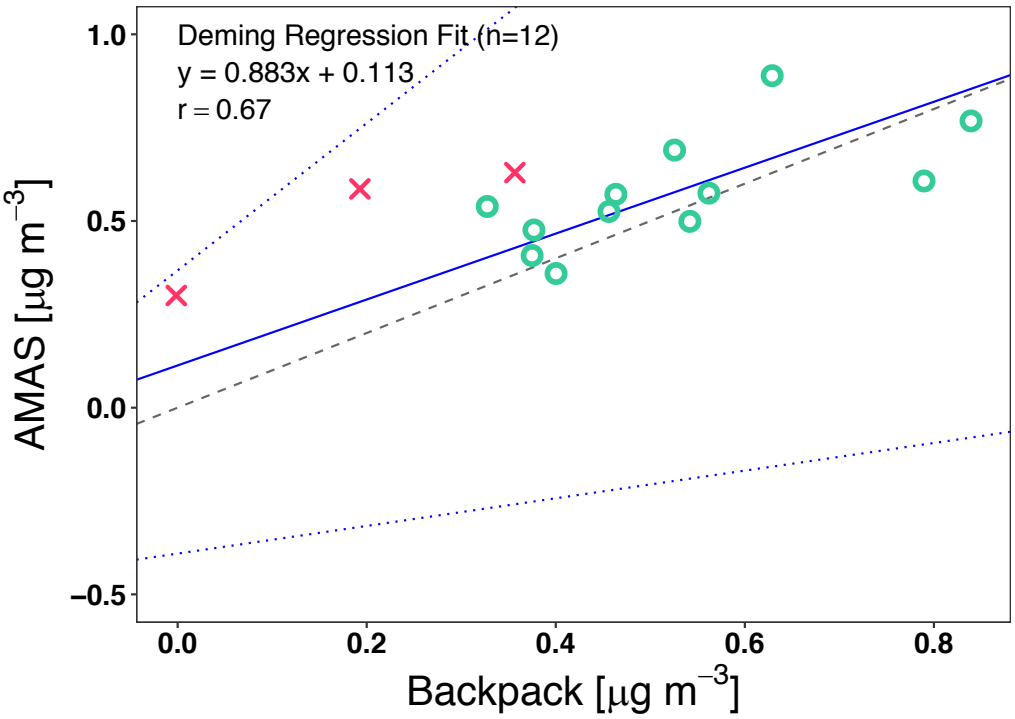

Figure B8: AMAS vs. backpack BC concentration. Comparison of the cumulative AMAS filter pair BC concentration to that of the measured backpack BC concentrations. A Deming regression was used to compare 12 of the 15 samples (green circles). The three samples that had backpack malfunctions (red multiplication signs) were excluded from the regression. The Deming regression (solid blue line) had a slope of 0.88 (0.37, 1.97) and an intercept of 0.11 (-0.39, 0.37). The 95% confidence intervals (dotted blue lines) and the 1:1 line (dashed gray line) are also shown in the figure.

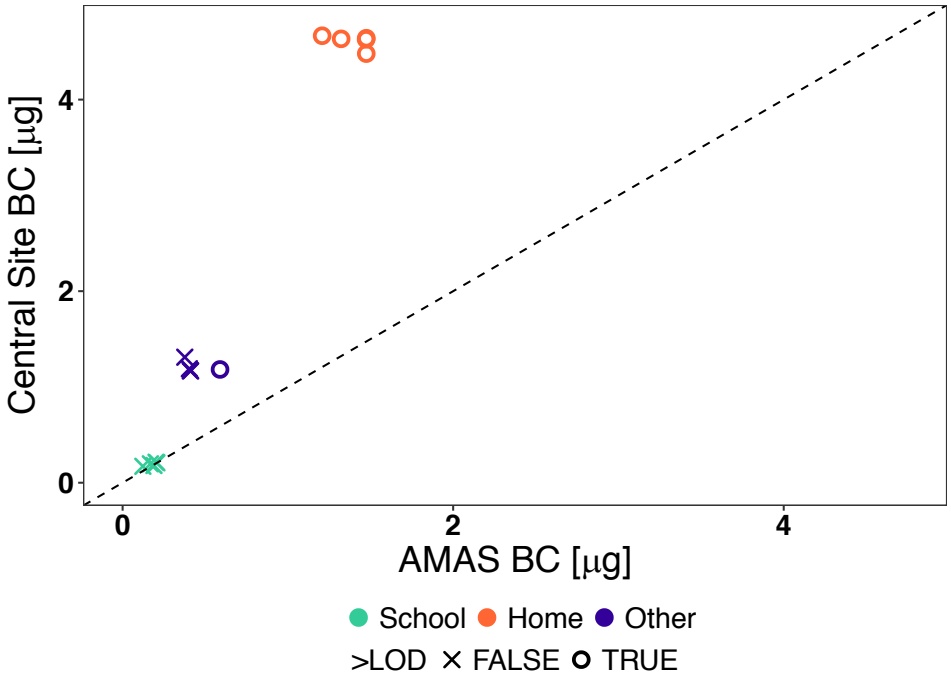

Figure B9: BC mass comparisons of AMAS collocation monitors to AE33.

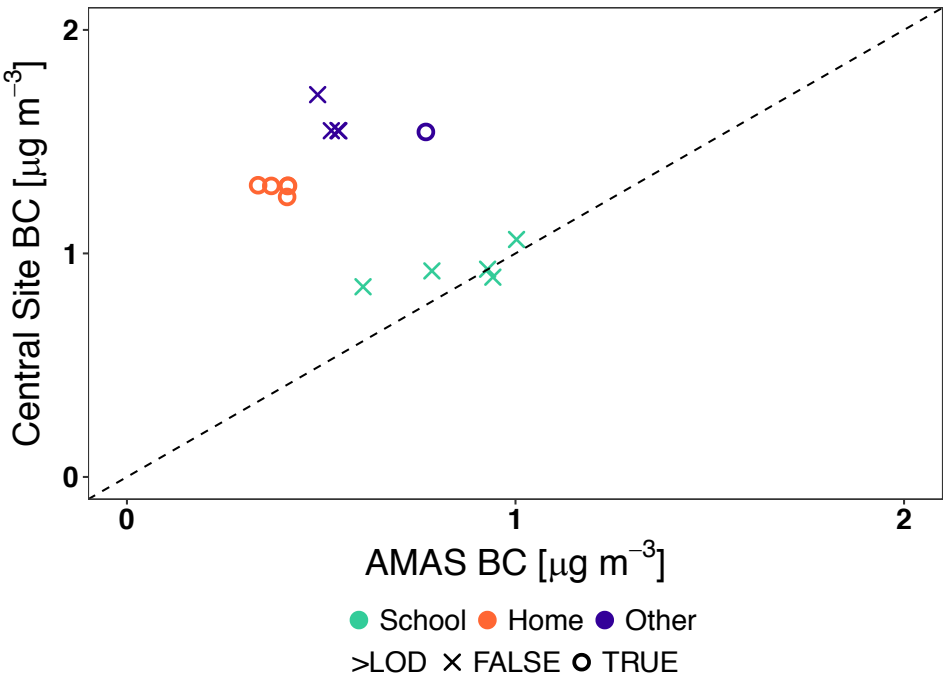

Figure B10: BC concentration comparisons of AMAS collocation monitors to AE33.

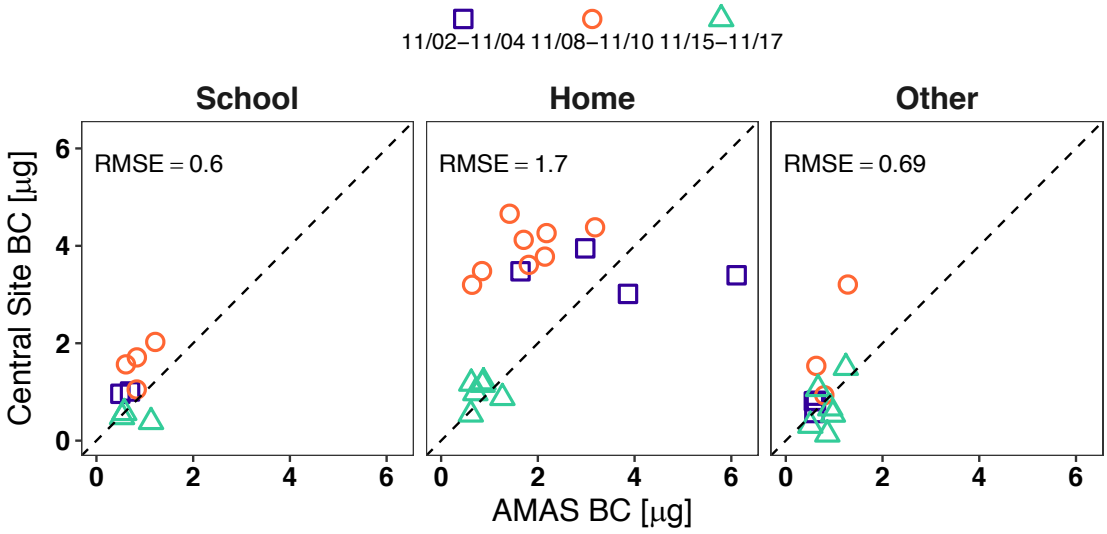

Figure B11: Central site BC mass compared to AMAS filter BC mass by microenvironment. The data shown in the plots only include samples which collected PM2.5 and AMAS data for the entire 48-hr period, had valid GPS coordinates, collected PM2.5 for more than an hour (0.1 m3) in each ME, and the BC measurement was above the LOD (0.49 µg) of the Magee Scientific Sootscan measurement (School, n = 9; Home, n = 18; Other, n = 12). The spearman correlation (ρ) is shown in each microenvironment panel.

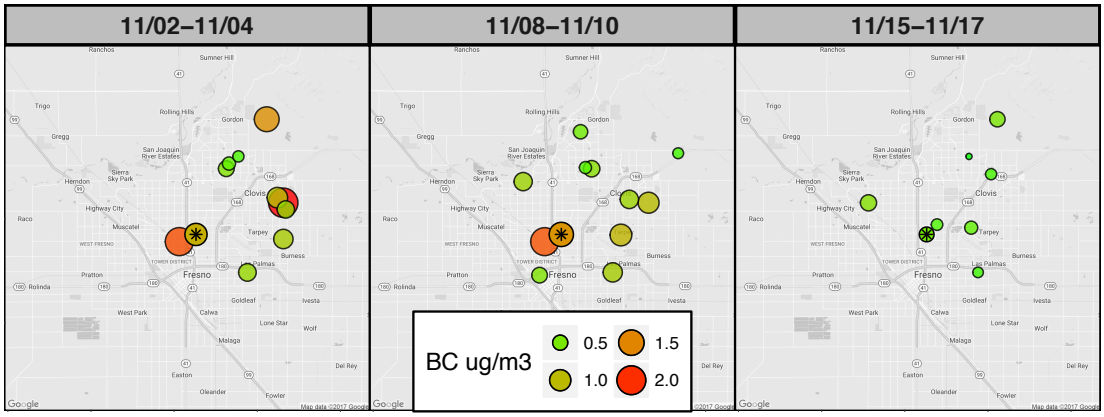

Figure B12: BC concentration spatial distribution. Home microenvironment concentrations and AE33 48-hour concentration (denoted with a "*") for the three 48-hour sampling periods.

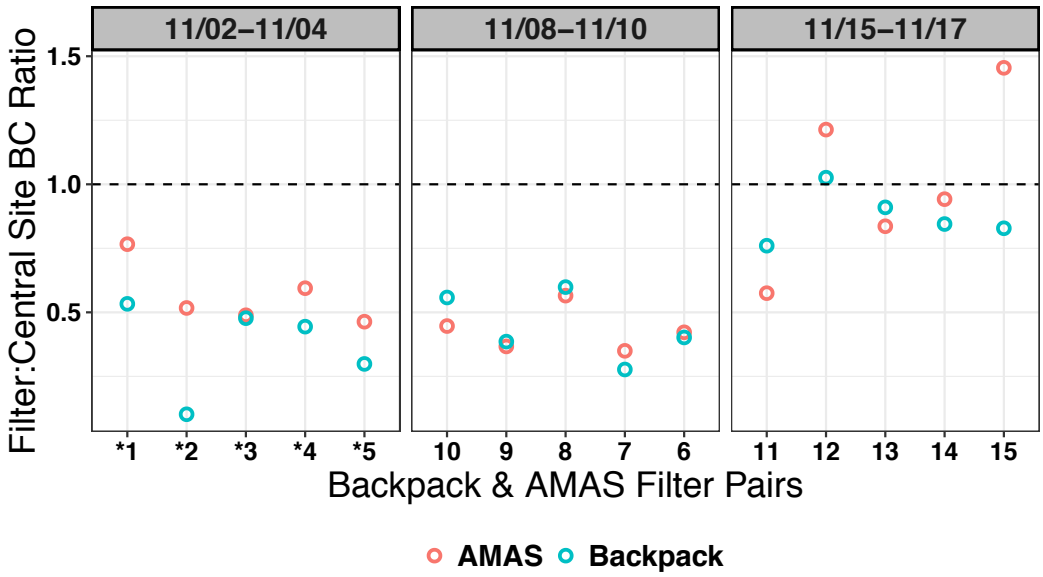

Figure B13: BC Comparisons of Backpack-AMAS pairs to AE33. This demonstrates that both the backpack and AMAS show some bias as compared to the AE33 measurements on high BC days, but not low BC days. The estimates come from using the hourly data for the AE33 to calculate the amount of mass expected compared to the mass found with the Magee Scientific Sootscan analysis.

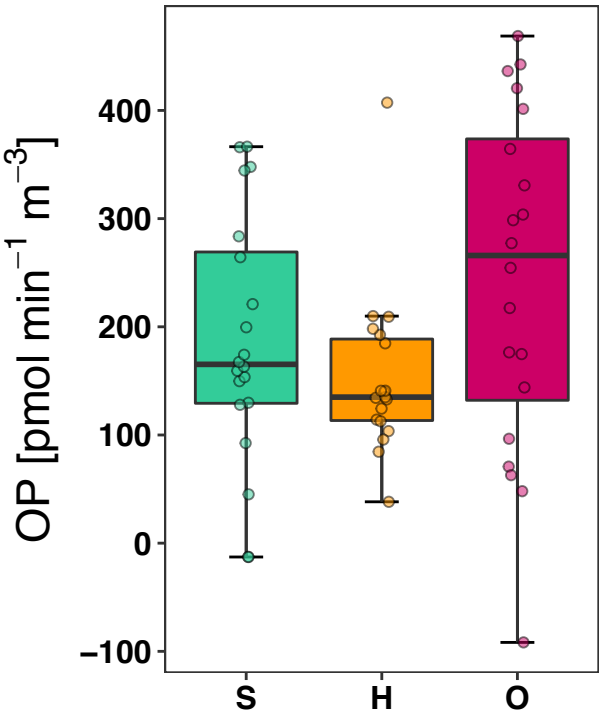

Figure B14: Oxidative potential boxplots. The data shown in the plots only include samples which collected PM2.5 and AMAS data for the entire 48-hr period, had valid GPS coordinates, and collected PM2.5 for more than an hour (0.1 m3) in each ME (n = 20, 19, 20 for S = school, H = home, and O = other).

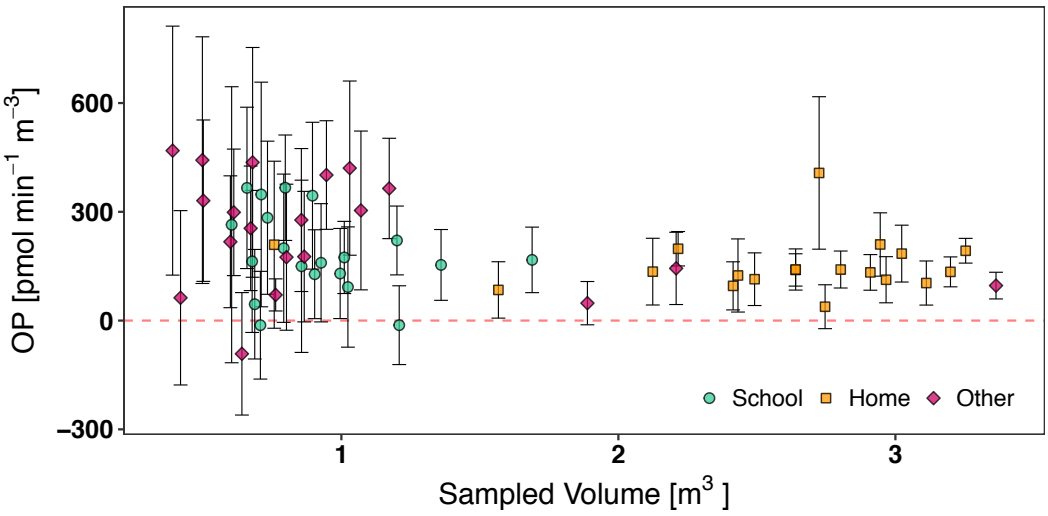

Figure B15: OP measurement uncertainty vs. sampled air volume. The data shown in the plots only include filter samples that collected $PM_{2.5}$ and AMAS data for the entire 48-hr period, had valid GPS coordinates, and collected $PM_{2.5}$ for more than an hour (0.1 m^3) in each microenvironment (n = 20, 19, 20 for S = school, H = home, and O = other).

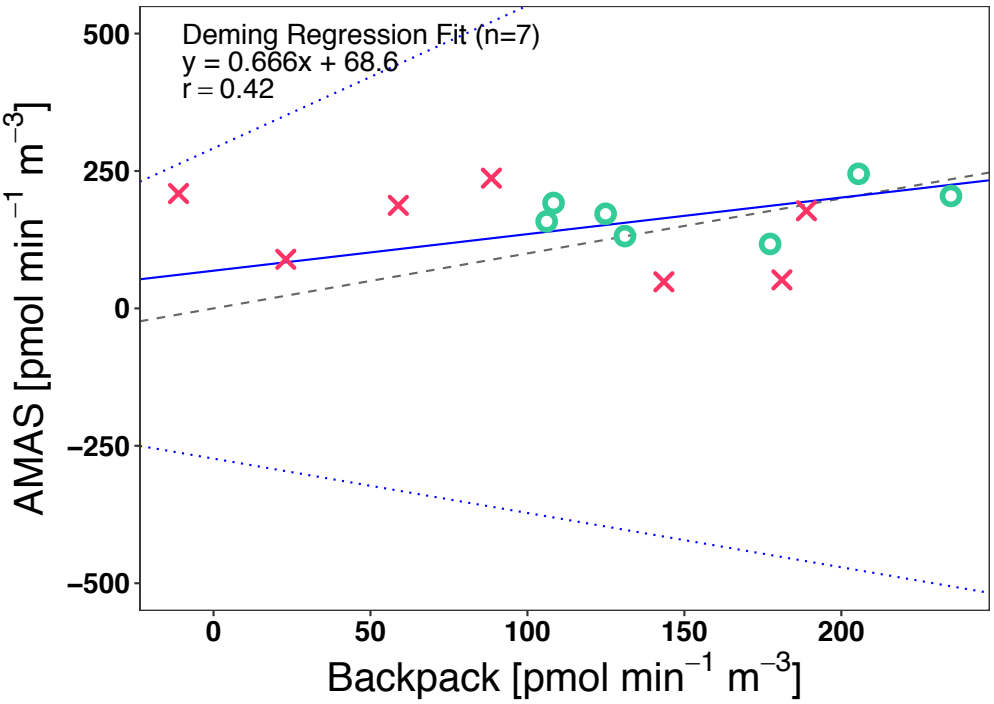

Figure B16: Deming regression of AMAS and backpack OP. Comparison of the cumulative AMAS filter pair OP measured using the dithiothreitol (DTT) assay to that of the measured backpack OP. The regression was evaluated using 7 of the 15 samples (green circles). The three samples that had backpack malfunctions or OP less than 100 pmol min-1 m-3(red multiplication signs) were excluded from the regression. The values less than 100 pmol min-1 m-3 were excluded due to the uncertainty of the assay when the reactivity of the sample was low. The Deming regression (solid blue line) had a slope of 0.67 (-0.99, 2.6) and an intercept of 69 (-270, 290). The 95% confidence intervals (dotted blue lines) and the 1:1 line (dashed gray line) are also shown in the figure.

$$BC_{\mu g} = \left(\frac{100 * ln\left(\frac{IR_{PRE}}{IR_{POST}}\right)}{\sigma_{ATN}} \right) * Area_{Filter}$$

Equation B1: Black carbon mass.

IR_{PRE}: Infrared filter transmitted intensity pre-sample

IR_{POST}: Infrared filter transmitted intensity post-sample

σ_{ATN}: Mass absorption cross-sections ($cm^2\ \mu g^{-1}$)

$Area_{Filter}$: Active filter area (cm^2):

15 mm: 13.2 cm^2; 25 mm Teflon: 3.50 cm^2; 25 mm Fiberfilm™: 3.66 cm^2

$$BC_{\frac{\mu g}{m^3}} = \left(\frac{BC_{\mu g}}{Vol} \right)$$

Equation B2: Black carbon mass concentration.

Vol: Sampled volume recorded for that filter (m^3)

$$Inhaled\ BC_{\mu g\ day^{-1}} = \frac{Inhallation\ Rate * BC_{\frac{\mu g}{m^3}} * Time_{ME}}{Total\ Sample\ Duration}$$

Equation B3: Inhaled black carbon mass.

Inhalation Rate: Long-term exposure inhalation rate ($m^3\ day^{-1}$)

$Time_{ME}$: Microenvironment sample time (day)

Total Sample Duration: Total sample period (day)

$$\sum AMAS\ BC_{\frac{\mu g}{m^3}} = \left(\frac{School\ BC_{\mu g} + Home\ BC_{\mu g} + Other\ BC_{\mu g}}{Vol_{School} + Vol_{Home}\ Vol_{Other}} \right)$$

Equation B4: Cumulative AMAS BC concentration.

$$[\boldsymbol{DTT}]_{\mu\boldsymbol{M}} = \left(\frac{\left(\frac{\boldsymbol{TNB\ abs.}}{\mathbf{14150}\ \frac{\boldsymbol{mole}}{\boldsymbol{liter}}} \right) * \mathbf{5}(\boldsymbol{dilution})}{\frac{\mathbf{2}\ \boldsymbol{moles\ TNB}}{\mathbf{1}\ \boldsymbol{mole\ DTT}}} \right) * \mathbf{1000000}\ \frac{\mu\boldsymbol{L}}{\boldsymbol{L}}$$

Equation B5: DTT concentration.

abs: UV-Vis absorbance

$$\boldsymbol{OP}_{\mu\boldsymbol{M}\ \boldsymbol{min}^{-1}} = -\mathbf{1} * \left(\left(\frac{\Delta[\boldsymbol{DTT}]}{\Delta \boldsymbol{t}} \right) - \boldsymbol{BFC} \right) * \boldsymbol{Ff}$$

Equation B6: Oxidative potential.

Δ [DTT]: Change in [DTT]

Δt: Elapsed time for all [DTT] measurements (min)

BFC: Blank filter correction (μM min^{-1})

Ff: Fraction of filter used for OP analysis (-)

Note: $\left(\frac{\Delta[\boldsymbol{DTT}]}{\Delta \boldsymbol{t}} \right)$ was calculated using the LINEST() function in MS Excel.

$$\boldsymbol{OP}_{\boldsymbol{pmol\ min}^{-1}\ \boldsymbol{m}^{-3}} = \left(\frac{\boldsymbol{OP}_{\mu\boldsymbol{M}\ \boldsymbol{min}^{-1}} * \boldsymbol{Vol}_{\boldsymbol{assay}}}{\boldsymbol{Vol}_{\boldsymbol{air}}} \right)$$

Equation B7: Oxidative potential per sampled air volume.

Vol_{assay}: DTT assay volume (μL)

Vol_{air}: Sampled volume recorded for that filter (m^3)

$$\boldsymbol{Inhaled\ OP}_{(\mu\boldsymbol{M}\ \boldsymbol{min}^{-1})\ \boldsymbol{day}^{-1}} = \frac{\boldsymbol{Inhallation\ Rate} * \left(\frac{\boldsymbol{OP}_{\mu\boldsymbol{M}\ \boldsymbol{min}^{-1}}}{\boldsymbol{Vol}} \right) * \boldsymbol{Time}_{\boldsymbol{ME}}}{\boldsymbol{Total\ Sample\ Duration}}$$

Equation B8: Inhaled oxidative potential.

Inhalation Rate: Long-term exposure inhalation rate (m^3 day^{-1})

$Time_{ME}$: Microenvironment sample time (day)

Total Sample Duration: Total sample period (day)

$$\sum \boldsymbol{AMAS\ OP}_{\frac{\boldsymbol{pmol}}{\boldsymbol{min}*\boldsymbol{m^3}}} = \left(\frac{\left(\boldsymbol{School\ OP}_{\mu \boldsymbol{M\ min^{-1}}} + \boldsymbol{Home\ OP}_{\mu \boldsymbol{M\ min^{-1}}} + \boldsymbol{Other\ OP}_{\mu \boldsymbol{M\ min^{-1}}}\right) * \boldsymbol{Vol_{assay}}}{\boldsymbol{Vol_{School}} + \boldsymbol{Vol_{Home}}\ \boldsymbol{Vol_{Other}}} \right)$$

Equation B9: Cumulative AMAS OP per sampled air volume.

Table B1: AMAS Sensor Components and Electronics.

Component	Manufacturer	Part Number
Microblower	Murata	MZBD001
Mass Air Flow Sensor	Honeywell	Omron D6F
Light Sensor (vis., UV, IR)	Silicon Labs	SI1145-A10-GMR
Temp., Pressure, RH Sensor	Bosch Sensortec	BME280
Accelerometer/Magnetometer	STMicroelectronics	LSM303DLHCTR
Bluetooth Low-Energy	Microchip	RN4677
MicroSD Card	Molex	5031821852
Memory (EEPROM)	Atmel	AT24CM01-XHM-T
Real-time Clock	Maxim Integrated	DS3231MZ+
Battery (2800 mAh)	Samsung	SAEBBG900BBU
Global Positioning System	Ublox	CAM-M8Q
Valve Manifold	Custom	N/A
Valve Manifold Gear Motor	Precision Microdrive	206-108

DTT Assay protocol: The 15 mm filters were cut in half and the 25 mm filters were quartered with ceramic scissors; one filter half or quarter was used for the DTT assay. The DTT assay was performed similar to the traditional method[4]; however, quenching with acid was not necessary as the samples were run immediately after DTNB addition, eliminating two pipetting/dilution steps in the process. The reaction of DTNB and DTT is near instantaneous at pH ~7.5, and we found a 1.5 molar excess (3 moles DTNB: 1 moles DTT) was sufficient for quenching, this then prevents the UV-Vis peak from DTNB interfering with the TNB peak at 412 nm.

To run the DTT assay, filters were placed in 1.5 mL centrifuge tubes (Eppendorf) and wet with 15 µL of 50/50 2,2,2,trifluoroethanol and MilliPore water. Trifluoroethanol has been reported to aid in wetting the surface of the filter and has been used previously in similar studies.[5] 500 µL of buffered 75 µM DTT solution was then added to the vials, which was made fresh minutes before running the assay. Stock 0.001 M phosphoric acid with a concentration of 4.5 mM of DTT, diluted by the Chelex buffer, was used to make the 75 µM DTT solution. The dilute acid stabilizes the DTT and enables the stock 4.5 mM DTT solution to be used through a day of testing, these solutions were remade fresh after 24 hours.

The vials were placed in a 37 °C water bath. At time points 0, ~15, ~30, and ~45 minutes 100 µL aliquots were removed from the vials and added to 400 µL of stock DTNB solution. The DTNB concentration was ~56 µM in 0.1 M phosphate buffer at pH of ~7.5. Spectra were measured four times (0, 15, 30, and 45 minutes) with a UV-Vis spectrophotometer (Agilent 8453, Santa Clara, CA, USA) within ~15 minutes of reacting DTT with DTNB. The absorbance at 412 nm was used to measure TNB concentration. The concentration was calculated with Beer's law using a molar extinction coefficient of 14150 M^{-1} cm^{-2}. For all trials two blank DTT decay rates were measured, blank rates were also recorded in the presence on non-PM loaded filters as a control for any filter related activity.

[4] Cho, A. K.; Sioutas, C.; Miguel, A. H.; Kumagai, Y.; Schmitz, D. A.; Singh, M.; Eiguren-Fernandez, A.; Froines, J. R., Redox activity of airborne particulate matter at different sites in the Los Angeles Basin. *Environmental Research* **2005,** *99*, (1), 40-47.

[5] Charrier, J. G.; McFall, A. S.; Vu, K. K. T.; Baroi, J.; Olea, C.; Hasson, A.; Anastasio, C., A bias in the "mass-normalized" DTT response – An effect of non-linear concentration-response curves for copper and manganese. *Atmospheric Environment*.

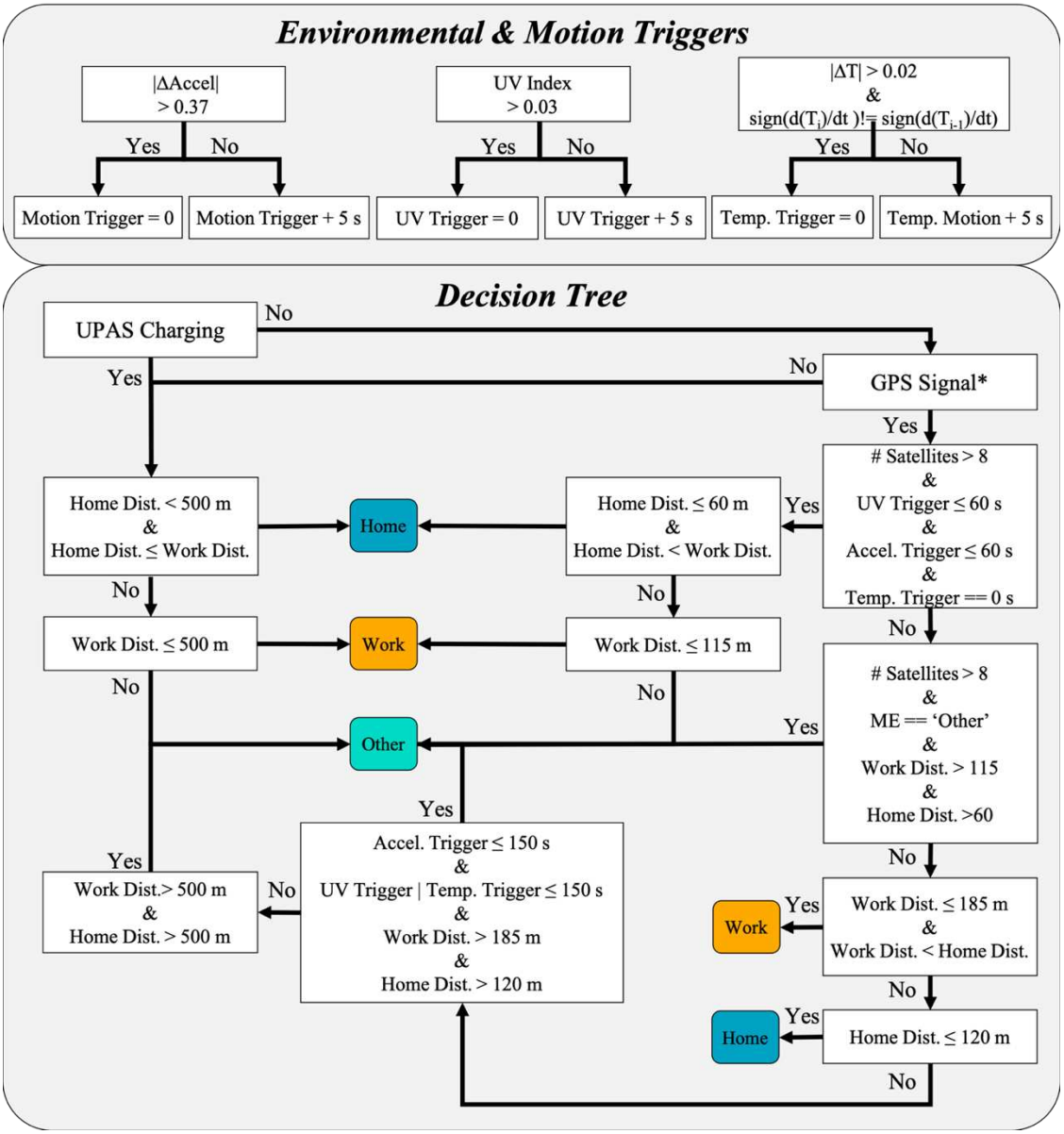

Figure C1: AMAS microenvironment classification AMAS. (*GPS Signal was considered valid only if the GPS had been connected to more than five satellites for a minimum of 30 s without signal loss).

Figure C2: Modified UPAS. An Ultrasonic Personal Aerosol Sampler (UPAS) was modified to include a pushbutton (mounted on the side) and global positioning system (GPS; mounted on the bottom). Volunteers used the three-point harness to wear the UPAS for multiple days to collect the GPS, environmental (temperature, pressure, relative humidity, UV light), and motion data..

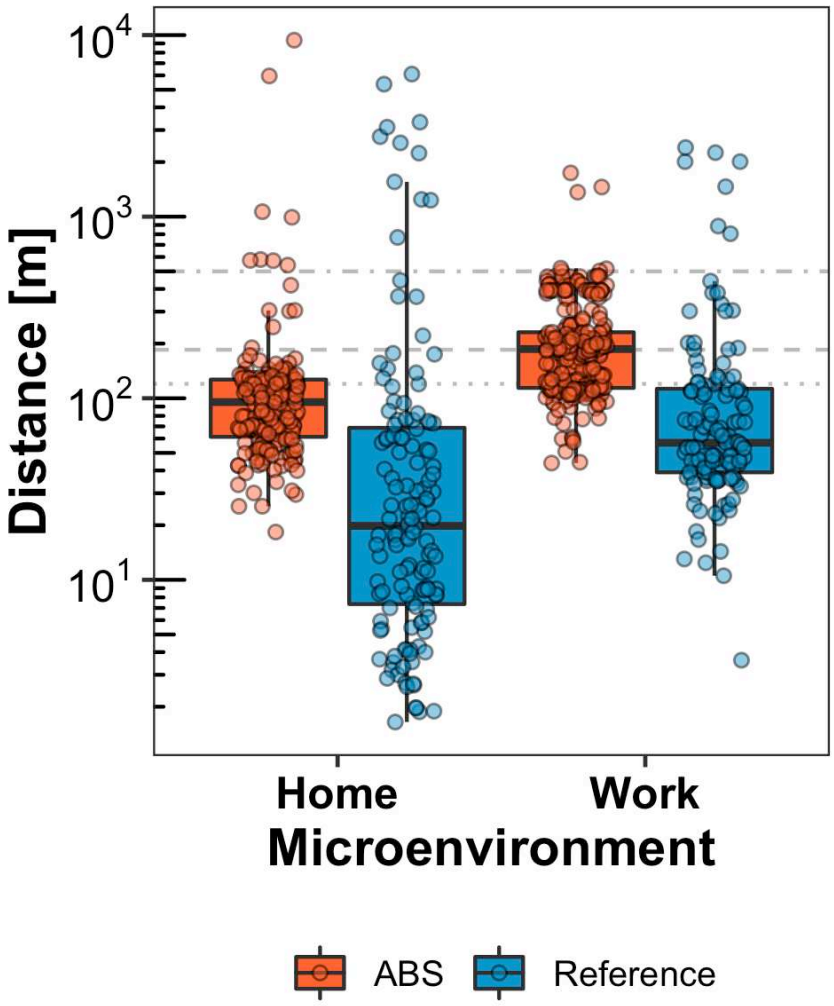

Figure C3: Microenvironment transition distance. Distance from microenvironment centroid at the time of transition. The ABS algorithm buffer sizes were based on the GPS distance recorded in the reference dataset. Distances equal to the 75th percentile (work: 115 m; home: 60 m), 85th percentile (work: 185 m; home: 120 m), and 500 m were used to define the buffer radii. The upper quartile of the volunteer record is the 75th percentile distances and the horizontal lines show the 85th percentile distances and 500 m. Sample sizes: ABS algorithm home, n=199; Reference dataset home, n=140; ABS algorithm work, n=280; Reference dataset work, n=132.

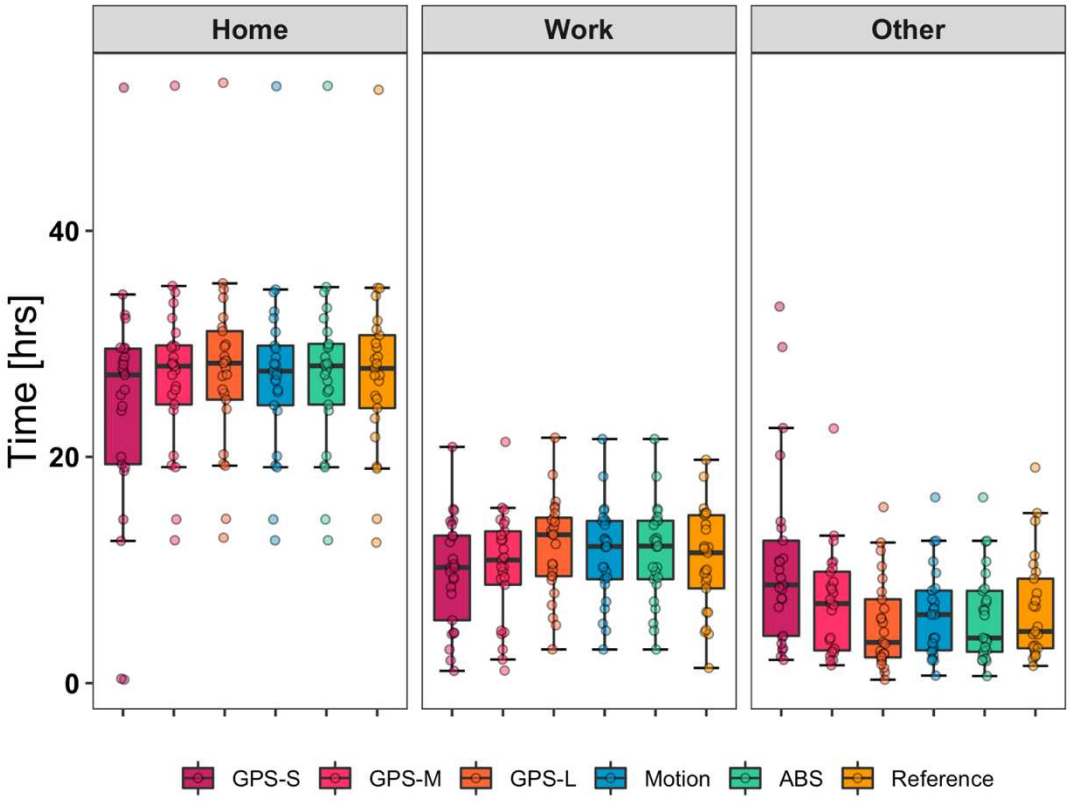

Figure C4: Microenvironment Time Estimates. Estimated or actual time spent in each microenvironment for all samples (n=25). A description of each algorithm (GPS-S, GPS-M, GPS-L, Motion, and ABS) can be found in the methods section of the main text. The reference dataset times are the times spent in each microenvironment as denoted by the volunteers in their diaries and/or using the pushbutton

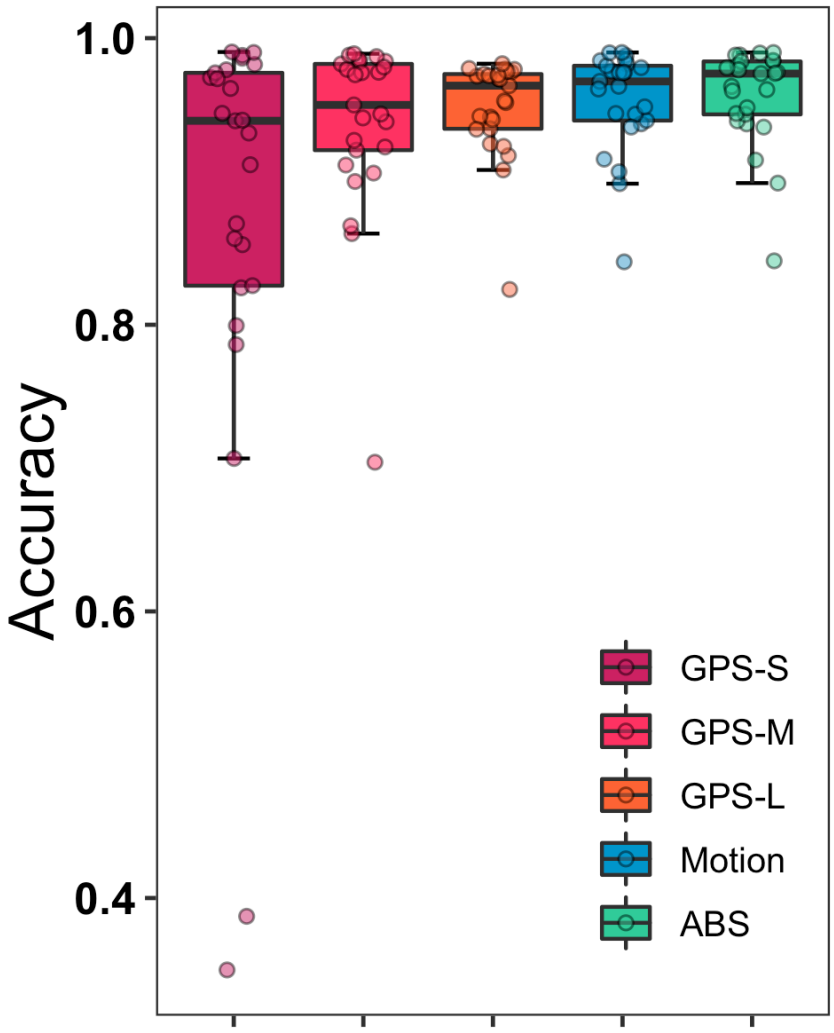

Figure C5: The accuracy for each of the five algorithms for predicting microenvironment classifications (n=25). The volunteer record data was used as the baseline.

$$Accel = \sqrt{Accel\_X^2 + Accel\_Y^2 + Accel\_Z^2}$$

Equation C1: Total Acceleration.

$$Sensitivity = \left(\frac{TP}{TP + FN}\right)$$

Equation C2: Sensitivity.

$$Specificity = \left(\frac{TN}{FP + TN}\right)$$

Equation C3: Specificity.

$$Accuracy = \left(\frac{TP + TN}{TP + TN + FP + FN}\right)$$

Equation C4: Accuracy).

True positive (TP) is defined as when the volunteer is inside a specific microenvironment and the designation determined by the algorithm developed in this work matches the microenvironment designation noted by the volunteer in their diary and/or via use of the push button.

(e.g. (ME_{Diary} = Home) = ($ME_{Algorithm}$ = Home))

True negative (TN) is defined as when the volunteer is outside a specific microenvironment and the designation determined by the algorithm developed in this work matches the microenvironment designation noted by the volunteer in their diary and/or via use of the push button.

(e.g. (ME_{Diary} != Home) = ($ME_{Algorithm}$!= Home)

False positive (FP) is defined as when the volunteer is inside a specific microenvironment and the designation determined by the algorithm developed in this work does not match the microenvironment designation noted by the volunteer in their diary and/or via use of the push button.

(e.g. (ME_{Diary} = Home) != ($ME_{Algorithm}$ = Home))

False negative (FN) is defined as when the volunteer is outside a specific microenvironment and the designation determined by the algorithm developed in this work does not match the microenvironment designation noted by the volunteer in their diary and/or via use of the push button.

(e.g. (ME_{Diary} != Home) != ($ME_{Algorithm}$!= Home))

Table C1: Modified UPAS Sensor Components and Electronics.

Component	Manufacturer	Part Number
Microblower	Murata	MZBD001
Mass Air Flow Sensor	Honeywell	Omron D6F
Light Sensor (vis., UV, IR)	Silicon Labs	SI1145-A10-GMR
Temp., Pressure, RH Sensor	Bosch Sensortec	BME280
Accelerometer/Magnetometer	STMicroelectronics	LSM303DLHCTR
Bluetooth Low-Energy	Switch Science	HRM1017
MicroSD Card	Molex	5031821852
Memory (EEPROM)	Atmel	AT24CM01-XHM-T
Real-time Clock	Maxim Integrated	DS3231MZ+
Battery (2800 mAh)	Samsung	SAEBBG900BBU
Global Positioning System	Adafruit	746
Pushbutton	Switchcraft Inc.	ED913

Table C2: Number of microenvironment transitions for the reference dataset or as determined via simulation for each of the algorithms.

	GPS-S	GPS-M	GPS-L	Motion	ABS	Reference
# of Transitions	1084	454	334	659	483	274

Table C3: The median (25^{th}, 75^{th} percentiles) time spent in each microenvironment for the reference dataset or as determined via simulation for each of the algorithms.

	GPS-S	GPS-M	GPS-L	Motion	ABS	Reference
Home	27.3 (19.4, 29.6)	28.0 (24.6, 29.9)	28.3 (25.1, 31.1)	27.6 (24.6, 29.8)	28.1 (24.6, 30.0)	27.8 (24.3, 30.8)
Work	10.2 (5.6, 13.0)	10.9 (8.7, 13.4)	13.1 (9.5, 14.6)	12.1 (9.2, 14.3)	12.1 (9.2, 14.4)	11.5 (8.4, 14.9)
Other	8.7 (4.2, 12.6)	7.0 (2.9, 9.8)	3.6 (2.3, 7.4)	6.1 (2.9, 8.2)	4.0 (2.8, 8.2)	4.6 (3.1, 9.2)

Table C4: Median (25th, 75th percentile) accuracy for the five microenvironment detection algorithms.

	Accuracy			Total Accuracy
	Home	Work	Other	All
GPS-S	0.981 (0.948, 0.994)	0.984 (0.914, 0.993)	0.942 (0.827, 0.975)	0.942 (0.827, 0.976)
GPS-M	0.989 (0.981, 0.994)	0.982 (0.947, 0.992)	0.953 (0.922, 0.982)	0.953 (0.922, 0.982)
GPS-L	0.987 (0.980, 0.994)	0.979 (0.954, 0.988)	0.967 (0.938, 0.975)	0.967 (0.937, 0.975)
Motion	0.990 (0.979, 0.994)	0.990 (0.959, 0.994)	0.970 (0.943, 0.981)	0.970 (0.943, 0.981)
ABS	0.992 (0.981, 0.994)	0.989 (0.959, 0.994)	0.975 (0.947, 0.984)	0.975 (0.947, 0.984)

Table C5: Pairwise comparisons of the total accuracy for all of the algorithms using the Nemenyi multiple comparisons test with q approximation. No p-value adjustment method was used. The green highlighted cells denoted the comparisons with significant differences.

	GPS-S	GPS-M	GPS-L	Motion
GPS-M	0.953	-	-	-
GPS-L	0.971	0.665	-	-
Motion	0.123	0.462	0.023	-
ABS	0.260	0.693	0.064	0.997

Table C6: Pairwise comparisons of the accuracy for all of the algorithms by microenvironment using the Nemenyi multiple comparisons test with q approximation. No p-value adjustment method was used. The green highlighted cells denoted the comparisons with significant differences

	Home				Work				Other			
	GPS-S	**GPS-M**	**GPS-L**	**Motion**	**GPS-S**	**GPS-M**	**GPS-L**	**Motion**	**GPS-S**	**GPS-M**	**GPS-L**	**Motion**
GPS-M	0.999	-	-	-	0.200	-	-	-	0.971	-	-	-
GPS-L	0.693	0.549	-	-	0.0008	0.380	-	-	0.984	0.773	-	-
Motion	0.462	0.607	0.026	-	0.9998	0.137	0.0004	-	0.137	0.434	0.034	-
ABS	0.329	0.462	0.013	0.999	0.9965	0.380	0.003	0.984	0.239	0.607	0.071	0.999

Table C7: Median (25th, 75th percentile) sensitivity and specificity for the five microenvironment detection algorithms

	Sensitivity			Specificity		
	Home	**Work**	**Other**	**Home**	**Work**	**Other**
GPS-S	0.990 (0.939, 1.000)	0.968 (0.711, 1.000)	0.892 (0.739, 0.947)	0.990 (0.984, 0.996)	0.992 (0.986, 0.996)	0.941 (0.846, 0.990)
GPS-M	0.997 (0.985, 1.000)	0.988 (0.860, 1.000)	0.830 (0.697, 0.934)	0.984 (0.976, 0.991)	0.989 (0.984, 0.995)	0.986 (0.941, 0.996)
GPS-L	1.000 (0.992, 1.000)	1.000 (1.000, 1.000)	0.711 (0.587, 0.816)	0.976 (0.965, 0.983)	0.975 (0.959, 0.985)	0.999 (0.987, 1.000)
Motion	0.998 (0.991, 1.000)	0.997 (0.989, 1.000)	0.856 (0.735, 0.921)	0.988 (0.983, 0.995)	0.986 (0.969, 0.992)	0.993 (0.972, 0.999)
ABS	0.998 (0.991, 1.000)	0.997 (0.989, 1.000)	0.832 (0.733, 0.870)	0.985 (0.982, 0.992)	0.986 (0.969, 0.992)	0.996 (0.979, 0.999)

Table C8: Pairwise comparisons of the sensitivity for all of the algorithms by microenvironment using the Nemenyi multiple comparisons test with q approximation. No p-value adjustment method was used. The green highlighted cells denoted the comparisons with significant differences.

	Home				Work				Other			
	GPS-S	**GPS-M**	**GPS-L**	**Motion**	**GPS-S**	**GPS-M**	**GPS-L**	**Motion**	**GPS-S**	**GPS-M**	**GPS-L**	**Motion**
GPS-M	0.0006	-	-	-	0.064	-	-	-	2.1e-5	-	-	-
GPS-L	2.7e-10	0.064	-	-	2.9e-7	0.03	-	-	3.5e-14	0.0003	-	-
Motion	0.044	0.721	0.001	-	0.219	0.984	0.005	-	0.008	0.607	1.7e-7	-
ABS	0.0007	1.000	0.056	0.747	0.056	1.000	0.034	0.978	8.0e-7	0.971	0.003	0.239

Table C9: Pairwise comparisons of the specificity for all of the algorithms by microenvironment using the Nemenyi multiple comparisons test with q approximation. No p-value adjustment method was used. The green highlighted cells denoted the comparisons with significant differences.

	Home				Work				Other			
	GPS-S	**GPS-M**	**GPS-L**	**Motion**	**GPS-S**	**GPS-M**	**GPS-L**	**Motion**	**GPS-S**	**GPS-M**	**GPS-L**	**Motion**
GPS-M	1.6e-8	-	-	-	3.3e-5	-	-	-	0.0006	-	-	-
GPS-L	4.5e-14	0.080	-	-	4.0e-14	0.0004	-	-	4.7e-14	7.6e-5	-	-
Motion	0.124	0.002	5.1e-9	-	0.005	0.747	1.0e-6	-	0.005	0.978	4.3e-6	-
ABS	7.6e-5	0.520	0.0004	0.219	0.4.0e-5	1.000	0.0003	0.773	4.3e-6	0.842	0.005	0.491